

## Copyright Undertaking

This thesis is protected by copyright, with all rights reserved.

**By reading and using the thesis, the reader understands and agrees to the following terms:**

1. The reader will abide by the rules and legal ordinances governing copyright regarding the use of the thesis.
2. The reader will use the thesis for the purpose of research or private study only and not for distribution or further reproduction or any other purpose.
3. The reader agrees to indemnify and hold the University harmless from and against any loss, damage, cost, liability or expenses arising from copyright infringement or unauthorized usage.

### IMPORTANT

If you have reasons to believe that any materials in this thesis are deemed not suitable to be distributed in this form, or a copyright owner having difficulty with the material being included in our database, please contact [lbsys@polyu.edu.hk](mailto:lbsys@polyu.edu.hk) providing details. The Library will look into your claim and consider taking remedial action upon receipt of the written requests.

The Hong Kong Polytechnic University

Department of Electrical Engineering

**Speciality Polymer Optical Fibres  
for Sensing Applications**

PUN CHI FUNG

A thesis submitted in partial fulfillment of the requirements for  
the degree of Doctor of Philosophy

JULY 2012

## **CERTIFICATE OF ORIGINALITY**

I hereby declare that this thesis is my own work and that, to the best of my knowledge and belief, it reproduces no material previously published or written nor material which has been accepted for the award of any other degree or diploma, except where due acknowledgement has been made in the text.

\_\_\_\_\_(Signed)

PUN CHI FUNG (Name of student)

## **Acknowledgments**

I offer my sincerest gratitude to my supervisor, Prof. Hwa-Yaw Tam, who has been fully supporting me throughout my Ph.D. study with his patience, knowledge and valuable advice.

I would like to show my gratitude to my co- supervisor, Prof. Tao Xiao-ming, who has been supporting me with her valuable guidance and suggestion.

I would like to show my gratitude to all my colleagues and note especially Dr. Ming-Leung Vincent, Prof. Zhao Guiyao, Mr. Cheng Xin, Mr. Zhengyong Liu, Mr. Yin Mingjie for their kindly collaborations, valuable discussion and suggestion.

Finally, I would greatly appreciate the financial support of the entire Ph.D programme from the Research Grants Council of the Hong Kong SAR Government.

## **Abstract**

The ultimate goal of our research is to develop an all-polymer fibre optic system for biomedical sensing application. This thesis introduces a paradigm shift in polymer optical fibre sensors that the light source and sensing elements are combined in a single laser-dye-doped polymer optical fibre without a coupling device. The light source is created by pumping the fibre with low-cost diode-pumped solid-state (DPSS) laser at any point along the fibre. Moreover, the sensing elements are allowed to be created anywhere along the POF as well, providing a low-cost technology platform for disposable biomedical sensors.

Our POFs are drawn by the preform drawing method. A reliable POF draw tower has been designed and built, which can handle preforms with diameter ranging from 6mm to 40mm and POF with diameter less than 3% tolerance. A specific pre-polymerization procedure is necessary to prevent bubble formation during the early stage of the polymerization of monomers.

The light source is created when the POF is doped with organic laser dye and pumped by a low-cost DPSS laser below 50mW by side-illumination fluorescence (SIF) technique. The Rh640 doped POF with cladding structure is fabricated and it is also calculated the optical conversion efficiency of the fibre is 1.509% with the laser dye concentration of 10ppm.

The SIF signal can be increased by tapering or bending method which is further studied experimentally, such that the fluorescence power in the fibre core is at least 4 times greater than that was achieved when side-illuminating without bends. The fluorescence power was further improved to greater than 10 times for multiple bends. The modelling of bending mechanism is done as well which supports and explains the experimental results.

There are two novel pumping schemes, based on a Switch-pumping (SwP) technique and a Scan-pumping (ScP) technique with single or multiple laser diodes, are invented to overcome the power degradation problems arising from the photobleaching of the dyes. The total output power deterioration is less than 10% when the dye doped POF has been continuously pumped by the laser diode(s) to give 1  $\mu$ W optical output for 90min.

## Contents

Acknowledgments .....	1
Abstract .....	2
Chapter 1    Introduction .....	7
1.1    Background.....	7
1.2    Objective.....	8
1.3    Structure of Thesis.....	10
1.4    Related Publications .....	13
Reference .....	14
Chapter 2    Literature Review .....	16
Reference .....	20
Chapter 3    Preform Fabrication .....	24
3.1    Introduction.....	24
3.2    Principle of Polymerization.....	26
3.2.1    Chain initiation .....	27
3.2.2    Chain Propagation .....	27
3.2.3    Chain Termination .....	28
3.3    Materials.....	29
3.3.1    Optimum Preform Composition .....	31
3.4    Fabrication Process.....	34
3.4.1    Importance of Pre-polymerization .....	35
3.4.2    Curing in Oven .....	38
3.5    Procedure of Fabricating Step-index Preforms .....	40
3.6    Conclusion .....	42
Reference .....	43
Chapter 4    Fibre Draw Tower.....	45
4.1    Introduction.....	45
4.2    Major Components.....	45
4.2.1    Main Structure Design .....	46
4.2.2    Preform Feeding Unit .....	47
4.2.3    Preform Heating Unit .....	49
4.2.4    Fibre Take-up Unit .....	52
4.2.5    Monitoring Devices.....	54

4.2.6	Control Unit .....	55
4.3	Overall Performance and Specification .....	56
4.4	Optimum Drawing Condition .....	58
4.5	Conclusion .....	62
	Reference .....	63
Chapter 5	Applications of Dye-Doped POF as Light Sources .....	64
5.1	Introduction.....	64
5.2	Dye-Doped unclad POF.....	65
5.2.1	Materials and fibres fabrication .....	66
5.2.2	Low Cost Pump Source .....	71
5.2.3	Experimental Setup and fluorescence Spectrum .....	76
5.2.4	Co-doping of Laser Dyes .....	82
5.3	Dye-Doped Fibres with Cladding.....	84
5.3.1	Fabrication Process.....	87
5.3.2	End-pump Versus Side Luminance Technique .....	89
5.3.3	Optical Conversion Efficiency .....	91
5.3.4	Fluorescence Characteristics .....	99
5.3.5	Enhancement of Optical Power by Gold Coating .....	103
5.3.6	Application as Light Source in Sensor System .....	106
5.4	Conclusion .....	108
	Reference .....	110
Chapter 6	Enhancement of Side-illumination Fluorescence by Bending Method.....	113
6.1	Introduction.....	113
6.2	Principle of Bending Method.....	114
6.3	Design of Dye-doped-clad PMMA-core POF .....	115
6.4	Experimental Setup .....	116
6.5	Experimental Results .....	118
6.6	Modelling of Bending Mechanism.....	120
6.7	Conclusion .....	123
	Reference .....	124
Chapter 7	Novel Pumping Scheme to Overcome Photobleaching Effect .....	126
7.1	Introduction.....	126



7.2	Bleaching Effect and Dye Recovery .....	127
7.3	Novel Pumping Scheme .....	129
7.3.1	Switch-pumping technique (SwP).....	130
7.3.2	Scan-Pumping (ScP) Technique .....	135
7.3.3	Comparison between SwP and ScP .....	142
7.4	Proposal of Various Pumping Scheme for Laser Dye-Doped POFs.....	143
7.5	Applications in Fibre Sensing Systems.....	144
7.6	Conclusion .....	146
	Reference .....	147
Chapter 8	Low-loss Single-mode Perfluorinated Polymer Optical Fibre .....	149
8.1	Introduction.....	149
8.2	Importance of fabricating low-loss single-mode PPOF .....	149
8.3	Design of single-mode PPOF.....	151
8.4	Fabrication of single-mode PPOF .....	153
8.4.1	Drawing Difficulty .....	154
8.4.2	Vacuum Pressure Control.....	156
8.5	Optical Characteristics .....	157
8.5.1	Far Field Profile.....	157
8.5.2	Cut-off Wavelength .....	159
8.5.3	Transmission Loss .....	160
8.6	Conclusion .....	162
	Reference .....	163
Chapter 9	Conclusion .....	165
Chapter 10	Future Work .....	169
10.1	Inscription of sensing elements in dye doped POF .....	169
10.2	Building POF Cleaver .....	169
10.3	Modification in Teflon Method .....	169
10.4	Building broadband fibre laser by dye doped POF.....	170
10.5	Fabrication of mPOF.....	170
10.6	Fabrication of Various Structures of Dye Doped POFs.....	173

## **Chapter 1 Introduction**

### **1.1 Background**

As early in 1960s, the first polymer optical fibre (POF) was manufactured by Dupont. At the same time, silica fibre had been introduced as well. Japanese companies had been putting a lot of effort in reducing the transmission loss of POFs [1]. In 1970s, the loss reduced to around 125db/km at wavelength 650nm, which was the theoretical limit. However, at that time, the loss of silica optical fibres was well below 1dB/km at C-band and L-band. POFs were not so competitive with the silica optical fibres and thus their development was slowed down. The situation had been gradually changed since 1990s, as the applications in optical fibres were not restricted to long-haul transmission. POFs were sometimes more suitable than silica fibres in specific requirement and applications. In recent years, POFs [2] are becoming increasingly attractive for sensing applications as well, particularly in biomedical, and in large strain measurement for health monitoring of civil infrastructure [3-6]. This is because unlike silica optical fibres, POFs are rugged, biocompatible, and do not produce shards when break. They have an eminent pliability, with a low Young's modulus of several GPa. As a polymeric fibre, POF can be easily interwoven with various common fibres and yarns to construct smart textile structures with sensing functions [7]. Other important merits of POFs are the ease of handling and flexibility in photosensitive design since various additives can be easily introduced into the fibre core during the fabrication process. The additives may include photosensitive materials and laser dyes such that the POFs can be used for fibre grating sensors as well as light

sources. Therefore this is a very good opportunity for us to explore the challenges in this exciting research area.

## 1.2 Objective

Our aim is to develop an all-polymer fibre optic sensor system. The four main components in the system are the source, the fibre sensing element, the coupling device and the detector as illustrated in Fig. 1-1.

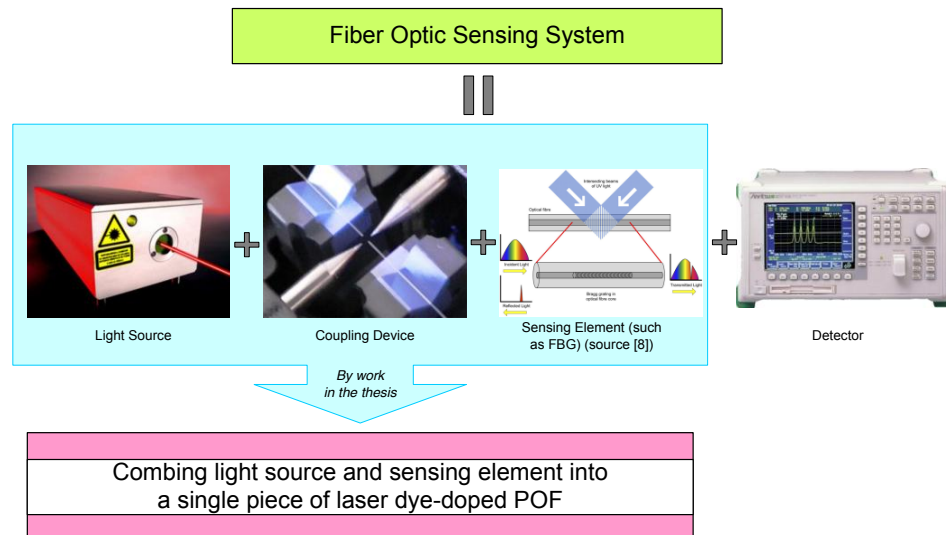


**Fig. 1-1. Diagram of main components in fiber optic sensing system.**

The ultimate goal is to create a complete low cost sensor system that is suitable for use as disposable devices in the biomedical industry. In order to achieve this, a few major issues need to be overcome. The light source should be cheap and easily coupled to polymer fibres. One suitable candidate is laser-dye-doped polymer fibre [9], which has a low production cost and should provide enough power for meters long biomedical devices. A reliable POF light source has to be built for sensing

applications. Therefore the bleaching effect of the dye doped POF has to be overcome. For the fibre sensing element, it can be inscripted into the dye doped POF directly, such that the light source and the sensing elements are combined into a single fibre. On the other hand, the sensing element can be built into other types of POF as well, so further research is required to improve the attenuation and uniformity of the fibre. This will in part facilitate a more reliable production of Bragg gratings that are difficult to achieve so far. The first single-mode poly-methyl-methacrylate (PMMA)-based POF with fibre Bragg gratings written in it was reported in 1999 [10]. It was demonstrated that the reflection wavelength of the polymeric FBGs could be tuned over a much larger range than those written in silica fibres. Since then however, virtually all reported polymeric FBGs were written at the 1550 nm transmission window [11-12], this limits their usable length to about 10 cm due to the extremely large attenuation of PMMA at 1550 nm. Therefore, devices operating at shorter wavelengths with lower loss windows in PMMA are preferred. Moreover, detectors for visible or near visible wavelengths are far cheaper than that for the 1550 nm window.

### 1.3 Structure of Thesis

In this thesis, firstly we will review the developments on dopant POFs and POF gratings, and some of the applications of POFs. At the beginning, we will show how POF preform to be fabricated and then introduce our in-house POF draw tower. We will demonstrate how the POFs, with different structures and dopants have been fabricated in our laboratory. Then we will investigate the optical properties of laser dye doped POF and how to make use of it as a light source for POF sensing system. After that, we will show how to couple light into the core of the dye doped POF efficiently by the bending method. Then we will focus on the possible ways to overcome bleaching effects in the dye doped POFs, so as to make our POF light source more practical and reliable. Later we will propose a possible low cost approach for an all-polymer optical sensing system. Then we will review our work in developing some special POFs, e.g. a low-loss, photosensitive single-mode POF which is suitable for the fabrication of FBGs operating at the 1310 nm - 1550 nm wavelength range by making use of perfluorinated polymer as the core material of the POF. Our work on designing hole-assisted POF for efficient FBG inscription will also be mentioned.

The thesis is organized as the following Fig. 1-2. In Chapter 2, we review some of the applications associate with POFs.

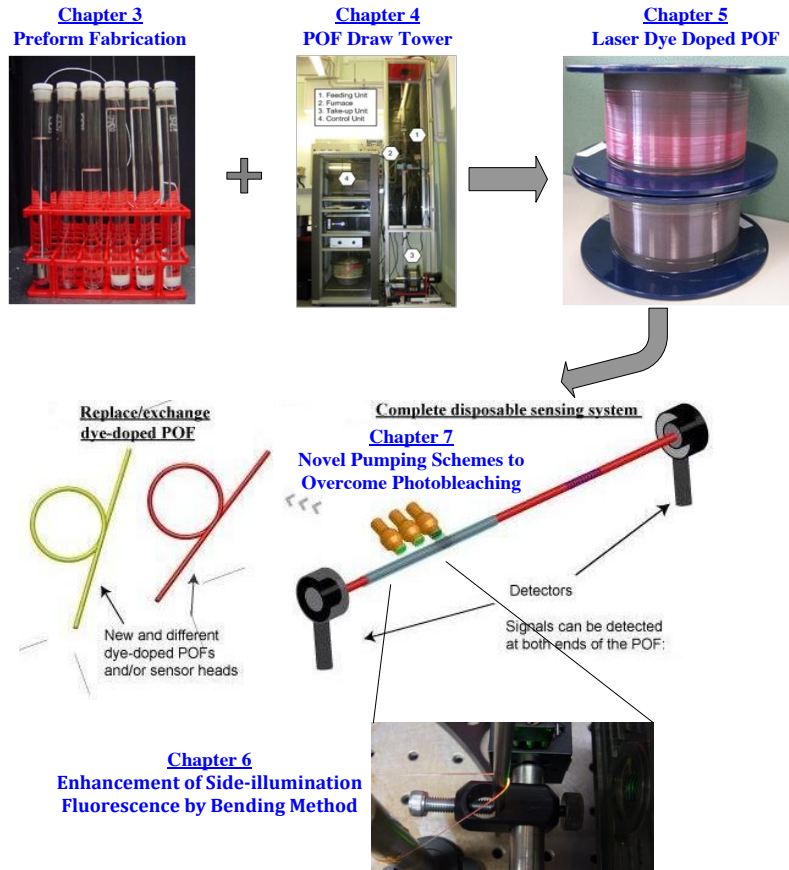


**Fig. 1-2. Diagram of structure of the thesis.**

In Chapter 3, we will go through the theory on how POF preforms we made. The process of fabrication of the preforms will be shown as well as the proper composition of the preforms. In Chapter 4, the building of the fibre draw tower will be introduced. The performance and the specification of the draw tower will be discussed and the optimum drawing conditions for various POFs will also be discussed. In Chapter 5, the experimental results of dopant POFs are demonstrated to show how the POFs can be doped with organic laser dyes and pumped by low

cost light source. The fluorescence characteristics of the dye doped POFs are investigated. Experiments have been done to realize the potential of the dye doped POFs to be used as light source for sensing applications. In Chapter 6, the bending method will be introduced, which its to increase the coupling efficiency of the pump source into the core of the dye doped POF. In Chapter 7, further experiments will be shown to overcome the bleaching effects of the dye doped POFs. Novel pumping schemes will be introduced to make the dye doped POFs as a reliable light source. Moreover, low cost polymer optical sensing systems will be proposed by making use of this dye doped POFs. Chapter 8 will conclude all the works and achievements done in this thesis. Lastly in Chapter 9, the relevant future work will be proposed in order to keep exploring in the area of POF sensing applications.

#### 1.4 Related Publications

The list of related publications about this thesis is summarized as follows:

1. CHENG, K.C., TSE, M.L., ZHOU, G.Y., PUN, C.F., CHAN, W.K., LU, C., WAI, P.K. and TAM, H.Y. "Optimization of 3-hole-assisted PMMA optical fibre with double cladding for UV-induced FBG fabrication", *Optics Express* 17, p.2080-2088 (2009)
2. ZHOU, G.Y., PUN, C.F. J., TAM, H.Y, WONG, A. C. L., LU, C. and WAI, P. K. A. "Single-Mode Perfluorinated Polymer Optical Fibres With Refractive Index of 1.34 for Biomedical Applications", *IEEE Photonics Technology Letters* 22, p.106-108 (2010)
3. TAM, H.Y., PUN, C.F., ZHOU, G.Y., CHENG, X. and TSE, M.L.V. "Special Structured Polymer Fibres for Sensing Applications", *Optical Fibre Technology* 16, p.357-366 (2010)
4. PUN, C.F., LIU, Z.Y., TSE, M.L.V., CHENG, X., TAO, X. M. and TAM, H. Y. "Side-illumination fluorescence dye-doped-clad, PMMA-core Polymer Optical Fiber: Potential Intrinsic Light Source for Biosensing", *IEEE Photonics Technology Letters* 24, p.960-962 (2012)



## Reference

1. OIKAWA, S., FUJIKI, M., and KATAYAMA, Y., “Polymer Optical Fibre with Improved Transmittance,” *Electron. Lett.* 15, 830–831 (1979).
2. BOSCH, D. and TOINEN, C., “Full polymer single-mode optical fibre,” *IEEE Photon. Technol. Lett.* 4, 749 (1992).
3. KUANG, K. S. C., QUEK, S. T., KOH, C. G., CANTWEL, W. J. and SCULLY, P. J., “Plastic optical fibre sensors for structural health monitoring: A review of recent progress,” *Journal of Sensors* 2009, Article ID 312053 (2009).
4. KIESEL, S., PETERS, K., HASSAN, T. and KOWALSKY, M., “Behaviour of intrinsic polymer optical fibre sensor for large-strain applications,” *Meas. Sci. Technol.* 18, 3144 (2007).
5. KIESEL, S., PETERS, K., HASSAN, T. and KOWALSKY, M., “Large deformation in-fibre polymer optical fibre sensor,” *IEEE Photon. Technol. Lett.* 20, 416 (2008).
6. CHANG, X., LI, M. and HAN, X., “Recent development and applications of polymer optical fiber sensors for strain measurement,” *Front. Optoelectron. China* 2, 362 (2009).
7. YE, C. C., DULIEU-BARTON, J. M., WEBB, D. J., ZHANG, C., PENG, G.-D., CHAMBERS, A. R., LENNARD, F. J. and EASTOP, D. D., “Applications of polymer optical fibre grating sensors to condition monitoring of textiles,” *Proc. of SPIE* 7503, 75030M-1 (2009).

8. JOHNSON, I., WEBB, D., "Polymer-fiber grating sensors", SPIE Newsroom, 10.1117/2.1201003.002867 (2010)
9. PENG, G. D., CHU, P. L., XIONG, Z. J., WHITBREAD, T. W. and CHAPLIN, R. P., "Dye-doped step- index polymer optical fiber for broadband optical amplification," *J. Lightwave Technol.* 14, 2215 (1996).
10. XIONG, Z., PENG, G. D., WU, B., and CHU, P. L., "Highly tunable Bragg gratings in single-mode polymer optical fibres," *IEEE Photon. Technol. Lett.* 11, 352 (1999).
11. KALLI, K., DOBB, H. L., WEBB, D. J., CARROLL, K., KOMODROMOS, M., THEMISTOS, C., PENG, G. D., FANG, Q. and BOYD, I. W., "Electrically tunable Bragg gratings in single-mode polymer optical fiber," *Opt. Lett.* 32, 214 (2007).
12. KIM, K. J., BAR-COHEN, A. and HAN, B., "Thermo-optical modeling of an intrinsically heated polymer fiber Bragg grating," *Appl. Opt.* 46, 4357 (2007).

## **Chapter 2 Literature Review**

In this section, we review some of the applications from the versatile polymer optical fibres (POFs).

The ability to detect and measure physical parameters such as strain, stress, load, temperature, displacement and pressure makes POF suitable for structural health monitoring applications. In addition to being cheaper than their glass-counterpart, polymer fibres offer better fracture resistance and flexibility. They also offer ease of termination, safe disposability and ease of handling. Moreover, POFs have a much larger elastic limit and can withstand larger strains; this makes POF particularly attractive in large strain measurement. For examples, POFs have been used in the study of the setting dynamics of concrete and cement paste [1-2], in aircraft structural health monitoring [3], and in the anti-squeeze sensing to improve safety in the automotive industry [4]. Furthermore, POF sensors based on the Optical Time Domain Reflectometry (OTDR) technique have been demonstrated in woven textiles to monitor earthwork structures such as slopes, dikes and embankments, enabling the detection of movement of soil and locate its position [5].

A self-referencing intensity sensor based on bending losses of a partially polished POF coupler has been demonstrated [6]. It can be used for measuring liquid levels in harsh environments such as oil/petrol tanks or bio-mass boilers to be used in condominiums and buildings.

Another key application area of polymer fibres is sensing in biomedicine, due to its biocompatibility. For examples, single-mode POFs have been used to detect ultrasound in the biomedical industry [7], and the mechanical characteristics of bone cement have been studied using polymer fiber Bragg grating sensors [8]. Fibre Bragg grating in single-mode POF have been reported since 1999, and many studies have been carried out on the temperature and strain characteristics together with the associated applications mentioned above. However, there is little work done on the polymeric FBG-based biomedical applications. Over the past few years, the advancement of microstructured polymer optical fibre (mPOF) leads to many interesting bio-based applications. For example, it is possible to selectively or locally detect antibodies in mPOFs [9], because sensor layers of bio-molecules can be immobilized inside the air holes of the mPOF, and localized sensor layers may be activated on the inner side of the air holes in a predetermined section of the mPOF [10]. By doping the mPOF with fluorescence dye, an optical pH sensor is also possible [11]. Further study should be carried out on biomedical applications using POFs and mPOFs with FBGs written in them.

It is possible to use tapered graded-index POFs for the measurement of a large range of refractive indices with improvement over glass fibres [12]. Graded-index optical fibres with appropriate geometries were used as refractive-index sensors without removing the cladding.

A POF sensor for short pulse duration x-ray dosimetry has been reported based on luminescence generated in the cladding with core doped with radioluminescent phosphor [13].

The optical properties of the polymeric material have been exploited by using the evanescent-wave interaction, which arises at the core-cladding boundary of step-index waveguides. For example, polymer-clad fibre-optic can be used as an evanescent field absorbance sensor for organic solvents [14], and a special ion-exchangeable polymer blend can be used in the cladding for spectroscopic sensing [15]. Other hybrid fibres such as silica/polymer fibre, metal coated polymer fibre and hybrid fibre with FBGs offer additional sensor applications. The following are a few examples: a high sensitivity pressure sensor is developed by embedding FBGs in a polymer surrounding [16], and a compact optical fibre distance sensor that is capable of measuring arbitrary small distance is produced by fabricating a micro-sized polymer core at the end of a single mode fibre [17]. An electric field sensor has been demonstrated by depositing the core of a D-shaped fiber with electro-optic polymer [18], and a high sensitivity temperature sensor is reported by replacing the core of a D-shape fiber with DR1-azo-dye-doped PMMA [19]. Furthermore, miniature fibre-optic temperature sensors based on silica/polymer microfibre knot resonators with  $\text{MgF}_2$  substrate have been demonstrated [20]. A surface-enhanced Raman scattering sensor has been reported by etching POFs and coated with gold nanorods [21]. Chromophore-Containing Polymers together with waveguide micro-ring resonator and fiber Bragg grating have been used for trace

explosive sensors [22]. Finally, it has been shown theoretically that surface plasmon resonance-like integrated sensor at terahertz frequencies for gaseous analytes is possible with subwavelength porous polymer fiber [23].

## Reference

1. RAJESH, M., SHEEBA, M and NAMPOORI, V P N, "POF based smart sensor for studying the setting dynamics of cement paste," *J. Phys.: Conf. Ser.* 85, 012016 (2007).
2. DOS REISA, J. M. L., NUNESA, L. C. S., TRIQUES, A. L. C., VALENTE, L. C. G. and BRAGAA, A. M. B., "Mechanical characterization using optical fibre sensors of polyester polymer concrete made with recycled aggregates," *Materials Research* 12, 269 (2009).
3. GOMEZ, J., ZUBIA, J., ARANGUREN, G., ARRUE, J., POISEL, H. and SAEZ, I., "Comparing polymer optical fibre, fibre Bragg grating, and traditional strain gauge for aircraft structural health monitoring," *Appl. Opt.* 48, 1436 (2009).
4. LINEC, M. and DONLAGIC, D., "A plastic optical fibre microbend sensor used as a low-cost anti-squeeze detector," *IEEE Sensors Journal* 7, 1262 (2007).
5. LIEHR, S., LENKE, P., WENDT, M., KREBBER, K., GLÖTZL, R., SCHNEIDER-GLÖTZL, J., GABINO, L. and KRYWULT, L., "Distributed polymer optical fibre sensors in geotextiles for monitoring of earthwork structures," in *Proc. SHMII-4*, Zurich, Switzerland, 22-24 (2009).
6. MONTERO, D. S., VÁZQUEZ, C., MÖLLERS, I., ARRÚE, J. and JÄGER, D., "A self-referencing intensity based polymer optical fibre sensor for liquid detection," *Sensors* 9, 6446 (2009).

7. GALLEGO, D. and LAMELA, H., "High-sensitivity ultrasound interferometric single-mode polymer optical fiber sensors for biomedical applications," *Opt. Lett.* 34, 1807 (2009).
8. FRIAS, C., FRAZÃO, O., TAVARES, S., VIEIRA, A., MARQUES, A.T. and SIMÕES, J., "Mechanical characterization of bone cement using fiber Bragg grating sensors," *Materials and Design* 30, 1841 (2009).
9. JENSEN, J. B., HOIBY, P. E., EMILIYANOV, G., BANG, O., PEDERSEN, L. H. and BJARKLEV, A., "Selective detection of antibodies in microstructured polymer optical fibres," *Opt. Express* 13, 5883 (2005).
10. EMILIYANOV, G., JENSEN, J. B., BANG, O., HOIBY, P. E., PEDERSEN, L. H., KJÆR, E. M. and LINDVOLD, L., "Localized biosensing with Topas microstructured polymer optical fiber," *Opt. Lett.* 32, 460 (2007).
11. YANG, X. H. and WANG, L. L., "Fluorescence pH probe based on microstructured polymer optical fibre," *Opt. Express* 15, 16478 (2007).
12. ARRUE, J., JIMÉNEZ, F., G. Aldabaldetrekul, G. Durana, J. Zubia1, M. Lomer and J. Mateo, "Analysis of the use of tapered graded-index polymer optical fibres for refractive-index sensors," *Opt. Express* 16, 16616 (2008).
13. FITZPATRICK, C., O'DONOGHUE, C., SCHÖBEL, J., BASTIAENS, B., VAN DER SLOT, P., LEWIS, E. and PENDRILL, D., "A large core polymer optical fibre sensor for x-ray dosimetry based on luminescence occurring in the cladding," *Meas. Sci. Technol.* 15, 1586 (2004).



14. DEGRANDPRE, M. D. and BURGESS, L. W., "A fibre-optic FT-NIR evanescent field absorbance sensor," *Applied Spectroscopy* 44, 273 (1990).
15. GAO, L., SELISKAR, C. J. and MILSTEIN, L., "Spectroscopic sensing with a highly transparent, ion-exchangeable polymer blend," *Applied Spectroscopy* 51, 1745 (1997).
16. AHMAD, H., HARUN, S. W., CHONG, W. Y., ZULKIFLI, M. Z., THANT, M. M. M., YUSOF, Z. and POOPALAN, P., "High-sensitivity pressure sensor using a polymer-embedded FBG," *Microwave and Optical Technology Letters* 50, 60 (2008).
17. MAJUMDAR, A. and HUANG, H., "Compact optical fibre whitelight interferometric distance sensor for arbitrary small distance measurement," *Appl. Opt.* 48, 3702 (2009).
18. JOHNSON, E. K., KVAVLE, J. M., SELFRIDGE, R. H., SCHULTZ, S. M., FORBER, R., WANG, W. and ZANG, D. Y., "Electric field sensing with a hybrid polymerglass fiber," *Appl. Opt.* 46, 6953 (2007).
19. SMITH, K. H., IPSON, B. L., SELFRIDGE, R. H. and SCHULTZ, S. M., "Versatile in-fiber sensing by use of core-replaced D-fiber," *Appl. Opt.* 44, 22 (2005).
20. WU, Y., RAO, Y.-J., CHEN, Y.-H. and GONG, Y., "Miniature fibre-optic temperature sensors based on silica/polymer microfibre knot resonators," *Opt. Express* 17, 18142 (2009).

21. XIE, Z., TAO, J., LU, Y., LIN, K., YAN, WANG, J., P. and MING, H.,  
“Polymer optical fiber SERS sensor with gold nanorods,” *Opt. Commun.*  
282, 439 (2009).
22. CHEN, A., SUN, H., PYAYT, A., ZHANG, X., LUO, J., JEN, A.,  
SULLIVAN, P. A., ELANGO VAN, S., DALTON, L. R., DINU, R., JIN,  
D. and HUANG, Diyun, “Chromophore-Containing Polymers for Trace  
Explosive Sensors,” *J. Phys. Chem. C* 112, 8072 (2008).
23. HASSANI, A. and SKOROBOGATIY, M., “Surface Plasmon Resonance-  
like integrated sensor at terahertz frequencies for gaseous analytes,” *Opt.*  
*Express* 16, 20206 (2008).

## Chapter 3 Preform Fabrication

### 3.1 Introduction

In general, there are two main methods for fabricating POFs: the extrusion process and the preform drawing process [1].

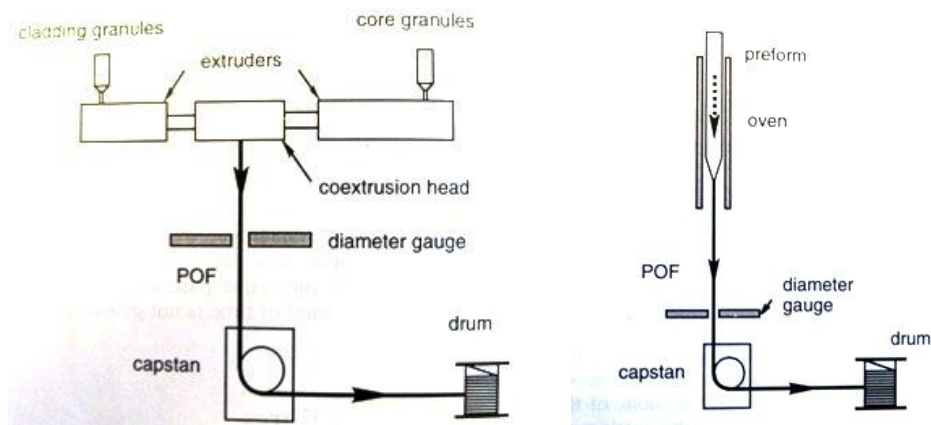


**Fig. 3-1. Schemetics of fibre drawing process: (left) extrusion and (right) preform drawing**  
(source: [2])

The left of Fig. 3.1 shows a schematic diagram of the extrusion process. The core and cladding materials are in the form of polymerized granules. They are fed into the extruders, and then melted and drawn from the co-extrusion head. The head contains two axial dies which determine the fibre core and overall diameter of the fibre. The extrusion method is suitable for a high-volume production process, as the core and cladding materials can be continuously fed into the system. Therefore commercial multimode POFs are often manufactured by this method.

In contrast, the right of Fig. 3-1 shows how POF is made from the preform drawing method. Initially a polymer rod, which is called “preform”, is fabricated with the similar geometrical dimension as the finished fibre. The preform is then heat-

drawn in a POF draw tower into the fibre, with the reduction of 10 to 50 times; while the fibre diameter is controlled by the relative speed of the preform feeder and the take-up unit. The preform drawing method is favorable for research purpose because it is more flexible for production of small quantity of POFs with different designs, and fabrication of different kinds of POFs by changing the physical and chemical properties of the preform. The preform drawing method also plays an important role in POF re-drawing process, making step-index singlemode or multimode POF, dye-doped POF and even microstructured POFs. One of the disadvantages of this method is that the total fibre drawn is limited by the volume of the preform. However it would not cause a big problem to our research purpose because unlike telecommunication, for our sensing applications, it required the fibre of meters long. Therefore the preform drawing method has been adopted for our application. The first main task for this research project was to build a reliable POF draw tower and fabricate POF preform with good optical quality.

In this Chapter, we firstly discuss how POF preforms were fabricated in our laboratory. In the next Chapter, we are going to show how a POF draw tower has been designed and built.

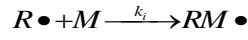
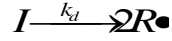
### 3.2 Principle of Polymerization

Our POF preforms are made from the polymerization of various monomers, added with initiator as well as chain transfer. The reason behind is that it provide us with freedom to alter the physical and chemical properties of the POF preforms for our specific purposes. These include the dimensions of the preforms, their molecular weight (MW), glass transition temperature ( $T_g$ ), refractive indexes, etc. In the following, firstly we are going to cover the principle of polymerization. Then we will talk about what basic materials to be used and the way to make our POF preforms.

The free radical polymerization involves four elementary reactions: chain initiation, chain propagation, chain termination, and chain transfer reaction. If the chain transfer reaction is ignored, the polymerization theory is expressed as follows:

### 3.2.1 Chain initiation

The initiator ( $I$ ) is decomposed into two primary radicals ( $R\bullet$ ), and then a primary radical combine with a monomer ( $M$ ) to compose a monomer radical ( $RM\bullet$ ). The reactions are as follows [6]:

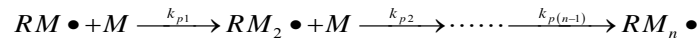


$$R_i = \frac{d[R\bullet]}{dt} = 2k_d[I] \quad \text{Equation 3-1}$$

where  $R_i$  is the decomposed rate of initiator,  $k_d$  is the decomposed rate coefficient of initiator,  $[I]$  is the concentration of the initiator.

### 3.2.2 Chain Propagation

The monomer radicals with an unpaired electron are easy to be composed into the macromolecule free radicals with individual monomers as follows [6]:



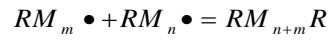
and  $k_{p1} = k_{p2} = \dots = k_{p(n-1)} = k_p$ , the total rate of polymerization is

$$R_p = -d[M]/dt = 2k_p[M][M\bullet] \quad \text{Equation 3-2}$$

where  $k_p$  is the polymerized rate coefficient of monomers,  $[M]$  is the concentration of the monomers.

### 3.2.3 Chain Termination

Two macromolecule free radicals are composed the larger macromolecule and the polymerization reaction is terminated.



Chain termination need two macromolecule free radicals, so the termination rate of polymer chain is

$$R_t = -d[RM_n \bullet] / dt = 2k_t [RM_n \bullet]^2 \quad \text{Equation 3-3}$$

where,  $k_t$  the termination rate coefficient of chain,  $[RM_n \bullet]$  is the concentration of the macromolecule free radicals.

If the initiated efficiency of initiator is ignored, from Equation 3-1, Equation 3-2 and Equation 3-3, the total polymerized rate of monomers can be achieved.

$$R_p = k_p (k_d / k_t)^{1/2} [M][I]^{1/2} = k[M][I]^{1/2} \quad \text{Equation 3-4}$$

With the viscosity of the solution increases, the diffusion movement of the macromolecule free radicals becomes slower because of the gel effect. The macromolecule free radicals are hard to encounter, and  $k_t$  decreases, but the small monomer molecules are hardly affected, and  $k_p$  is invariant. Thus  $k_p / \sqrt{k_t}$  increases, we can see that  $R_p$  increases from Equation 3-4.

### 3.3 Materials

Poly (Methyl methacrylate) (PMMA) plays a very important role among polymer optical materials. A great majority of POF products are based on PMMA [3]. Other types of polymers are also available, which include polycarbonate (PC). PC has relatively high refractive index of 1.59, thus the NA is higher. However, it has a poor stability in regard to humid heat. Other candidate can be polystyrene (PS). However, besides of higher refractive index of 1.58, PS does not shows any practical significance comparing with PMMA. Consequently our POFs are mainly based on PMMA. Other monomers can be co-polymerized with MMA to modify the properties of the resultant polymer preform. For instance, the overall  $T_g$  of preform can be decreased by adding suitable amount of Butyl methacrylate (BMA), which has a lower  $T_g$  of 54 °C comparing with MMA of 114°C [4]. With lower  $T_g$ , the flow property is improved, such that the preform can be drawn easily at lower temperature. Besides that, Benzyl methacrylate (BzMA) has a higher refractive index of 1.5680 comparing with PMMA of 1.490 [4] so that it can be used to increase the overall refractive index of the polymer by following the calculation described in [5]. Then the polymer can be used as the core material.



**Table 3-1. Summary of materials used to fabricate POF preforms and their usage.**

Chemical name (Abbreviation)	Chemical structure	Purity	Role	Function
Methyl methacrylate (MMA)	$H_2C=C(CH_3)CO_2CH_3$	99%	monomer	Preform main body
Butyl methacrylate (BMA)	$H_2C=C(CH_3)CO_2(CH_2)_3CH_3$	99%	monomer	Improve drawability
Benzyl methacrylate (BzMA)	$H_2C=C(CH_3)CO_2CH_2C_6H_5$	96%	monomer	Increase refractive index
Lauroyl peroxide (LP)	$[CH_3(CH_2)_{10}CO]_2O_2$	97%	initiator	Adjust initial rate of polymerization
1-Decanethiol (DT)	$C_{10}H_{22}S$	99+ %	Chain transfer	Adjust molecular weight of polymer
<i>Trans</i> -4-Stilbenemethanol (TS)	$C_6H_5CH=CHC_6H_4CH_2OH$		Photo isomer	UV-photosensitive material

Table 3-1 shows a list of chemicals (purchased from Aldrich) to fabricate POF preforms and their usage. The PMMA based preforms are made by thermal bulk polymerization of various monomers. Monomers are often added with MEHQ to prevent them from polymerization during storage. Therefore they have to be filtered by a column of inhibitor remover (Sigma-Aldrich) before using them in the preform fabrication process.

Small amount of initiator is added to trigger initiation of the polymer chain and accelerating the polymerization rate at the beginning stage [65]. Azo compounds, organometallic reagents, Lewis acids and peroxides are typically used as the initiators. In our case, Lauroyl peroxide (LP) was used.

1-decanethiol (DT) is used as the chain transfer which is employed as a regulator of molecular weight of polymer [7]. DT is important in determining how easily the preform can be processed into fibres. In the past, there was an alternative which was called 1-butanethiol. However, due to its extremely foul smelling odor, it was later replaced by 1-decanethiol, which smell was moderate and did not affect the polymerization efficiency.

In the case of writing FBGs on POF, a photosensitive chemical, namely trans-4-stilbenemethanol (TS), is added to the core of the POF preforms. The material has been proved to be photosensitive at the UV wavelength of 325 nm [8] and so it is possible to write FBGs in TS-doped POFs.

### **3.3.1 Optimum Preform Composition**

The optimum composition of our POF preform was obtained after a large number of trials and experiments had been conducted. There were two important observations to ensure the quality of the preforms. First is to observe the appearance of the preform after curing in the oven. A good preform would show its clear and transparent appearance and not contain bubbles throughout its structure. Second is to examine its drawing condition to see if it would deform or evolve bubbles during the fiber drawing process.



**Fig. 3-2. Photo of (left) preform with MMA:BMA ratio of 90:10 and (right) preform with MMA:BMA ratio of 75:25.**

Fig. 3-2 shows two preforms with different MMA:BMA composition. Both preforms were drawn at tension of around 20cN. For the left one, the molar ratio of MMA:BMA was 90:10. It needed to be drawn at around 265°C. It could be observed that depolymerization took place and bubbles were formed. For the right one, it only needed to be drawn at around 235°C, because more BMA was added that effectively lowered the overall glass temperature of the preform. Then the preform could be drawn perfectly. In this thesis, the composition of MMA:BMA with a molar ratio of 75:25 was usually used to make the preforms.

Different concentrations of LP, such as 0.02, 0.05 and 0.1mol.%, have also been tried. It was found that if the concentration was too low, the polymerization would start too slowly. The preform would not fully polymerized even after leaving in the oven for few days. Therefore the amount of LP was increased each time. Finally we got 0.1% as the optimum concentration of LP such that the pre-polymerization

stage would be controlled within 20min (which will be discussed in the following section).

The effect of different concentrations of chain transfer on the molecular weight (MW) of polymer performs was investigated and reported in [9]. It was found that PMMA preforms with MW of around  $9 \times 10^4$  can be drawn into fibre easily, in which the corresponding concentration of chain transfer was 0.25mol%. Therefore we made it as the reference for the concentration of DT and proved experimentally that it was feasible to draw the POFs.

**Table 3-2 Summary of preform composition for cladding and photosensitive core system**

	Copolymer (mol%)			Initiator (mol%)	Chain Transfer (mol%)	Photo isomer (wt%)
Chemical Name	MMA	BMA	BzMA	LP	DT	TS
Cladding	75	25	-	0.1	0.25	-
Photosensitive Core	75	19	6	0.1	0.25	0.1-0.5

Table 3-2 indicates a summary of typical preform composition of the cladding and photosensitive core system respectively. In the core, a certain amount of BMA is replaced by BzMA, to raise its refractive index. Moreover the phenyl group in BzMA structure enhances UV absorption [10] which makes the core material more efficient for writing gratings with 325nm laser.

### 3.4 Fabrication Process

Generally the process of fabricating POF preform involves mixing the desirable composition of monomers and putting them into moulds for curing inside an oven. As mentioned before, the monomers have to pass through columns of inhibitor remover to get rid of the MEHQ. The process has to be done just before mixing the monomers at the beginning of the preform fabrication process. Otherwise, the monomers will undergo polymerization at room temperature. As a result, the partly polymerized monomers affect their mixing properties and induce adverse effects to the quality of the final polymer preforms.

The preform moulds is usually made of commercially available glass test tubes. Thus, the dimension of the perform is limited by the inside diameter and the length of test tubes. Therefore we choose to make our own preform moulds by cutting long hollow glass tubes into short pieces and sealing them at one end using oxyhydrogen fire. Fig. 3-3 shows photo of glass moulds with 8mm in inner diameter and 200mm in length.



**Fig. 3-3. Photo of a bunch of glass moulds cleaned by ultrasonic cleaner.**

### 3.4.1 Importance of Pre-polymerization

The mixture of filtered monomers, initiator and chain transfer must undergo pre-polymerization before curing in the oven. According to the principle of polymerization [6], the viscosity of the monomer solution increases with conversion rate, and results in gel effect, which decreases the diffusion movement of macromolecule free radicals, but the monomer molecules are hardly affected.  $k_t$  is reduced and  $k_p$  keeps constant. From Equation 3-4, we can achieve the total polymerized rate ( $R_p$ ) of monomers rapidly with the increase of  $k_p / \sqrt{k_t}$ , however, the polymerization reaction induce temperature rise. According to Arrhenius Equation:

$$k = A \exp\left(-\frac{E}{RT}\right) \quad \text{Equation 3-5}$$

where,  $A = A_p (A_d / A_t)^{1/2}$ ,  $R$  is molar gas constant,  $E = E_p + E_d / 2 - E_t / 2$  ( $E_p$  is polymerization energy,  $E_d$  is the decomposed energy of initiator,  $E_t$  is terminal energy of chain). Fig. 3-4 shows the relationship between polymerization rate ( $k$ ) of MMA and temperature, using LPO as the initiator.

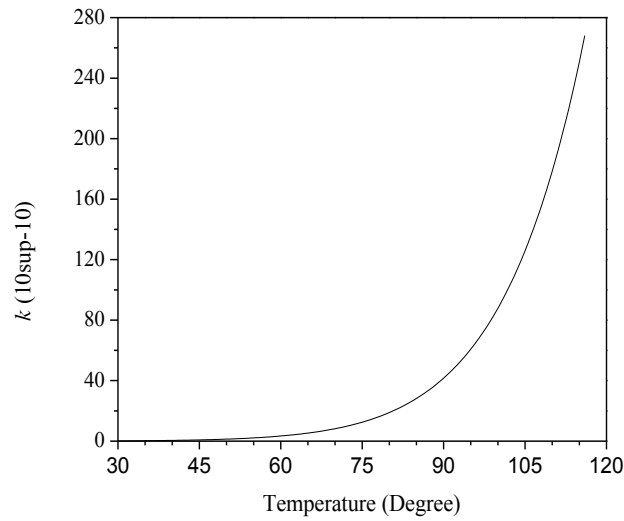


**Fig. 3-4. Relation between polymerization rate ( $k$ ) of MMA and temperature.**

From Fig. 3-4, the polymerization rate ( $k$ ) of MMA increases rapidly with temperature. The polymerization rate ( $k$ ) of MMA increases by around 2.5 times when the temperature changes from 60°C to 70°C, and the polymerization reactant almost stops when the temperature is below 60°C. Both the gel effect and high temperature increase the polymerization rate ( $k$ ) further, eventually bubbles appear in the POF preforms because the monomers are vaporized under the high temperature in a small area (see Fig. 3-5).

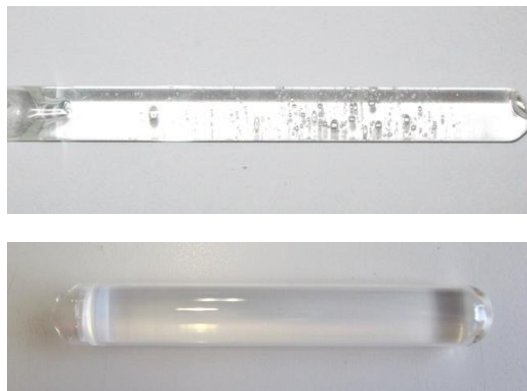


**Fig. 3-5. (upper) Photo of preform without going pre-polymerization; (lower) that with pre-polymerization**

In order to avoid occurring explosive polymerization, we accelerate the diffusion movement of the macromolecule free radicals by external force and prevent localized temperature to rise. These are the essential steps during the pre-polymerization process.

In the pre-polymerization process, firstly the filtered monomers are poured into a conical flask. Then suitable amount of initiator and chain transfer are added. In order to prevent the thermal volatilization of the solution, the conical flask is sealed with aluminum foil. The conical flask with solution is heated in a water bath and stirred on a hot-stirring plate as shown in Fig. 3-6.



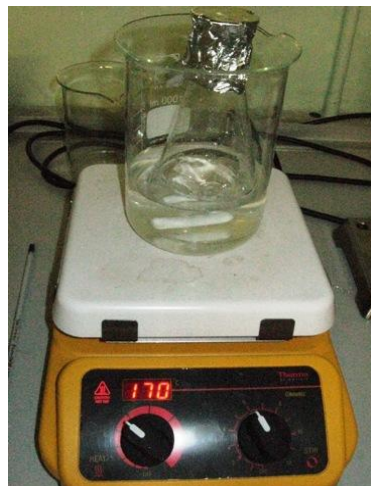


**Fig.3-6. Photo of polymer undergoing pre-polymerization on hot-stirring plate.**

The temperature is maintained at around 75°C. The solution mixture is heated until it has a syrup-like consistency. Many bubbles and heat would be released throughout the pre-polymerization process. Typically the pre-polymerization process takes about 20 to 25 minutes to complete for mixtures with LP concentration of 0.25mol%. After that the solution will be transferred into glass tubes for further polymerization inside the oven.

### **3.4.2 Curing in Oven**

The prepolymerized reactants are poured into POF preform moulds and put into the oven for further polymerization.



**Fig. 3-7. Photo of (left) glass test filled with monomers mixture and (right) computer controlled oven.**

The temperature of the oven is computer controlled to give a pre-programmed temperature profile. Fig. shows the relationship between actual and preset temperature against time.

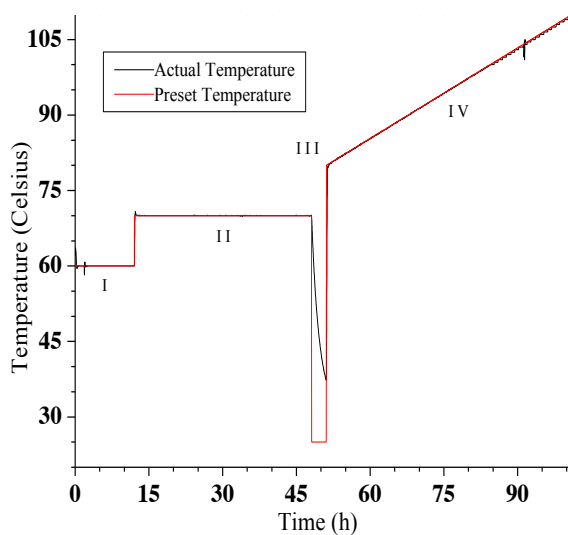


**Fig. 3-8. Actual and preset temperature for polymerization of MMA monomers.**

Because the viscosity of pre-polymerized reactant is high, it is very easy for the gel effect to occur, in which the polymerization occurs from the inner wall of the tube [11]. Therefore at Stage I, polymerization has to start at a low temperature of 60°C for preventing explosive polymerization. Stage II offers sufficient time for reactants to reach conversion equilibrium that monomers are converted to polymer. Such conversion equilibrium for PMMA can be calculated using the following equation [6]:

$$\text{Conversion (\%)} = 0.225T(^{\circ}\text{C}) + 78.25 \quad \text{Equation 3-6}$$

It implies that at the end of Stage II, for T=70°C, conversion = 94%. This means that only 6% of monomer residue is left in the mixture. Then the temperature decreased to room temperature to let the polymer contract from the interface with the moulds. Otherwise, it is hard to remove the polymer preforms from the moulds after polymerization. Then during Stage IV, the temperature is elevated from 80 to 110°C gradually for the fully polymerization of the polymer preform. At the end, the moulds are taken out from the oven and cooled slowly at room temperature. Then the glass tubes is broken carefully and the POF preforms are obtained.

### 3.5 Procedure of Fabricating Step-index Preforms

In this section, we will discuss the procedure to make a step-index POF preform. The “Teflon Technique” described in [12] is adopted to fabricate such kind of preforms. There are other techniques available to make POF preforms, such as centrifugal deposition method [13], inter-facial gel method [14] and drilling holes

[15]. However, for the first two techniques, they are mainly used for fabricating graded-index POF. We have tried out the drilling method but the result was not satisfactory that leaving the drilled surface too rough. Finally, “Teflon Technique” is adopted which has advantages in giving smooth interface, easy to setup, and flexibility in making preforms of different diameters. The technique is illustrated in Fig. 3-9.

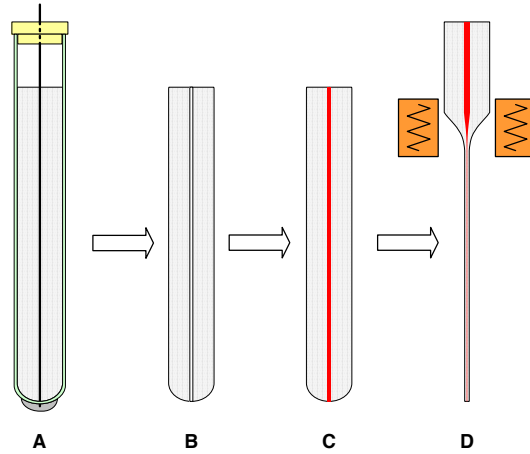


**Fig. 3-9. Schematics of preform fabrication process.**

As illustrated in Fig. 3-9 (A), a Teflon string/rod was fixed along the central axis of a glass tube by epoxy adhesive and filled with the cladding monomers. The cladding monomers were fully polymerized in an oven with specific temperature profile, mentioned in our previous section. After that, both string/rod and glass tube were removed, leaving with a centered hole as shown in Fig. 3-9 (B). Then the core monomers, which can be mixed with photosensitive material TS or organic laser dyes (will be discussed in Chapter 6) were injected into the hole and went through

the polymerization process again in Stage C. Finally at Stage D the POF preform was heat-drawn into fibre on our home-built POF draw tower.

By using this technique, as the Teflon is elastic, it can be pulled out easily from the preform at Stage B. Besides that, the central hole at stage B would have a smooth surface. Different dimensions of the preform can be easily obtained by using different sizes of Teflon string/rod and glass tubes. From our experience, the size for Teflon string/rod can vary from 0.8mm to 5mm; while the inner diameter of the glass tubes ranges from 6 to 22.2mm, which are sufficient to cover almost all dimensions of POFs for our study.

### **3.6 Conclusion**

In this chapter, we described the fabrication of POF preforms in our laboratory. A brief polymerization theory has been explained, which guided us how the polymerization process should be done and revealed the importance of pre-polymerization. The chemicals for fabricating POF preforms was listed, in which PMMA was the main component used in making the preforms. Each of the chemicals had their own role and function. For their quantity usage and preform composition, a series of trials and experiments had been done to obtain the optimum values. Details of preform polymerization process were also discussed. In case of making step-index POF preform, the procedure of Teflon Technique was shown and explained why it was superior to other methods, such as drilling and inter-facial gel method, in our applications.

## Reference

1. KUZYSK, M. G., "Polymer Fibre Optics – Materials, Physics and Applications," CRC Press (2007)
2. MARCOU, J., "Plastic Optical Fibres – Practical Applications," John Wiley & Sons (1997)
3. DAUM, W., KRAUSER, J., ZAMZOW, P. E., and ZIEMANN, O., "POF- Polymer Optical Fibres for Data Communication", ISBN: 3-540-42009-6, Springer-Verlag Berlin Heidelberg, Germany (2002)
4. BRANDRUP, J., IMMERGUT, E. H. and GRULKE, E. A., "Polymer handbook," ISBN: 0471166286, a Wiley-Interscience publication, 4th edition (1999)
5. ASKADSKII, A. A., *Physical properties of polymers prediction and control*, ISBN: 2- 88449-155-4, Gordon and Breach Publishers, The Netherlands (1996)
6. Robert O. Ebewele, "Polymer Science and Technology", CRC Press, ISBN: 978-0-8493-8939-9 (2000)
7. Seymour, Carraher, "Polymer Chemistry," 7<sup>th</sup> Edition, ISBN: 1-4200-5102-4, CRC Press (2008)
8. YU, J. M., TAO, X. M., TAM, H. Y., "Trans-4-stilbenemethanol-doped photosensitive polymer fibres and grating," *Opt. Lett.* 29, 156 (2004)
9. YU, J. M., TAO, X. M., TAM, H. Y., "Fabrication of UV sensitive single-mode polymeric optical fibre," *Optical Materials* 28, 181 (2006)

10. SUGITA, K., ISHIDA, T., KUSHIDA, M., “Photodegradation mechanism of phenylisopropenyl ketone – methyl methacrylate copolymers in the solid phase and their performance as a deep UV resist,” *Canadian J. of Chemistry-Revue Canadienne de Chimie* 73, 1841 (1995)
11. KOIKE, Y., NIHEI, E., TANIO, N., OHTSUKA, Y., “Graded-index plastic optical fiber composed of methyl methacrylate and vinyl phenylacetate copolymers”, *Appl. Opt.* 19, 2686 (1990)
12. PENG, G. D., CHU, P. L., XIONG, Z. J., WHITBREAD, T. W., and CHAPLIN, R. P., “Dye-Doped Step-Index Polymer Optical Fibre for Broadband Optical Amplification”, *J. of Lightwave Technol.* 14, 2215 (1996)
13. SHIN, B. G., PARK, J. H., and KIM, J. J., “Low-loss, high-bandwidth graded-index plastic optical fibre fabricated by the centrifugal deposition method,” *Appl. Physics Lett.* 82, 4645 (2003)
14. RUCKENSTEIN, E., “On the gel effect in the presence of a chain transfer agent in methyl methacrylate polymerization and its copolymerization with various acrylates,” *J. Appl. Polymer Sci.* 49, 2179 (1993)
15. BARTON, G., VAN EIJKELNBORG, M. A. and HENRY, G., “Fabrication of microstructured polymer optical fibres,” *Opt. Fibre Technol.* 10 (2004)

## **Chapter 4 Fibre Draw Tower**

### **4.1 Introduction**

In Chapter 3, we have discussed how to make good polymer performs, that are free of voids or bubbles due to incomplete polymerization, for drawing into polymer optical fibres. Obviously, to make good quality polymer optical fibres, we need a reliable fibre drawing tower. In this Chapter, we are going to describe a POF draw tower that has been designed and built by the PhD candidate for drawing different types of POFs. The major components of the tower, such as feeding unit, furnace, take-up unit and control unit will be introduced and explained. The specification and the performance of the tower will be discussed. There are several reasons to build our own fibre draw tower. Firstly, there are only a few POF draw tower manufacturers, and their draw towers are extremely expensive. Secondly, we can design and build the draw tower to satisfy our precise needs. Thirdly, we can modify the draw tower easily to fine tune the drawing conditions for different types of POFs.

### **4.2 Major Components**

The in-house POF draw tower is situated at our Specialty Optical Fibre Fabrication Laboratory. The tower mainly consists of the feeding unit, two exchangeable furnaces, the take-up unit and the control unit as shown in Fig. 4-1. The tower is integrated with suitable commercially available apparatus and necessary metal parts which are specifically designed and CNC machined. Temperature sensors for monitoring the furnaces are also integrated to the furnaces. The control system and



graphical user interface are designed by the PhD candidate. The furnaces are enclosed inside an aluminium frame, about 3-m tall, covered with acrylic panels and equipped with a fume extractor that offers HEPA filtration, capable of capturing 99.97% of particles down to 0.3  $\mu\text{m}$ .

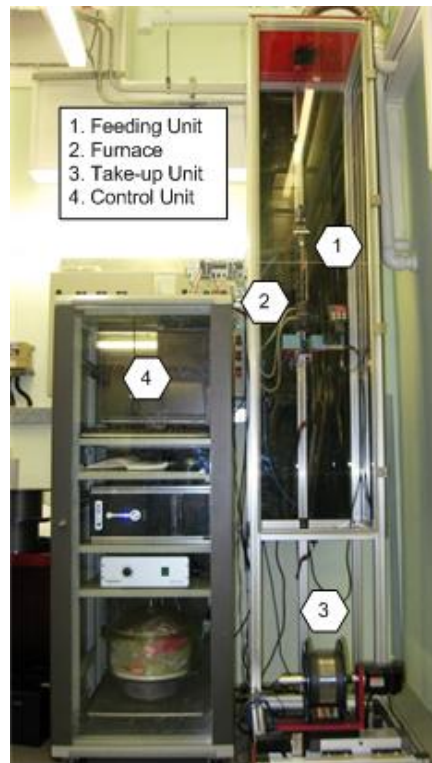


**Fig.4-1. Photo of home-built POF draw tower at the Photonics Research Centre of PolyU.**

#### **4.2.1 Main Structure Design**

The main frame holds the structure of the tower. It is built up of aluminium alloy profiles which are light in weight and resistant to weathering and many chemicals. The basic elements of the frame are Aluminum Alloy Profiles and Universal Fasten Sets (©item, Germany); Fig. 4-2 shows how they are connected firmly together.

They also provide the flexibility to change the whole structure of the tower conveniently.

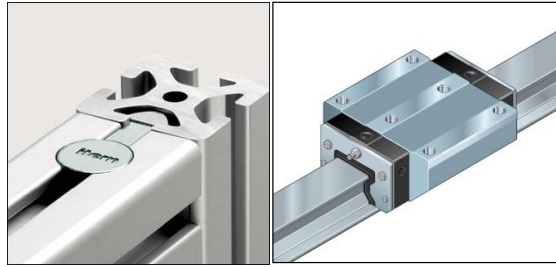


**Fig.4-2. Photo of (left) two Aluminum Alloy Profiles connected with Universal Fasten Sets (©item Germany); (right) roller rail system (©Rexroth, Germany).**

The overall height of the tower is 3 meters. It has to be tall enough to allow the fibre drawn from the furnace sufficient time to cool down before being collected in the optical fibre spool. Otherwise the fibre will deform as it remains in the molten state.

A roller rail system (©Rexroth, Germany), shown on right of Fig. 4-2, with two runner/carrier blocks used to anchor the feeding unit and the furnace. The system is especially designed for machine tool requiring compact linear motion guideway with high load capacity and high rigidity, to provide easy movement of the feeding unit and the furnace for operation and investigation.

#### **4.2.2 Preform Feeding Unit**

There three main components in the preform feeding unit: translation stage (LSR300A, Zaber), drill chuck and preform adaptor are shown in Fig. 4-3.



**Fig. 4-3. Photo of preform feeding unit.**

The translation stage can be controlled by computer and it has a travel range of 300 mm and speed resolution of 0.93 $\mu$ m/s. Different sizes of POF perform can be held by the specially designed preform adaptor with any size (see Fig. 4-4) from 6 mm to 22 mm in diameter.



**Fig.4-4. Photo of preform adaptors with different sizes, integrated with gas fittings.**

The preform adaptor is sealed at one end and connected with a pneumatic pipe fitting. A vacuum controller, as shown in Fig. 4-5, is linked to the preform adaptor so as to control the pressure inside the preform, especially for fabrication of microstructured polymer optical fibres. The pressure can be varied from 0 to -80kPa for various drawing requirement.



**Fig. 4-5. Photo of the vacuum controller.**

### **4.2.3 Preform Heating Unit**

We have designed two types of furnaces for the fibre draw tower. At the early stage, the furnace was built by electric band heater; and later on infra-red (IR) heater was used. Details of the two furnaces are described in the following sections.

#### **4.2.3.1 Electric Heater Furnace**

The preform heating unit is where the POF perform is heated and neck-down. For the electric heater furnace, it is composed of upper and lower heating zones, which are the pre-heating zone and heat-melt zone respectively [1]. As shown in Fig. 4-6, the two band heaters (Mi-Plus<sup>®</sup>, Tempco) are used as the heating elements, which are individually controlled and their temperature can be increased up to 700°C. The

pre-heating zone heats the POF perform first, and then the temperature of the heat-melt zone can be lower, so that the preform will not easily form bubbles during the drawing process.

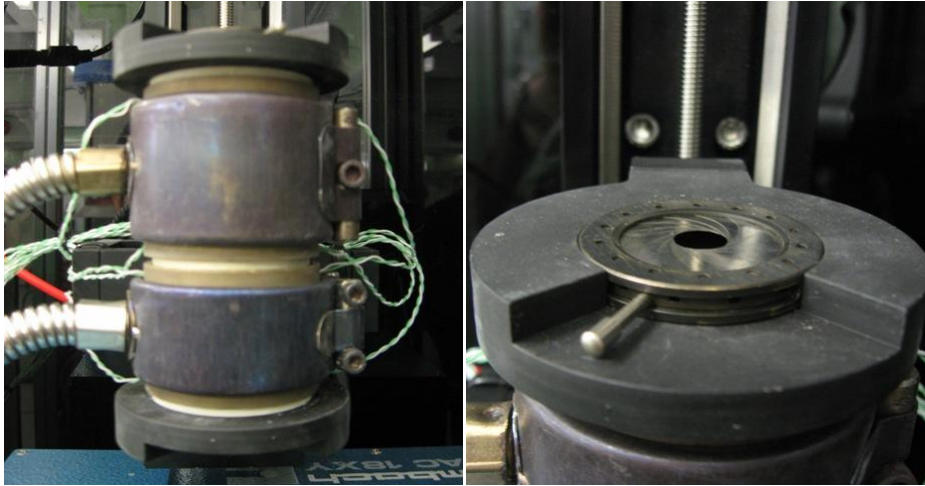


**Fig.4-6. Photo of (left) side view and (right) top view of electric heater.**

The heaters heat the inside copper cylindrical dies with inner diameter of 25mm to achieve even distribution of heat. 4 pairs of thermocouples are evenly located in each copper die to monitor the temperature. Insulating layers, made of calcium silicate plane (750 Insulation Board, Duratec), are inserted in between to minimize heat flowing between the two heat zones. Iris diaphragms (ID25, Thorlabs) are added on both end of the furnace to minimize the heat loss and temperature fluctuation due to convection of air. The drawing temperature can be lowered by 20°C with the present of the iris diaphragms.

#### **4.2.3.2 IR Emitter Furnace**

There are some limitations for our electric heater furnace. It restricts the diameter of the preform up to 22mm. Moreover, as the preform is heated by conduction, it leads to uneven heat distribution within the preform. Sometimes, the outer part of the preform has already decomposed and formed bubbles, but the inner part of it is not hot enough to be drawn. To solve these problems, we designed another type of furnace, which was built by IR emitter as shown in Fig. 4-7.



**Fig. 4-7 (a) Photo of the infrared emitter**

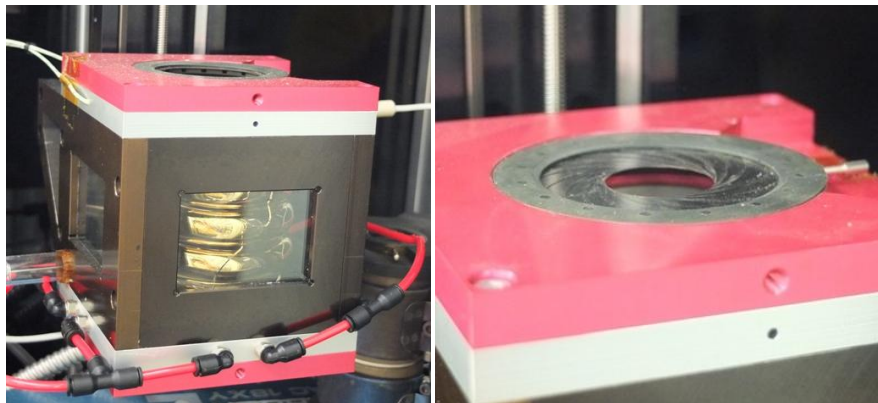
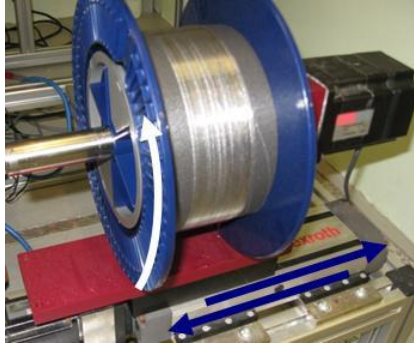


**Fig. 4-7 (b). Photo of (left) side view and (right) top view of IR heater furnace.**

The main component of the furnace is the IR emitter (Spiralform, Heraeus). The IR emitter is specially made and bent into a spiral shape. The rated power of the IR emitter is 2000W with inside diameter of 50-mm and height of 10-cm. The outer surface is coated with thin layer of gold to increase IR radiation back to the inner part. A larger furnace using the IR emitter was designed and built by the student to draw preforms of larger diameter. A pure silica tube with inner diameter of 45mm is placed inside the IR emitter to protect the IR emitter. The furnace can draw preforms with diameter up to 40mm. Iris diaphragms (ID25, Thorlabs) are also added on both end of the furnace to minimize the effect of convection. The gas inlets are built around the bottom part of the furnace. Pure nitrogen can be feed into the furnace to purge the IR emitter during the drawing process to ensure that the perform is drawn in a clean environment.

Generally the IR emitter furnace is better than the electric one. Firstly, the spiral shape of the IR emitter radiates the heat evenly; while the opening part of the electric heater causes some temperature difference to the furnace. Secondly, the IR emitter furnace heats preforms through IR radiation of heat transfer, the heat transfer to the inner part of the preform is faster, thus permitting preforms to be drawn at a lower temperature. Thirdly, the start-up time and the power control of the IR emitter are better than that of the electric heater, so that the IR emitter furnace can control the drawing temperature more preciously.

#### **4.2.4 Fibre Take-up Unit**



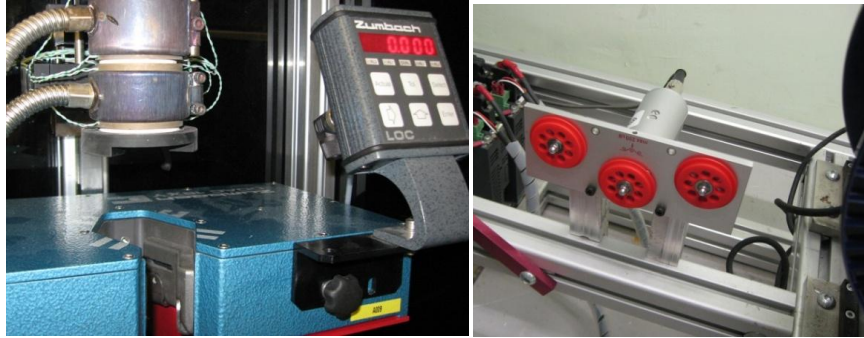
**Fig. 4-8. Photo of the fibre take-up unit.**

Fig. 4-8 shows the fibre take-up unit, a fibre spool is used to collect the fibre, which is driven by a servomotor (BL Super P5, Sanyo Denki). The whole setup stands on a ball-screw translation stage (CKK 12-90, Bosch), also driven by a servomotor (BL Super P3, Sanyo Denki), to allow linear movement of the spool so that the fibre is being wrapped neatly and smoothly onto the spool with minimum fibre crossover. Both servomotors are associated with their controller (Sanmotion R, Sanyo Denki) and then connected to the computer. The resolution of the motor is 8000 steps/rev.



#### 4.2.5 Monitoring Devices

Two monitoring devices were added to the POF draw tower, namely diameter gauge and tension meter, to read the diameter of the drawn polymer optical fibres and fibre tension.



**Fig. 4-9. Photo of (left) diameter gauge and (right) tension meter.**

The diameter gauge (Zumbach) is shown in the left photo of Fig. 4-9. It is located near the exit of the furnace for better feedback and control [2]. It gives the diameter information of the processing fibre with accuracy up to  $1\mu\text{m}$ .

The right photo of Fig 4-9, shows the tension meter (TSL-200-T-A2, Schmidt). The tension meter gives the value of tension in the drawing fibre up to 200cN. The tension value gives important information for judging the suitable drawing temperature in the furnace. Generally, the fibre tension increases when the furnace temperature decreases and vice versa.

#### 4.2.6 Control Unit

The schematic control diagram of the POF tower is shown in Fig. 4-10.

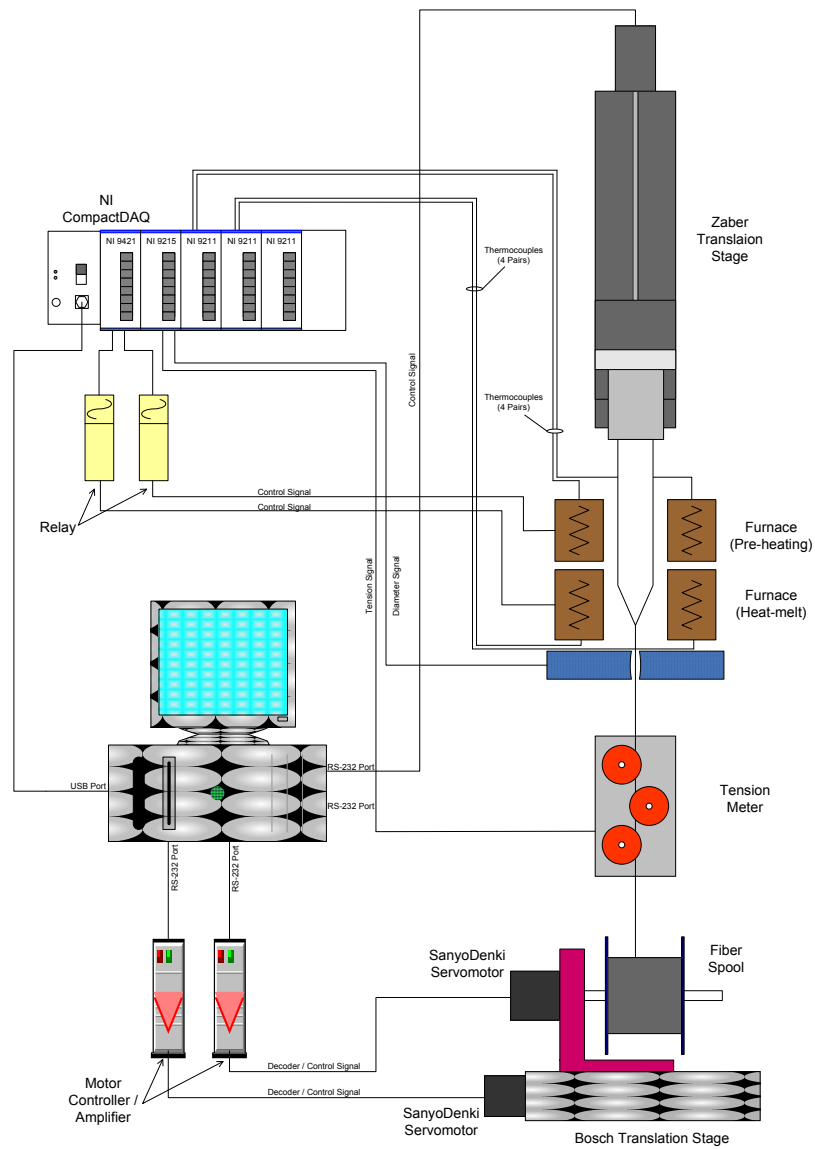


**Fig. 4-10. Schematic control diagram of POF tower.**

The main components of the POF tower control unit are the data acquisition unit (NI cDAQ-9172 from National Instrument) and the PC. The data acquisition unit acquires the signals from the furnace, diameter gauge and tension meter through the USB port to the PC. The control program is written in LabView™ (National Instrument) in the PC, which integrates and analyzes all the relevant signals and then generates suitable commands to the furnace through the data acquisition unit; and to the feeding unit and take-up unit directly through the RS-232 ports.

### **4.3 Overall Performance and Specification**

Generally the POF draw tower is capable of drawing preforms with diameters of 6mm to 22mm. The diameter of the fibres produced ranges from 50µm to 4000µm. The accuracy in the diameter is within 3% after the operation of the tower has become stable. Normally the tower reaches the stable stage after 10-20m of fibre drawn. The specifications of the home-built POF draw tower and its various components is summarized in Table 4-1.

**Table 4-1. Specification of POF Draw Tower.**

<b>General Specification</b>	<b><i>Electric Heater Furnace</i></b>	<b><i>IR Emitter Furnace</i></b>
Preform Size	6mm up to 22mm in O.D.	6mm up to 40mm in O.D.
Max. Length of Preform Drawn	300mm	
Fibre Drawn Size	100µm up to 4000µm in O.D.	
Accuracy	±3%	
Draw Ratio	5.575 to 272 in O.D.	
<b>Feeding Unit</b>		
Travel Range	300mm	
Accuracy	±3%	
Max. Speed	4mm/s	
Min. Speed	0.93µm/s	
Max. Cantilever Load	200 N-cm	
<b>Heating Unit</b>		
<b><i>-Pre-heating</i></b>		
Power	350W	-
Effective Heating Length	26mm	-
Max. Temperature	760°C	-
Accuracy	<±2%	-
<b><i>-Heat-melting</i></b>		
Power	400W	2000W
Effective Heating Length	37mm	100mm
Max. Temperature	760°C	Depends on material absorption
Accuracy	<±2%	<±1%
<b>Take-up Unit</b>		
<b><i>-Motor (for Fibre Spool)</i></b>		
Rated Torque	0.637N.m	
Decoder Resolution	8000steps/rev	
Max. Velocity	600rpm	
<b><i>-Bosch Translation Stage</i></b>		
Travel Range	150mm	
Max. Velocity	55cm/s	
<b>Measuring Devices</b>		
<b><i>-Diameter Gauge</i></b>		
Diameter Range	80µm to 18mm	
Accuracy	±0.05µm	
<b><i>-Tension Meter</i></b>		
Tension Range	0-200cN	
Accuracy	±1% on full scale	

#### 4.4 Optimum Drawing Condition

We regard the optimum drawing condition as the condition that the fibre can be continuously drawn from its preform without bubbles formed inside and deformation of its structure. There are generally three drawing parameters to be optimized for drawing POFs. They are: (1) the feed speed of the preform, (2) the take-up speed of the fibre spool, and (3) the furnace temperature. In case of drawing special fibres such as mPOF or fibre with holey structure, vacuum and pressure inside the preform are also needed to be adjusted. Moreover, to draw POF with different sizes, different sets of parameters have to be adopted in order to achieve the optimum drawing condition. It is a very time consuming process. Many experimental trials were carried out with different drawing parameters until the optimum drawing condition was reached.

In order to draw POFs with specific diameter, the ratio of the feeding speed to take-up speeds needs to be controlled, which can be calculated from mass conservation [3]:

$$\frac{V_{take}}{V_{feed}} = \sqrt{\frac{D_p}{D_f}} \quad \text{Equation 4-1}$$

where  $V_{take}$  is the linear speed on the fibre spool,  $V_{feed}$  is the feed speed of the preform,  $D_p$  is the diameter of the preform and  $D_f$  is the diameter of the fibre.

The actual feed and take-up speed depends on the preform size, the furnace temperature as well as under what tension the fibre to be drawn. Usually the feed speed is kept constant throughout the drawing process while the take-up speed is finely tuned to obtain the desired fibre diameter.

The correct value of the feed speed is to ensure the preform getting sufficient heat energy to melt and to be drawn into fibre under certain furnace temperature. In most of our experiments, only the upper heating zone of the furnace was used; and the temperature was set to between 200 and 280°C. If the furnace temperature is too low, fibre perform drop will not occur. Besides, during drawing process, the fibre will break if the furnace temperature is not high enough. Conversely, if the furnace temperature is too high, the preform will undergo depolymerization process, monomers will be formed which are volatile and bubbles are formed immediately inside the preform as shown in the left preform of Fig. 4-11.



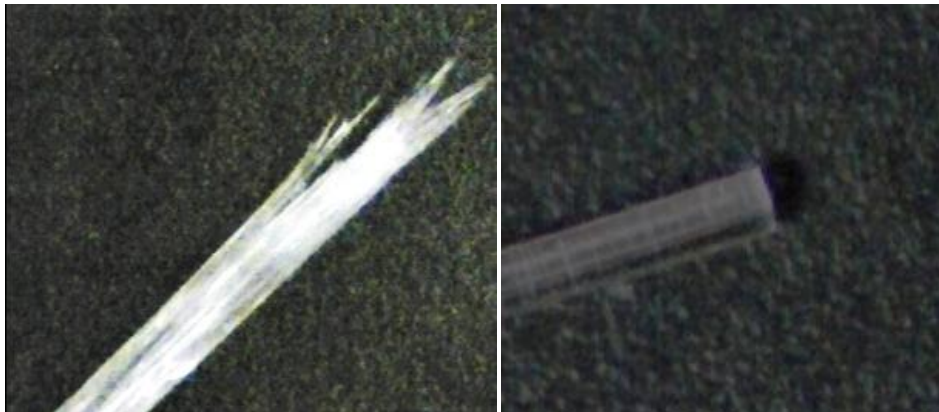
**Fig. 4-11. Photo of (left) preform under too high furnace temperature and (right) preform drawn with suitable temperature.**

Table 4-2 gives a summary of sets of drawing parameters for drawing different sizes of preform from 6mm to 22.2mm in diameter. The preforms are made from copolymer of methy methacrylate (MMA) and butyl methacrylate (BMA) with molar ratio 75/25.

**Table 4-2. Drawing parameters for different sizes of MMA/BMA preform.**

<b>Preform Diameter (mm)</b>	<b>Furnace Temperature (°C)</b>	<b>Feed Speed (um/s)</b>	<b>Take-up Speed (mm/s)</b>	<b>Rotational Speed of Fibre Spool (rpm)</b>
6	215 - 230	120	~17.28	~2.129
8	220 - 235	120	~30.72	~3.785
13.6	230 - 250	60	~44.39	~5.469
22.2	235 - 260	30	~59.14	~7.287

The tension of the drawing fibre is also an important factor for the drawing process. After the feed and take-up speed have been determined, the drawing tension can be changed by varying the furnace temperature. From our experience, we can increase the drawing tension by decreasing the furnace temperature. However, if the tension is too high, the fibre is likely to break. Even if not broken, the physical structure inside the fibre will be deformed. It can be explained that high tension drawing leads to significant molecular alignment along the fibre axis, which results in the reduction of failure strain of the POF [4]. Fig 4-12 shows the differences of fibre drawn with high tension and low tension respectively.



**Fig. 4-12. Photos of fibre drawn with (left) high tension and (right) low tension, when they were cleaved with razor blade.**

Both fibres are made from MMA/BMA with ratio 75/25 and their outer diameter is around 500 $\mu$ m. The left one was drawn with tension over 200cN; the right one was drawn with tension around 20cN. When they were cleaved by a razor blade, the one drawn with high tension would shatter instead of a clean break with smooth endfacet. To solve the problem in this case, the furnace temperature has to increase to lower the drawing tension. However, if the temperature is too high, bubbles will evolve as stated above. Therefore we have to optimize the drawing tension and the furnace temperature.



## 4.5 Conclusion

A POF draw tower has been built for the research project to fabricate various types of polymer optical fibres. The POF tower's designs, features and functions of its major components have been introduced in this chapter. The draw tower mainly comprises of the feeding unit, the furnace, the take-up unit and the control unit. Two types of furnace, i.e. the electric heater and the IR heater, for different purposes were designed and built to investigate their pros and cons in fabricating different types of polymer optical fibres. For the performance, the POF draw tower can handle preform sizes from 6 to 24mm and produce POFs with outer diameter from 100 $\mu$ m to as large as 4mm, with better than 97% accuracy. Great efforts have been put in optimizing the drawing parameters and conditions. Different combinations of the feed speed, the take-up speed as well as the furnace temperature have been tested to produce POFs with quality high enough for research purpose.

## Reference

1. Shinichi Matsumoto, US Patent No.: “6,042,755” (2000)
2. YOSHIMURA, I., MATSUDA, Y. and CHIGUSA, Y., Us Patent No.: “5,073,179” (1991)
3. KUZYK, M. G., “Polymer Fibre Optics – Materials, Physics and Applications,” CRC Press (2007)
4. WEBB, D. J., KALLI, K., “Fiber Bragg Grating Sensors: Recent Advancements, Industrial Applications and Market Exploitation”, p.292-312 (2011)

## Chapter 5 Applications of Dye-Doped POF as Light Sources

### 5.1 Introduction

The intrinsic low threshold and high tunability of dye lasers have made a variety of applications and key advances in laser technology possible [1]. The laser dyes have been incorporated into solid state materials to enable various optics developments, such as tunable lasers, amplifiers as well as nonlinear optical devices like switches and modulators [2]. Organic dyes are usually used as they have high quantum efficiency, high nonlinearities and availability of wide spectral range. Typically, PMMA is employed to act as the medium for the laser dyes. PMMA is superior to silica in that it has a low processing temperature of less than 300°C [2]. Otherwise, at 300-500°C, organic dyes start to deteriorate [2]. It is also expected that dye-doped polymer fibre lasers would play an important role in the integration of light sources into polymer FBG based sensing devices. It is also important to note that commercial broadband light sources operating in the visible region are not readily available. For example, superluminescent light-emitting diodes operating at the visible wavelength have spectral width of less than 10 nm [www.exalos.com].

In 1995, researchers in Japan demonstrated the first polymer optical amplifier by doping laser dye into a graded-index POF [3], which was prepared by the interfacial-gel polymerization technique. The laser dye they used was rhodamine B and the POF was based on PMMA. They utilized doubled *Q*-switch Nd:YAG laser as the pump source, in which the power was 690W, the repetition rate was 10Hz

and the center of wavelength was 532nm. A year later, Peng *et al.* demonstrated a rhodamine B doped step-index (SI) POF also for optical amplification [4], in which they utilized a 950W input pump power at 532nm wavelength in which the repetition rate was 10Hz and the pulse width was 5ns.. More recently, Sheeba *et al.* investigated the multimode laser emission from POF doped with a mixture of Rhodamine 6G and Rhodamine B [5]. Commonly, the pump sources they used came from big lasers at power level of several hundreds Watts, which were too bulky, not portable and so limit the practical applications.

This chapter will demonstrate how the dye-doped POF is pumped from a low-cost, low-energy and compact laser diodes and to show the feasibility to implement as light sources for sensing applications. A simple all polymer bending sensor was demonstrated by coupling a commercial polymer fibre (Asahi Lucina<sup>TM</sup>) with the light source, where the output signal was detected by a low cost spectrometer.

## 5.2 Dye-Doped unclad POF

Solid-state dye-doped light sources are usually made by dissolving the dye in a monomer followed by polymerization [6]. The resultant doped polymer can be used in its bulk form or drawn to make a polymer fibre. In our case, we produced the dye-doped POF without outside cladding, which made the fabrication process simpler and taking shorter time. Different organic laser dyes were mixed with the monomers, chain initiator and chain transfer. They went through the copolymerization process as described in Chapter 3.4. Finally the preforms were drawn into fibre using our in-house POF draw tower.

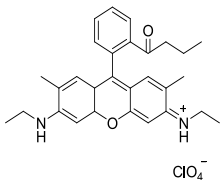
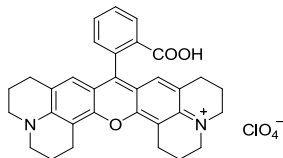
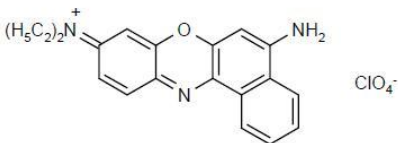
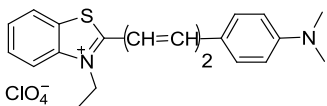
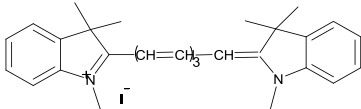
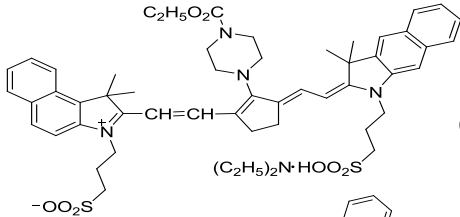
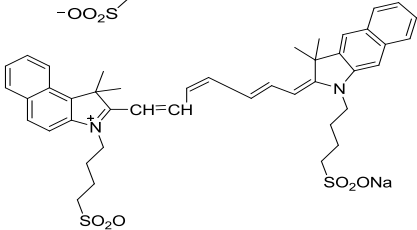
### **5.2.1 Materials and fibres fabrication**

The composition of the dye-doped fibres is just like that of the photosensitive core described in Chapter 3.3. The fibres were composed of MMA, BMA and BzMA with molar ratio of 75:19:6, added with 0.1mol% of LP and 0.25mol% of DT. The fibres were doped with laser dyes with concentration from 10ppm to 20ppm.

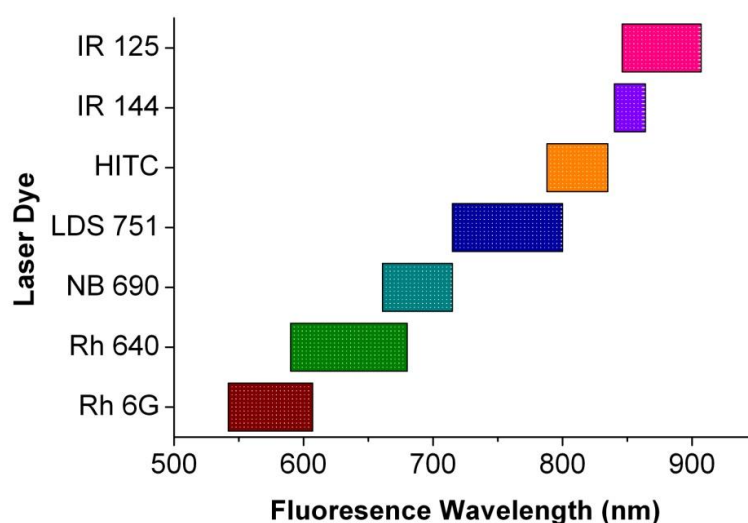
The laser dyes used in our experiments were all purchased from Exciton Co. Totally we have used 7 types of organic laser dye, which all belongs to the category of Nd:YAG excitation. The laser dyes have been developed for over 30 years for lasing applications.

Table 5-1 shows the different types of organic laser dyes used in our experiments, including their structures, chemical formulas and molecular weights.

Table 5-1. Types of organic laser dyes used in the experiments.

Name of Laser Dye	Structure	Chemical Formula	Molecular Weight
Rhodamine 6G (R6G)		$C_{32}H_{31}N_2O_7Cl$	479.01
Rhodamine 640 (Rh640)		$C_{32}H_{31}N_2O_7Cl$	591.05
Nile Blue 690 (NB690)		$C_{20}H_{20}O \cdot ClO_4$	417.85
LDS751		$C_{21}H_{23}N_2SO_4Cl$	472
HITC		$C_{29}H_{33}N_2I$ $C_{29}H_{33}N_2ClO_4$	536.5 509.04
IR144		$C_{56}H_{73}N_5O_8S_2$	1008.36
IR125		$C_{34}H_{47}N_2O_6S_2Na$	774.97

The reason for choosing these laser dyes is that their fluorescence emission spectra lie around the low-loss absorption wavelength windows of polymers. Many of the emission spectra overlapping each other (see Fig. 5-1), providing a continuous spectrum ranging from 542nm to 907nm. It would be possible for us to mix them together to achieve broadband light sources.



**Fig. 5-1. Fluorescence emission spectrum of various laser dyes.**

To study the laser dye fluorescence properties inside solid polymer, PMMA-based preforms were doped with various types of laser dyes. All the laser dyes were in solid form. They were added into the mixture of the monomers at the beginning, in which the concentration of the dye was 10ppm. Then it had to assure that the dyes totally dissolved into the solution at the pre-polymerization stage. After that, they underwent the conventional polymerization process which is mentioned in Chapter 3, Section 3.4. Dye-doped preforms with 1.36cm outer diameter were made as shown in Fig 5-2.



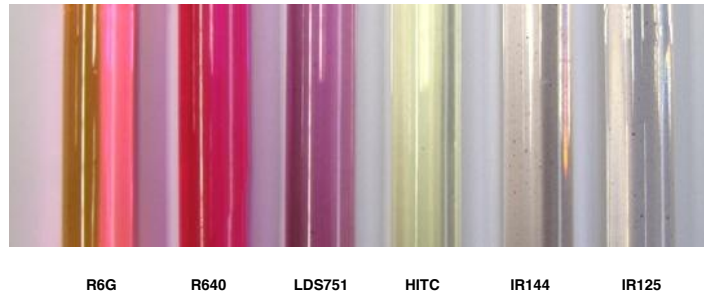


**Fig. 5 2 (a). Photo of preforms doped with various laser dyes.**



**Fig. 5-2 (b). Photo of dye-doped POFs where the fibre in the top reel is doped with Rh640 and the bottom reel with LDS751.**

At room environment, the dye-doped preforms do not show their fluorescence colors. For example, LDS751 emits fluorescence from 715 nm to 850 nm, which is infrared in color, but the color of the preform is purple. The situation is similar for R6G, Rh640 and HITC, which preform colors are light yellow, crystal red and mild orange respectively. IR 125 and IR 140 behave differently from others. Their preforms are nearly transparent and only show a very light pink color. Apart from that, the dye granules have not totally dissolved and stay in the preforms. It can be explained by the energy concern. According to

Table 5-1, the molecular weights of IR 125 and IR 140 are relatively high. The usual driving force for mixing and dissolving materials (entropy) is larger for large molecules [7]. Consequently, they have poorer solubility.

The next step was to draw the dye-doped preforms into fibres. As the quantity of the dyes was relatively small (10ppm), it would not cause significant change in the drawing condition of the POF draw tower. The doped preforms were heat-drawn, similar to drawing the undoped PMMA-based preforms into fibres, with outer diameter of around 500 $\mu$ m for ease of handling and coupling. The fibres were wound onto fibre spools as shown in Fig. 5-2(b).

### **5.2.2 Low Cost Pump Source**

The fibres can be optically pumped and used as polymer light sources. Typically a frequency double Q-switched Nd:YAG laser at 532nm is used as the pump source. For our experiments, Nd:YAG laser was replaced by a low-cost and compact laser diode, which can be easily found in a conventional green laser pointer.

The working principle of the green laser pointer is illustrated in Fig. 5-2. The laser pointer contains a composite Nd:YVO<sub>4</sub>/KTP crystal which Nd:YVO<sub>4</sub> stands for neodymium-doped yttrium aluminum vanadate and KTP stands for potassium titanyl phosphate. The crystal emits 1064 nm light when pumped by a high power infrared ALGaAs laser diode which operates with typically 100-300mW and at

808nm wavelength. Then the KTP side acts as a frequency doubler which halves the wavelength to desired 532nm.

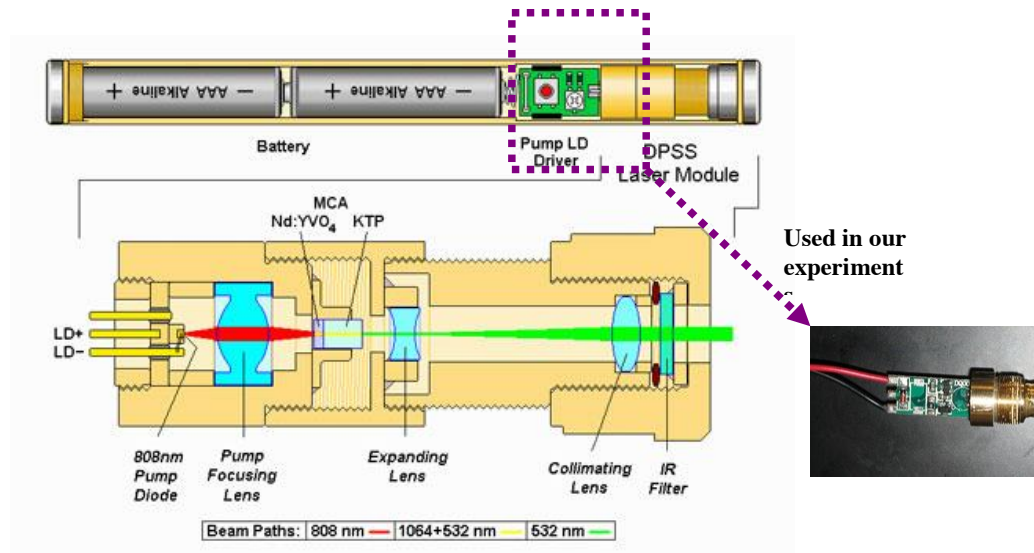


**Fig. 5-2. Working principle of green laser pointer. (source: Wikipedia)**

To make the pump source more compact, only the parts of pump driver, pump diode, pump focusing lens and Nd:YVO<sub>4</sub>/KTP crystal from the laser pointer were used, as shown in the inset of Fig. 5-2. Thus, the dye-doped fibre could be placed in front of the lasing crystal as close as possible. The cost of the pump is less than USD 10 for a 50mW power module.

The driver board is needed to protect the pump diode from burning by over-current. To control the whole pump source, the lead-out wires were connected to a power supply. Then the pump power was simply controlled by adjusting the current flowing through it. Fig. 5-3 shows the relationship between the output power of

one of the pump source laser and its input current. The lasing power was measured by an optical powermeter (Thorlabs, model no.: PM100).

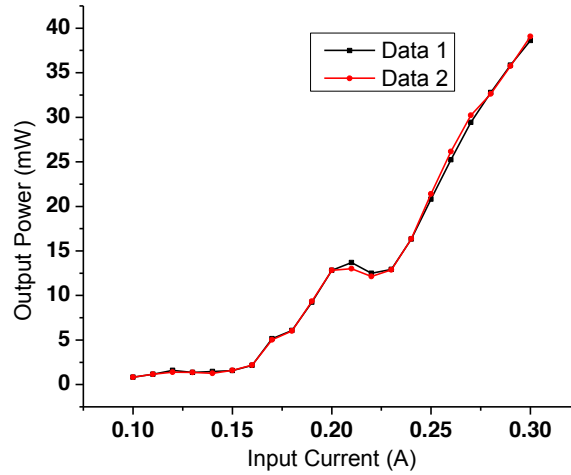


**Fig. 5-3. Graph of output pump power against input current.**

The measurement was done twice, which shows in the graph at Date 1 and Data 2. It can be seen that the power of the laser can be easily controlled by its input current. Moreover, the control of the laser is stable and repeatable. However, each of the pump source laser has different output characteristics. Therefore they should be calibrated individually if more than one is used in the experiments.

A stability test was also conducted for the pump laser. We set the output power of the laser to its maximum value, which was the state we assumed the heat produced was the highest. The output power was measured by the powermeter for 100min, where the sampling interval was 20sec. The result is shown in Fig. 5-4.

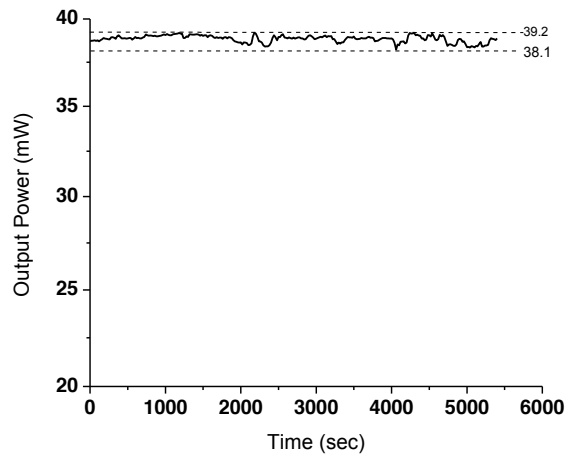


**Fig. 5-4. Output power of laser at its maximum power "on" for 100min.**

It is amazing to see that the low-cost laser performed very well and that the power fluctuation was just within 38.1-39.2mW, a small variation of less than 3%. It demonstrated that the laser was good enough for our applications.

The beam profile of the laser diode was obtained by scanning the beam by a CCD chip (Model: TCD1304AP, Toshiba). The CCD chip contained a linear array of high sensitive pn photodiodes. Fig. 5-5 shows the experimental setup.

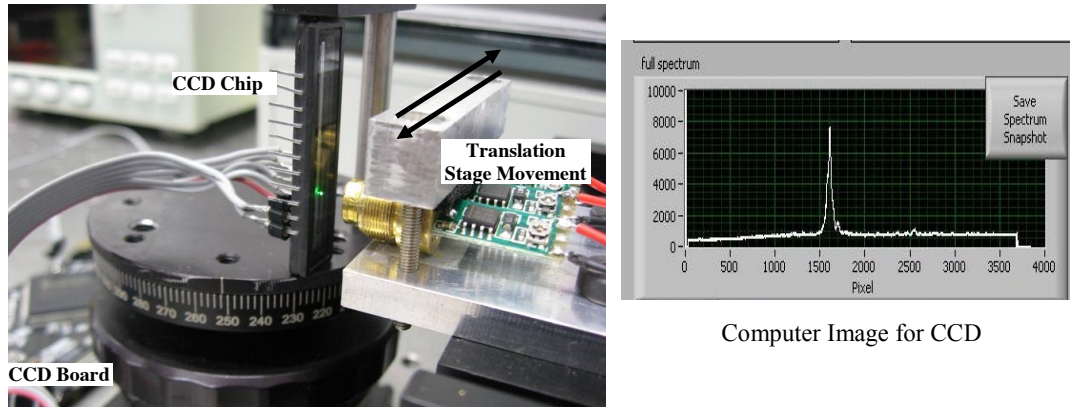


**Fig. 5-5. Photo of (left) experimental setup for scanning beam from laser diode; (right) computer image for the beam profile.**

The laser diode was mounted on a translation stage, the CCD chip was placed vertically in front of the laser at a distance of 3mm. Then the laser diode was moved horizontally and the beam was scanned. The resolution depends on the size of the pixel of the photodiode, which was  $8\mu\text{m}$ . During the horizontal scan, the beam profile was recorded for every  $250\mu\text{m}$  of stage movement, The results were then computed and shown in Fig. 5-6

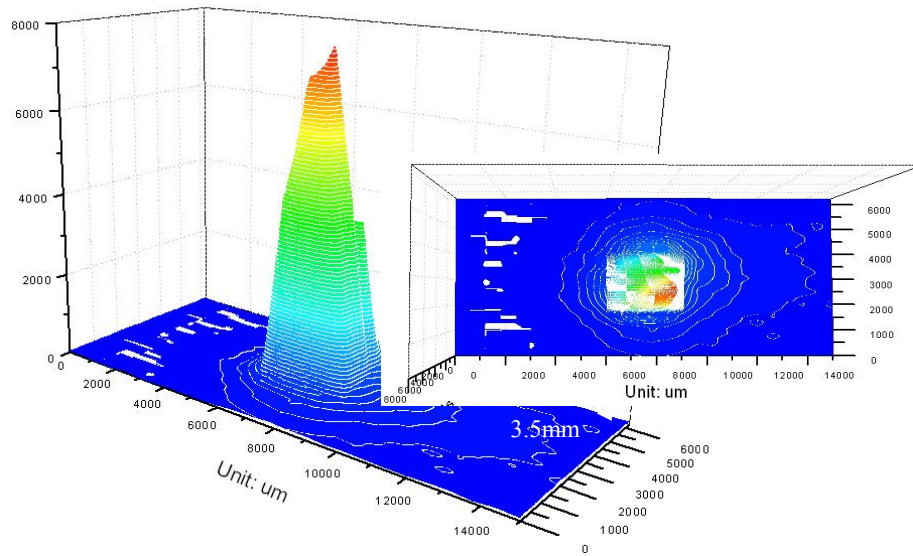


**Fig. 5-6. Beam profile of laser diode and (right top corner) the top view of it.**

It is seen that the beam size was around  $3.5\text{mm} \times 2.5\text{mm}$  a distance of 3mm. The intensity of the beam was nicely concentrated at the centre.

### **5.2.3 Experimental Setup and fluorescence Spectrum**

In order to test the fluorescence of the dye-doped fibre, each of the fibres doped with different types of organic laser dye was end-pumped by the 532nm laser diode. At the other end, the emission spectrum of the fluorescence was detected by a low-cost, CCD based spectrometer (Ocean Optics - USB650 Red-Tide™) as shown in Fig. 5-7. The output of the laser diode was 25mW and the length of each of the fibres was around 10cm, and both ends of the fibre was cleaved by a hot razor blade.

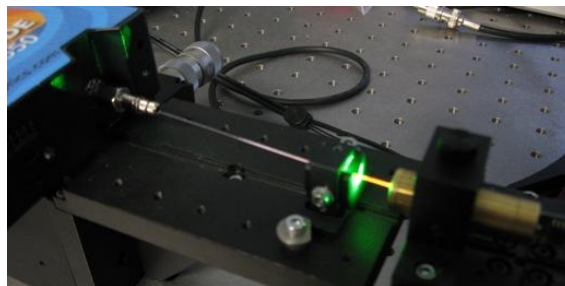


**Fig. 5-7. A photo of the experimental setup of testing the emission spectrum of Rh640 dye-doped fibre.**

#### ***5.2.3.1 Fibres Doped with Various Laser Dyes***

Totally, seven fibres were under tested which were doped with R6G, Rh640, NB690, LDS751, HITI, IR144 and IR125 and their concentrations were all 10ppm. The fibre diameter was around 500 $\mu$ m. To connect the fibre to the spectrometer, SMA-905 fibre adaptor with similar diameter was used. The objective of the experiment was to observe the fluorescence of the dye-doped fibres and their elementary spectra. Therefore the spectrum intensities were normalized and shown in Fig. 5-8.



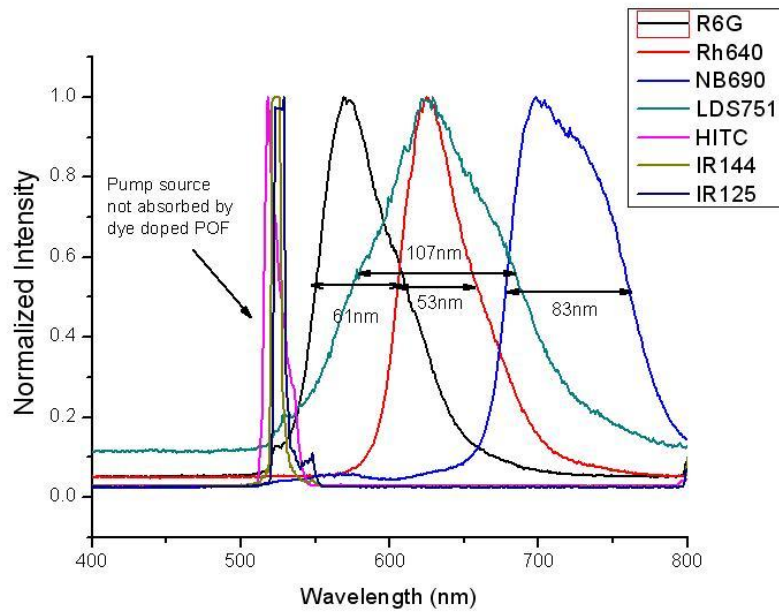


**Fig. 5-8. Spectra of various dye-doped POFs.**

The results show that not all the dye-doped fibres could be pumped to induce fluorescence. It can be clearly read from the graph that R6G, Rh640, NB690 and LDS751 doped fibres absorbed the pump source power and excited fluorescence at particular wavelength ranges. The spectra overlap each other and the measured Full-Width Half Maximum (FWHM) of their spectrum were around 61nm, 53nm, 83nm and 107nm respectively, as shown in the graph.

On the other hand, HITI, IR144 and IR125 doped fibres seemed to be transparent to the pump source and no fluorescence was observed. The result was the same even the power of the laser diode was turned to maximum (nearly 40mW).

After checking with the manufacturer's data sheet, it is found that researchers mainly use methanol as the solvent for R6G, Rh640, NB690 and 751. On the other hand, they mainly use dimethyl sulfoxide (DMSO) as the solvent for HITI, IR144 and IR125. DMSO is a kind of polar aprotic solvent which has excellent solvating power so that the large molecules of IR144 and IR125 can dissolve in DMSO and kept their fluorescence ability, but not for the case of our monomers solvent. Another suspect is that the dyes did not just dissolve but reacted with monomers to form other substances which were not fluorescent in nature. Referring to

Table 5-1, HITI, IR144 and IR125 have a common structure that the centre of the molecule is linked by C=C double bond. They dissolve in the monomers in the pre-polymerization stage at high temperature of 75°C. The C=C double bonds in the dye molecules might break just like the monomers and linked with other monomers. In this way, the original structure of the dye molecules was destroyed and thus the fluorescence disappeared.

#### ***5.2.3.2 Fibre Doped with Rh640 with Different Concentrations***

To investigate the effect of the dye concentration on the fluorescence spectrum, the preforms were doped with Rh640 with different concentrations of 5ppm, 10ppm, 15ppm, 20ppm and 25ppm (see top of Fig. 5-9). They were drawn into fibres and 10cm of each of them were put in the above setup for testing their spectra. The result is shown in bottom of Fig. 5-9.

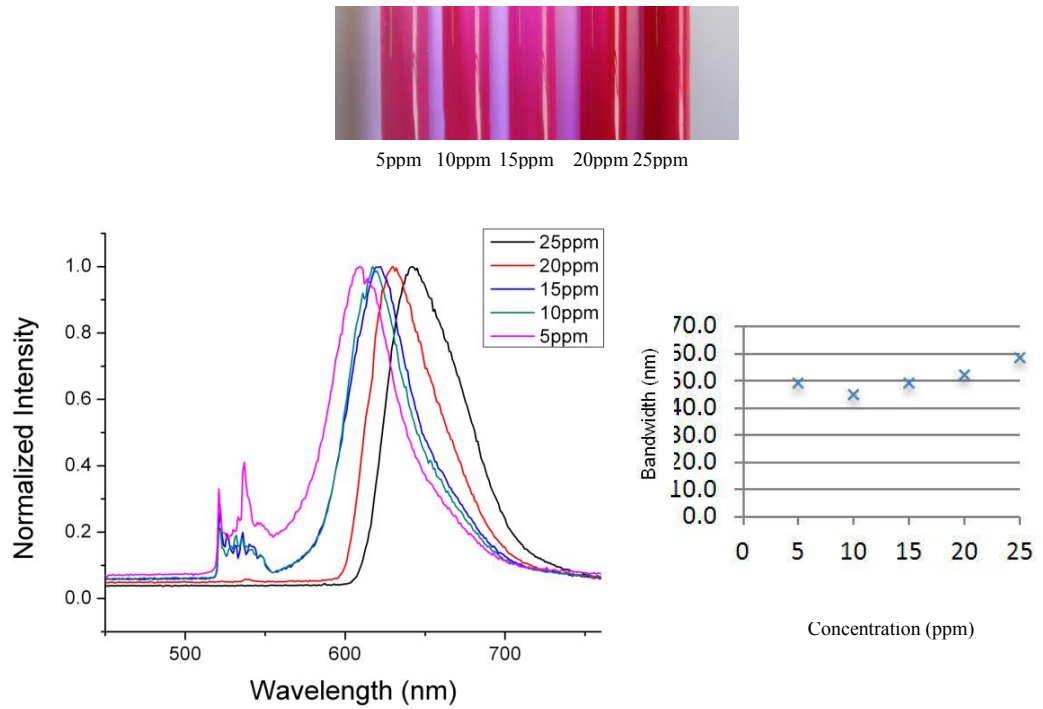


**Fig. 5-9. (Top) Photo of dye-doped preforms with different concentrations; (bottom) graph of respective fluorescence spectra of their fibres. Inset shows the FWHM of the fluorescence spectra of the fibres with different ppm.**

From the photo of the preforms, it can be observed that higher the concentration of Rh640, the darker the appearance of the preform. When their fibres are excited by the 532nm laser diode, it is interesting to note that the fluorescence peak shifts from around 608nm to 642nm, and the FWHM of the spectra decreases from 49 nm to 45 nm and then increases to about 60 nm, when the concentration of the dye increases from 5ppm to 25ppm. It can be explained that more fluorescence light is re-absorbed by the dye and re-emit as fluorescence again, causing the spectrum to red-shift. Another interesting observation is that the residue of the pump source became smaller if the concentration of the dye is getting higher. It is because if the

concentration of the dye is higher, which means more dye molecules could absorb the power of the pump light source. It is expected the optical conversion efficiency is higher for higher dye concentration. More about this matter will be covered in Section 5.3.3.

#### 5.2.4 Co-doping of Laser Dyes

In order to increase the emission bandwidth, PMMA-based preforms co-doped with various laser dyes were fabricated. A long fibre has been drawn from the preform, 10cm of it was pumped by the 532nm laser diode. The spectrum of R6G and Rh640 co-doped fibre was shown in Fig. 5-10. The concentration of both laser dyes was 20ppm.

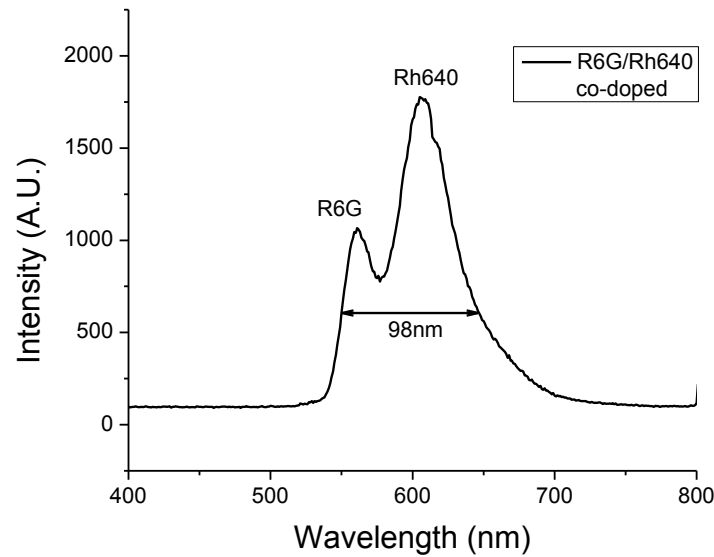


**Fig. 5-10. The emission spectrum of Rh640 and R6G co-doped PMMA fibre pumped at 532 nm.**

From the figure, two emission peaks are observed at around 560nm and 610nm, corresponding to R6G and Rh640 respectively. The two spectra overlapped with each other, and give a wider emission bandwidth than fibre doped with just R6G or Rh640 (see Fig. 5-9). The FWHM of the spectrum is as large as 98nm.

Similar experiment has been done on the fibre co-doping with three laser dyes, which were R6G, Rh640 and LDS751. The spectrum is shown in Fig. 5-11. The concentration of three laser dyes were 20ppm.

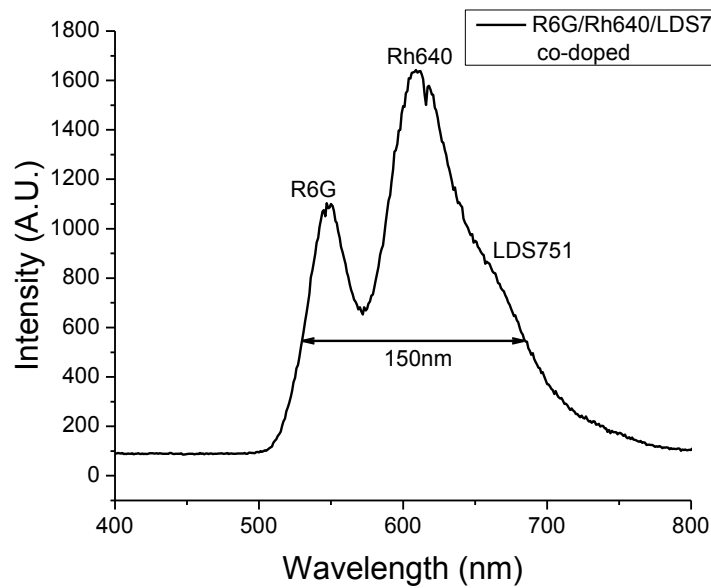


**Fig. 5-11. The emission spectrum of R6G, Rh640, and LDS751 co-doped PMMA fibre pumped at 532 nm.**

The co-doped fibre was still able to be pumped by the 532nm laser diode and emit fluorescence spectrum. The emission spectra got even broader, with FWHM of as

large as 150nm. This suggests that it is possible to co-dope more dye components in PMMA to make a broadband source with an even broader spectrum.

### **5.3 Dye-Doped Fibres with Cladding**

To implement the dye-doped fibre as a light source for a sensing system, it has to be coupled to a sensing/receiving fibre. In our experiment, the butt-coupling method is used. In order to minimize the coupling loss between them, the dye-doped fibre is designed using a tailor-made structure to match the sensing/receiving fibre to decrease the optical loss due to core size mismatch. Also, the refractive indexes of the core and the cladding of the dye doped fibre are designed to give a suitable NA value, preferably a bit smaller than that of the sensing/receiving fibre, such that the loss due to NA mismatch is minimized.

In our case, a commercial polymer fibre (Asahi Lucina<sup>TM</sup> fibre) was used the sensing/receiving element fibre. Rh640 was used as the laser dye. Fig. 5-12(a) shows the structure of the Asahi fibre. In order to increase the coupling efficiency between the two fibres, the dye-doped fibre was designed to have a similar core and cladding dimensions as the Asahi fibre, see Fig. 5-12(b).

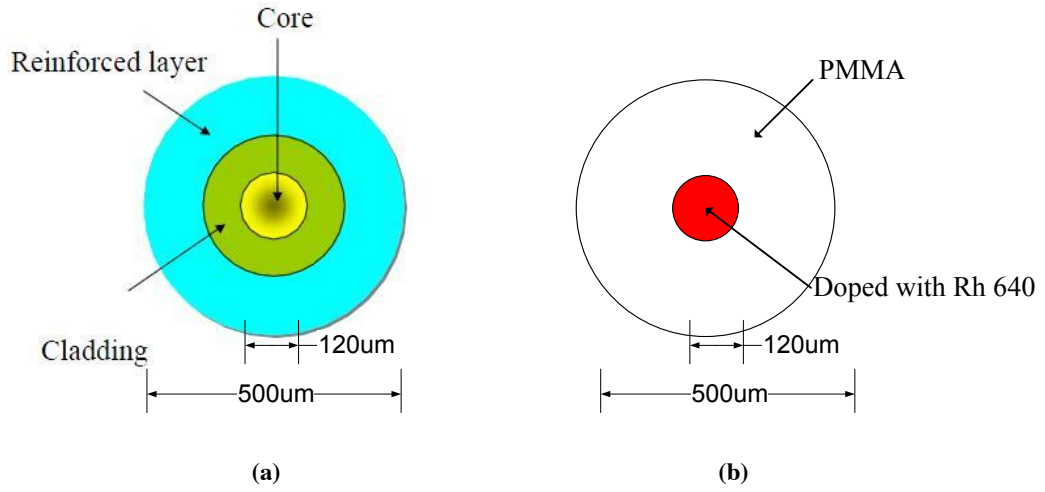


**Fig. 5-12. (a) Structure of the Asahi graded-index multimode fibre. (b) Structure of the Rh 640-doped fibre with similar core/cladding ratio as the Asahi fibre.**

After determining the dimension, we had to design the refractive index of the cladding and the core of the dye doped fibre. The refractive index of polymers can be calculated by Equation 5-1[8]:

$$\frac{n^2 - 1}{n^2 + 2} \cdot \frac{N_A \sum_i \Delta V_i}{K_{av}} = f \quad \text{Equation 5-1}$$

where  $n$  is refractive index at 589.3nm,  $N_A$  is Avogadro constant ( $6.023 \times 10^{23}$ ),  $\Delta V_i$  is Van-der-Waals volume of  $i$ -th atom in the chemical structure of the repeating unit,  $K_{av}$  is molecular packing coefficient (0.681 for bulk polymer) and  $R$  is molar refraction of the repeating unit.



For amorphous and glassy copolymers or polymer blends, R is calculated by Equation 5-2 [8]:

$$\frac{n^2 - 1}{n^2 + 2} \cdot \frac{N_A [\alpha_1 (\sum_i \Delta V_i)_1 + \alpha_2 (\sum_i \Delta V_i)_2 + \dots + \alpha_n (\sum_i \Delta V_i)_n]}{K_a} = \alpha_1 R_1 + \alpha_2 R_2 + \dots + \alpha_n R_n$$

**Equation 5-2**

where  $\alpha_n$  is the molar fraction for each component in a copolymer. The values of R for the monomers were checked, which were 24.744, 38.598 and 48.851 for MMA, BMA and BzMA respectively. By substituting the values into Equation 5-3 and solving it, we got the value of the refractive index. In our case, the composition of the core was MMA:BMA:BzMA (molar ratio=75:19:6), doped with 10ppm Rh640. By neglecting the effect of the dye, the evaluated refractive index was 1.4990. For the cladding, the composition is MMA:BMA (molar ratio=75:25), then the evaluated refractive index was 1.4941.

The samples of the core and the cladding were measured by spectroscopic ellipsometry for further clarification. It was found that for the values were 1.499 and 1.493 respectively, which were quite close to the evaluated values. NA for step index fibre can be calculated by Equation 5-3 [9]:

$$NA = n_c \cdot \sqrt{2 \cdot \frac{n_{co}^2 - n_{cl}^2}{2 \cdot n_{co}^2}} \quad \text{Equation 5-3}$$

The NA for the dye doped fibre was 0.134 which was smaller than that of the Lucina<sup>TM</sup> fibre of 0.185. Therefore the coupling loss by NA mismatch was not so significant.

### **5.3.1 Fabrication Process**

The fabrication of the dye-doped preform followed the procedure described in Chapter 3. The cladding was composed of MMA, and BMA with molar ratio of 75:25. The core was composed of MMA, BMA and BzMA with molar ratio of 75:19:6. For both cladding and core, 0.1mol% of LP and 0.25mol% of DT were added. The laser dye, Rh640, was doped with concentration of 10ppm into the core.

Glass tubes were used as the moulds which has an inner diameter of 22.23mm; for the core, Teflon rods with outer diameter of 5mm were used and secured at the centre. The ratio of preform cladding/core was 22.23:5, which was similar to that of the Lucina<sup>TM</sup> fibre of 500:120. Thus, if the preform was drawn down into fibre with outer diameter of 500 $\mu$ m, then the core diameter would be around 112 $\mu$ m, which was slightly smaller than that of the receiving fibre. The draw-down ratio was around 44.

The preform were shown in Fig. 5-13a. The total drawable length of the preform was around 7cm. By considering the draw-down ratio, theoretically the maximum length of the fibre can be drawn was around 135m, which was far enough for our usage. Fig. 5-13b shows the dye-doped fibre wound onto a spool.

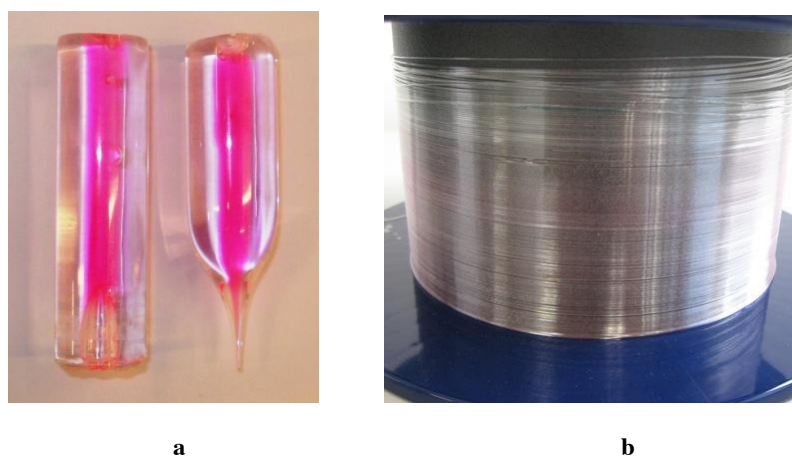


**Fig. 5-13. (a)Photo of preform with Rh640 doped (10ppm) core and undoped PMMA-based cladding (left) before and (right) after being drawn to fibres. (b) Photo of dye-doped fibre drawn from the preform.**

### 5.3.2 End-pump Versus Side Luminance Technique

The dye-doped fibre with cladding was end-pump by the laser diode as like as Fig. 5-7. The total length of the fibre was 10cm. The power of the laser diode was around 25mW. The resultant fluorescence spectrum is shown in Fig. 5-14.

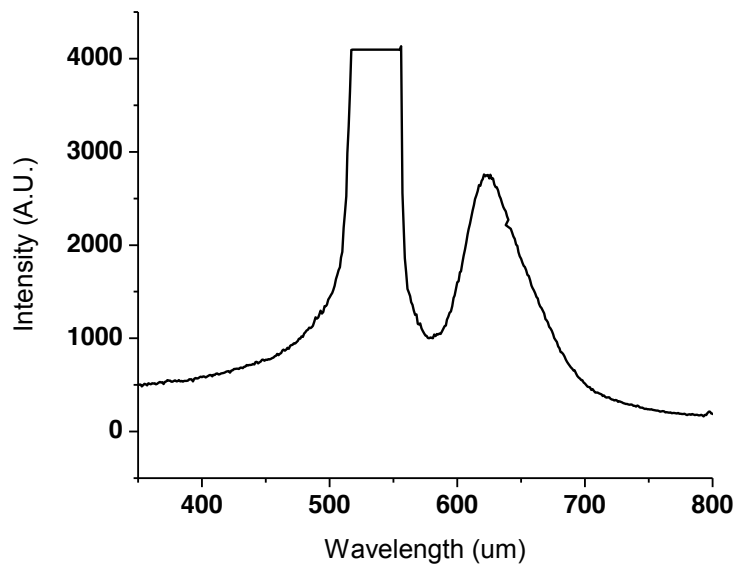


**Fig. 5-14.** Spectrum of dye-doped fibre with cladding end-pumped by the laser diode.

It shows that a large amount of the light from the pump source was collected by the spectrometer (the intensity at 532nm was cutoff by the scale of the graph). The light from the pump and the fluorescent light most were guided through the fibre together.

To suppress the pumping spectrum, the technique of side illumination fluorescence (SIF) can be used. The side-illumination fluorescence (SIF) technique on dye-

doped fibres has been studied by Kruhlak and Kuzyk [10] for measuring the linear absorption spectrum in POF. The SIF technique was also carried by Rosa-Cruz [11] and Sheeba [12] on dye-doped fibres to study their emission characteristics. However, their pump source was high-power laser which was bulky and the uncladded dye doped fibres were used. In our experiments, the SIF technique was applied to our dye-doped fibre with core and cladding. The fibre was pumped by the low-cost laser diode perpendicularly to the fibre axis, as shown in Fig. 5-15. The resultant spectrum is shown in Fig. 5-16. Note that the intensity at 532nm was significantly suppressed, leaving the fluorescence spectrum dominant. The intensity of the fluorescence spectrum was still high enough for data transport as well as sensing applications.

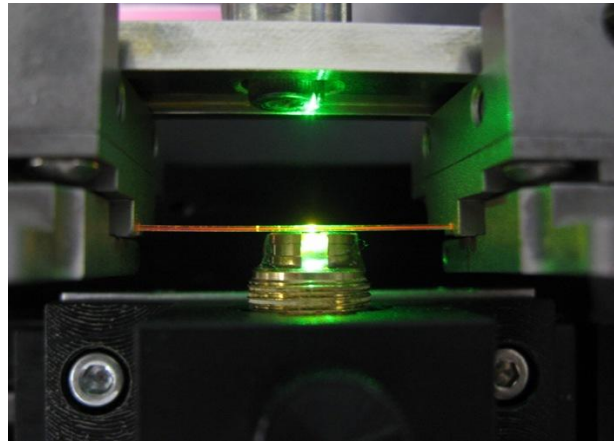


**Fig. 5-15.** Close view of how the dye doped fibre was side-pumped by laser diode.

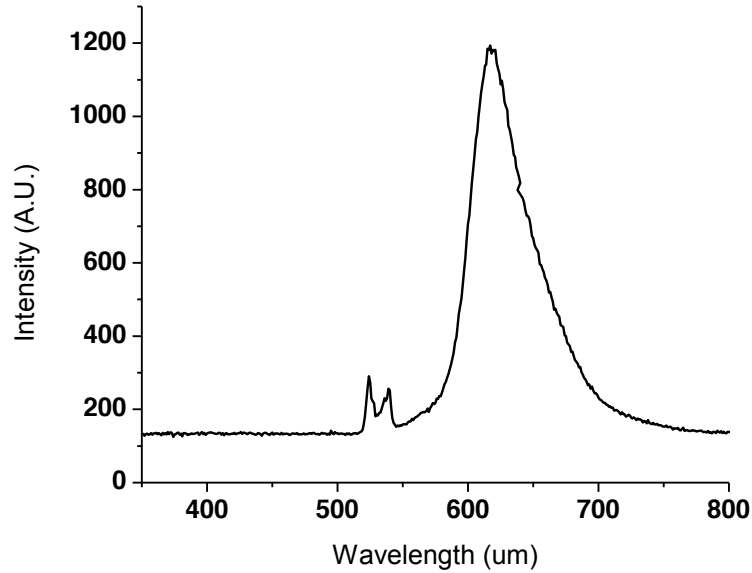


**Fig. 5-16 Spectrum of dye doped fibre side pumped by laser diode.**

### **5.3.3 Optical Conversion Efficiency**

To realize a practical low-cost system, the expensive visible-spectrometer is replaced by a low-cost photodiode. Therefore we have to know the actual spectrum power emitted from the dye-doped fibre to see if it is powerful enough to be detected by the photodiode. Moreover, we have to know the dye-doped fibre loss as well as the conversion efficiency of the fibre, so that we can determine the power requirement of the pump.

It is well known that the quantum efficiency of Rh640 in methanol solution is around 0.75-0.8 [13,14]. However for our practical application, we need to know the optical conversion efficiency for the dye doped in POF. In order to calculate the

value, we have to know how much pump power the fibre absorbs and how much power the fibre emits as fluorescence.

First of all, we estimate the power illuminating onto the core of the dye doped fibre. As illustrated in Fig. 5-17, it is assumed that the dye-doped fibre is pumped by the laser diode in such orientation, i.e. in the middle of the laser diode beam.

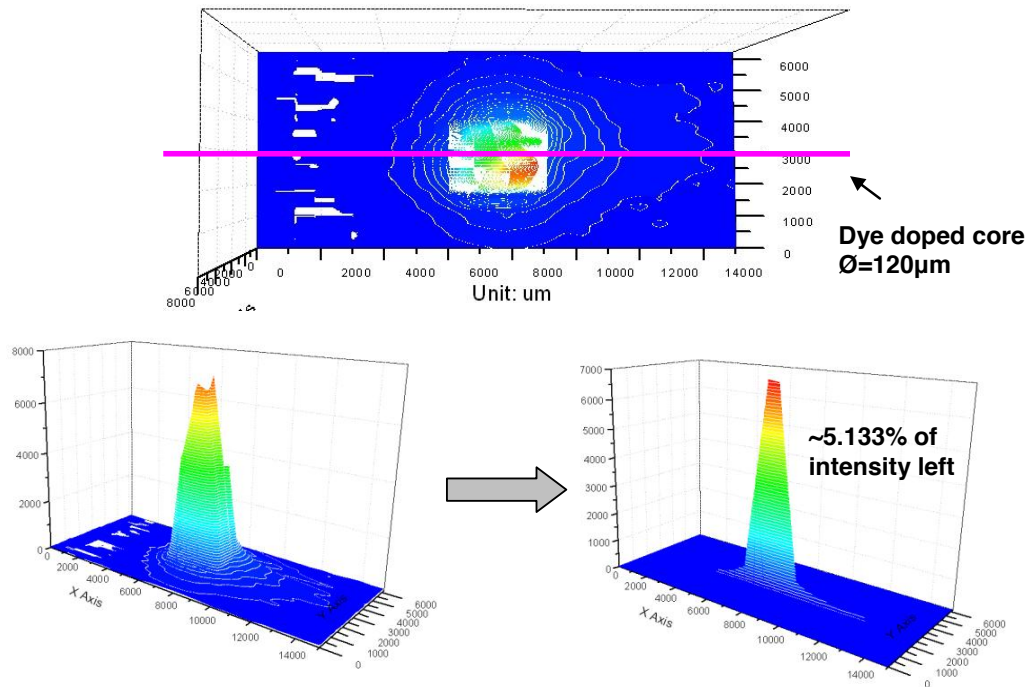


**Fig. 5-17. Estimation of power illuminating on dye-doped fibre.**

The diameter of the fibre is around 120 $\mu\text{m}$ . The beam profile with width of 120 $\mu\text{m}$  is taken away from the original profile. The volume beneath surface was computed by Origin<sup>®</sup> and compared with that of the original profile. It is concluded that around 5.133% of the pump power illuminates onto the core.

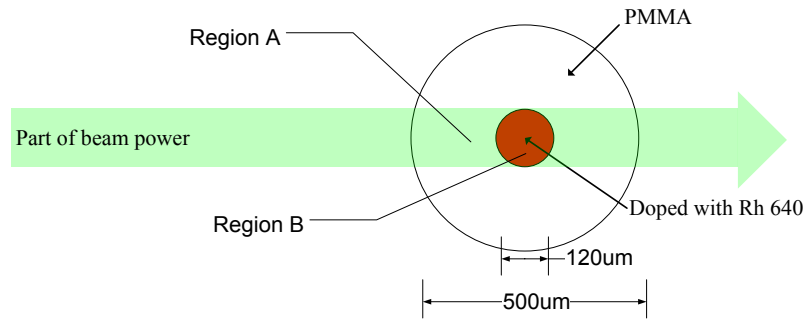


**Fig. 5-18. Path of laser beam travelling through the dye-doped fibre.**

According to Fig. 5-18, to know how much power is absorbed by the core, we have to know the absorption loss if the dye material at 532nm wavelength, i.e. absorption in Region B. Also the loss of PMMA-based cladding at this wavelength is taken into account, i.e. loss in Region A.

The loss of the cladding material can be obtained by doing a cutback test on a pure PMMA fibre. The 532nm laser diode is used as the light source. A 1.9m long fibre is cut back by about 2cm and the process was repeated for 61 times. The result is shown in Fig. 5-19. It is seen from the graph that the fibre loss is 0.045dB/cm at 532nm wavelength.



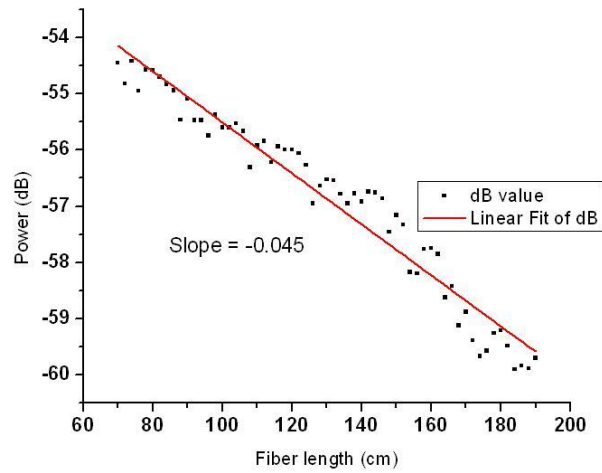


**Fig. 5-19. Result of cutback test on PMMA-based fibre at 532 nm.**

Similar test is conducted on the dye-doped material. However, this time, we used thin slabs instead of fibres. Again 532nm laser diode is used as the light source and the power is measured by the powermeter. In between them, a slice of the dye-doped polymer with different thickness acts as the obstacle. The relationship of the receiving power and the slice thickness is shown in Fig. 5-20.

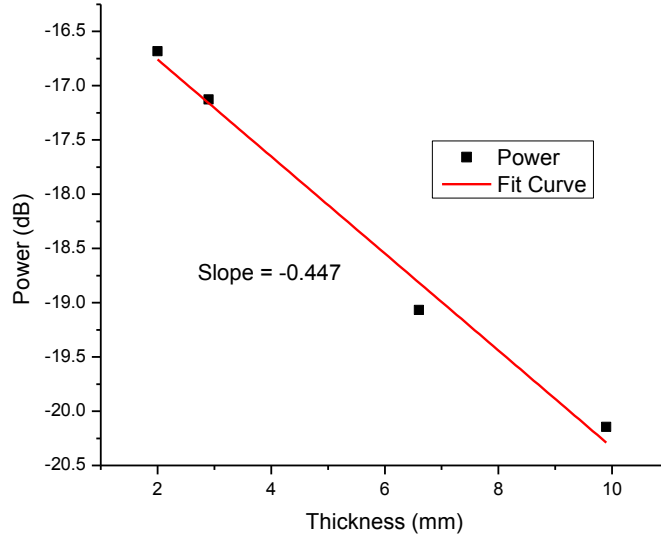


**Fig. 5-20. Relationship between receiving power and thickness of laser dye-doped polymer slabs.**

The absorption loss of the dye-doped polymer can be read from the slope of the graph. The value for it is 0.447dB/mm (3% tolerance) which is much higher than that of the PMMA-based polymer. Referring to Fig. 5-18, the optical loss in Region A becomes negligible in our calculation.

The transmission loss of the dye-doped fibre at wavelength around 640nm is also useful in our calculation. Thus, we perform cutback test on the fibre using red laser pointer as the light source which has centre wavelength of 658nm. The fibre was cut back 32 times and Fig. 5-21 shows the result that the loss is 0.233dB/cm.

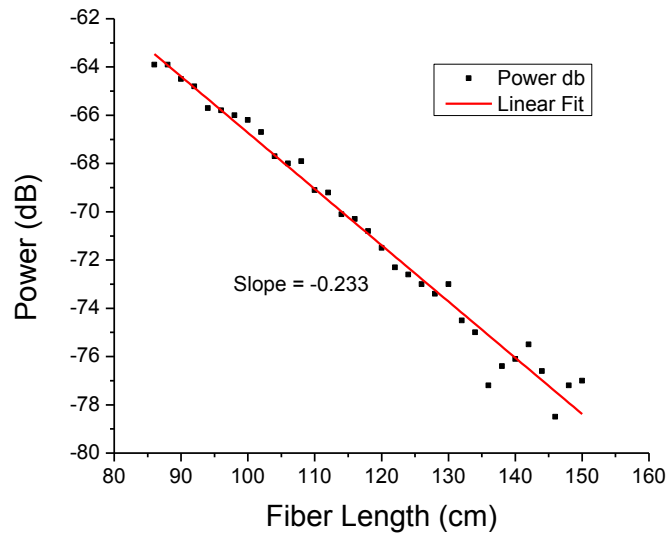


**Fig. 5-21. Result of cutback test on PMMA-based fibre by red laser at 658 nm wavelength.**

Now we have sufficient information to calculate the conversion efficiency of the dye-doped fibre. A simple experimental setup used for evaluating the conversion efficiency is shown in Fig. 5-22.

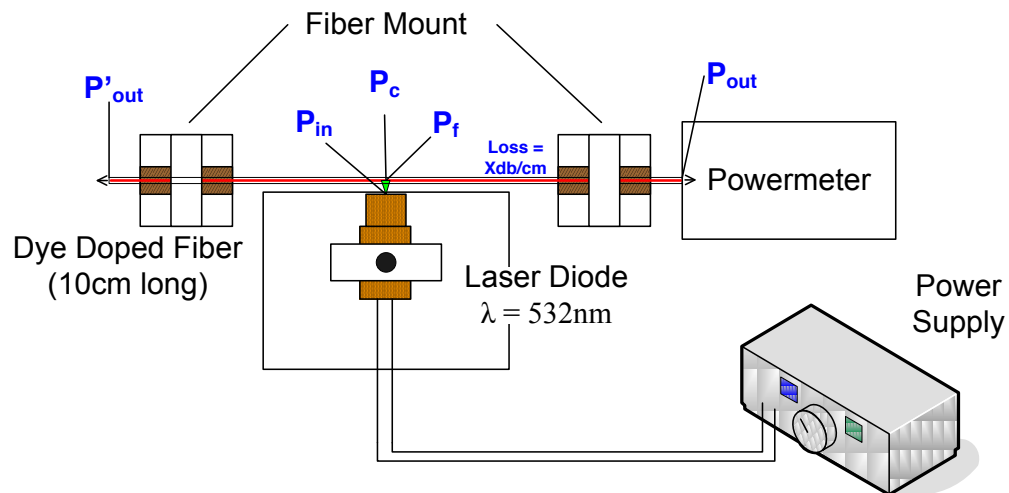


**Fig. 5-22. Experimental setup to evaluate conversion efficiency.**

The middle of a 10cm long dye-doped fibre is pumped by the 532nm laser diode. The power of the laser diode,  $P_{in}$ , is 4.146mW. The output power of the dye-doped fibre,  $P_{out}$ , is 1.223μW. Theoretically, the fibre output power of the fibre,  $P'_{out}$ , should be equal to  $P_{out}$ .

The power of the pump source passing through the core of the dye-doped fibre,  $P_c$ , can be obtained from the previous result:

$$P_c = 541219\mu W \quad \text{Equation 5-4}$$

The loss of the fibre from  $P_f$  to  $P_{out}$  is:

$$\text{Fibre loss} = (0.233 \times 5)dB = 1.165dB \quad \text{Equation 5-5}$$

The fluorescence power of the dye doped fibre,  $P_f$ , is a function of  $P_{out}$ , can be calculated by:

$$P_f = 2.41 \times 10^{-4} W \quad \text{Equation 5-6}$$

Hence, the optical conversion efficiency of the fibre,  $\eta$ , can be obtained by:

$$\eta = \frac{P_f}{P_a} = 1.50\% \quad \text{Equation 5-7}$$

The optical conversion efficiency is 1.509%, which means such percentage of the incident optical pump power is converted to fluorescence power by Rh640 doped POF with concentration of 10ppm. Similar result was reported by Drake [14], but the Rh640 doped polymer was in slab form instead of fibre. The conversion efficiency of the slab was 3.6% at a dye concentration of  $3 \times 10^{-5} \text{M}$ . Another researcher, Costela, doped Rh640 into a cylindrical rod made from PMMA and poly-2-hydroxyethyl methacrylate (PHEMA), in which the measured lasing efficiency was 4% [15] and dye concentration is  $1 \times 10^{-3} \text{M}$ .

The optical conversion efficiency for our fibre is relatively low. The main reason is that the concentration of the dye is lower (10ppm). It is expected increasing the dye concentration could increase the conversion efficiency. However there would be a trade off with the transmission loss of the fibre.

The objective behind the calculations is that we can find the required power of the pump source as well as the length of the dye doped fibre in order to achieve a practical light source for a sensing system.

### 5.3.4 Fluorescence Characteristics

To study the fluorescence characteristics of the dye-doped fibre by the SIF technique, we used the following setup:

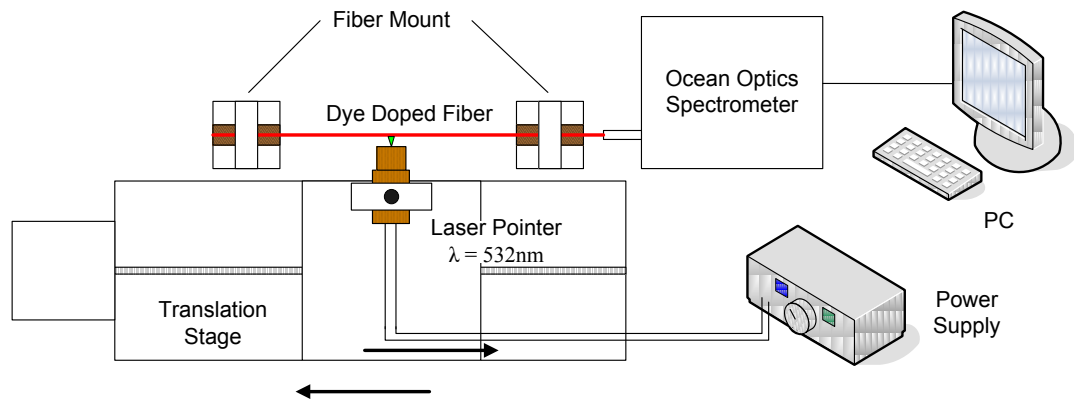


**Fig. 5-23. Experimental setup for investigating fluorescence characteristics of dye-doped fibre.**

A 10cm-long dye doped fibre is mounted and side-pumped by the laser diode. The laser was mounted on a translation stage such that it can move horizontally along with the dye doped fibre. The spectrum was taken by the spectrometer and recorded in the computer. We will see how the difference in the dye concentration, pump power and pump position affects the fluorescence of the dye doped fibre.

#### 5.3.4.1 Intensity Calibration for UV-spectrometer

The unit of the spectrum intensity used in our UV-spectrometer is an arbitrary value (A.U.). It has also been seen from many research papers that A.U. was almost used as the unit when similar spectrometers were used. However, the A.U.

unit can be meaningless for a practical system. Before further doing our experiments were carried out, the intensity of the UV-spectrometer was calibrated.

A broadband SLED light source (Model: SLD-35-HP, Superlum Diodes Ltd.) was used, which wavelength was centered at 830nm. The light source was connected to FC/APC single-mode fibre pigtail, coupled to SMA-905 multimode fibre pigtail, then to the UV-spectrometer. It was assumed that there was not coupling loss between the single-mode and multimode fibre. The power of the light source was turned to nearly the maximum level shown in the UV-spectrometer. Then the light source was collected to an optical spectrum analyzer (OSA) (Model: AQ6370, Fugokawa). The resolution was adjusted to 1nm for both UV-spectrometer and OSA. The spectra were compared in Fig. 5-24.

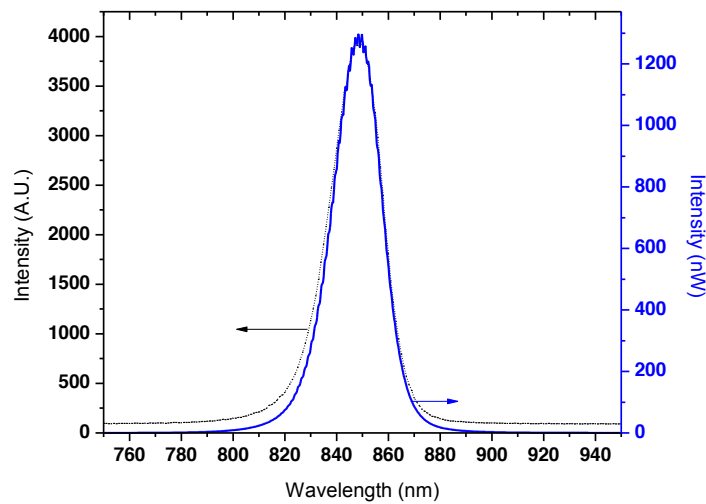


**Fig. 5-24. Spectra from UV-spectrometer and OSA by same light source.**

The dotted line is the reading from the UV-spectrometer and the solid line is that from the OSA. They nearly overlapped with each other. It is concluded that 1 A.U  $\approx$  0.322nW (with 1% tolerance). In the latter part of the thesis, all the intensity reading from the UV-spectrometer will be converted to nW based on this scale.

#### 5.3.4.2 Effect of Input Power

As shown in Fig. 5-23, the total length of the dye doped fibre was 10cm. The position of the laser pointer was adjusted so that it emitted the pump source at the middle (5cm) of the dye doped fibre. The power of the laser pointer was adjusted by limiting the current flowing through it by the external power supply. The relationship between the pump source power (5-25W) and the florescence emission spectra was shown in Fig. 5-27.

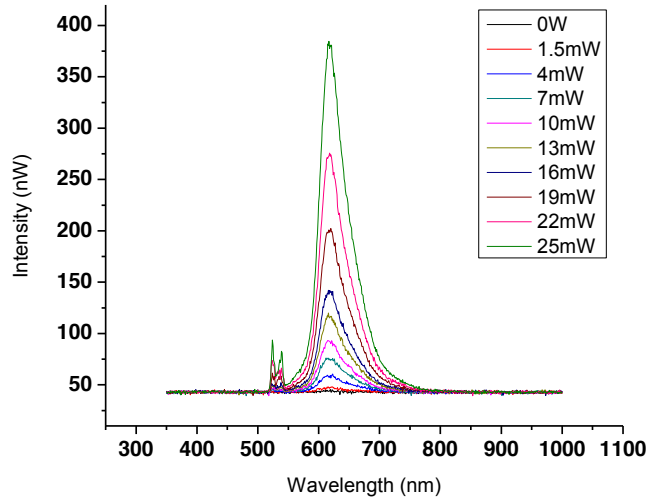


Fig. 5-25. Graph of fluorescence emission spectrum against different pumping power.



Once again, comparing with the end-pump technique, the intensity at 532nm was significantly suppressed, leaving the fluorescence spectrum dominant. The intensity of the fluorescence can be easily controlled by the power of the pump source. Another important point is about the power independence of the fluorescence emission wavelength. For end-pumping technique, it has been investigated by Rajesh that fluorescence blueshift was observed as the pump power increased [16]. In contrast, for our side pump technique, the wavelength of the peak of the emission spectrum was independent to the pump power. In other words, it is possible to control the intensity of the emission spectrum without shifting it.

#### ***5.3.4.3 Effect of Pump Position***

The experimental setup shown in Fig. 5-23 was used to investigate the change in the emission spectrum when the dye doped fibre was pumped at different section with constant pump power. The total length of the fibre was 10cm. The power of the laser pointer source remained at 25mW. It was carried by a translation stage so that the light from it illuminated the dye doped fibre at the length from 5cm to 8cm to the spectrometer. In other words, the propagation distance of the fluorescence emission was changed. The shortest propagation distance was limited to around 4cm as fibre had to be inserted into the spectrometer and certain length was taken up by the mounts. At each distance, the emission spectra were recorded three times. The averaged values are shown in Fig. 5-26.

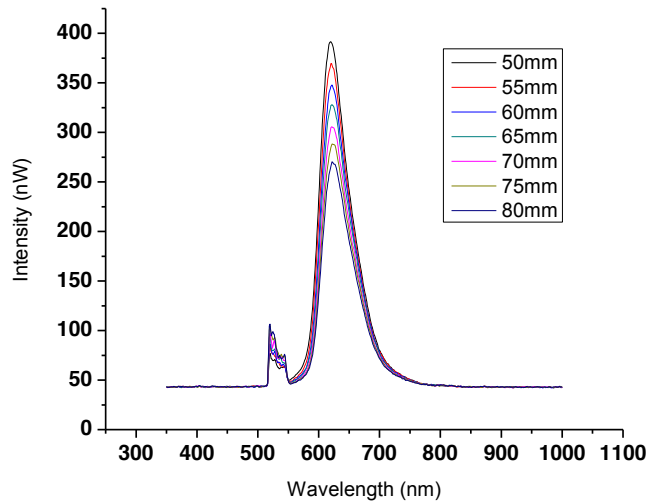


**Fig. 5-26. Graph of fluorescence emission spectrum against different pumping position.**

It can be observed that the fluorescence power deteriorated when the pump source illuminated the fibre at longer distance from the spectrometer. It could be explained by the loss of the fibre by adsorption and scattering of the fluorescence. The peak of the fluorescence experienced red shift when the propagation distance was increased. The red shift was from 622nm to 627nm when the propagation distance was increased from 5cm to 8cm. It was suggested that the peak fluorescence wavelength can be finely tunable by this mechanism. Moreover, the power of the pump residue was increased with the propagation distance.

### **5.3.5 Enhancement of Optical Power by Gold Coating**

One of the disadvantages of SIF technique is that the light comes out from both ends of the fibre. If the one end is connected to the spectrum, the light from the opposite end come out as a waste. To solve the problem, it was suggested that gold

is coated on one end of the fibre so that the waste light is reflected back into the fibre to enhance the optical output power of the dye doped fibre.

Before coating with gold, the fibre end should be cleaved nicely and perpendicularly to its axial direction. A 193nm ArF excimer laser (Coherent Model no.: Pro F2) was used to cleave the fibre. A similar experiment has been done by Canning [17], but it was on air-polymer structure fibre. A cylindrical lens was used to compress the beam from the laser as “knife-edge”. Then the fibre was placed in front of the beam and the images are captured by a CCD camera. The angle of the fibre was tilted such that the one end of the fibre was cut at right angle to its axis as shown in Fig. 5-27.

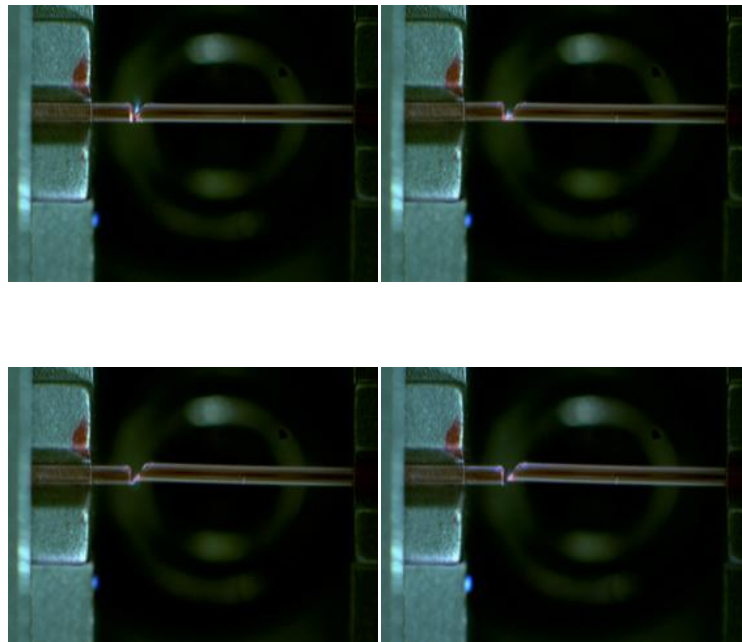


**Fig. 5-27. Photos of dye doped fibre being cut by 193nm ArF laser.**

The dye doped fibre was then put into the chamber to undergo gold coating process. As shown in Fig. 5-28, for each time, a pair of fibre were held by the reinforced fused silica tubes leaving a tip of the fibre emerging towards the gold. The current and pressure of the chamber were adjusted such that gold was coated on the fibre end without melting the fibre.

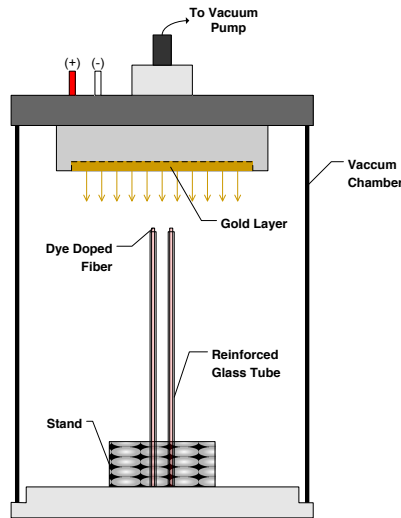


**Fig. 5-28. Schematic diagram showing how the end of dye doped fibre to be coated with gold.**

Totally there were 4 pieces of dye doped fibre were coated with gold at one end. From our measurement, the thickness of the gold was around 200nm. They were 10cm long each. They were put in the SIF setup as Fig. 5-23 respectively, where the pump was located in the middle of the fibre, i.e. 5cm. Their spectra were recorded and averaged. The result was compared with the spectrum of the dye doped fibre without gold coating shown in Fig. 5-29.

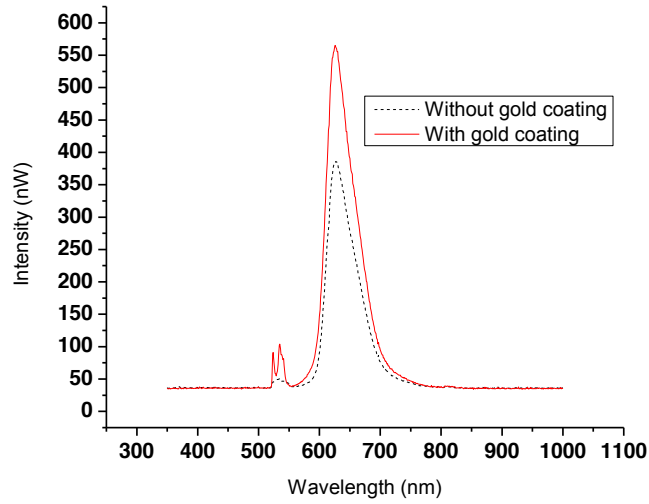


**Fig. 5-29. Graph of comparing fluorescence emission spectrum between dye doped fibre with and without gold coating.**

It was observed that emission spectrum from the dye doped fibre with gold coating experienced a bit red-shift. It could be explained that the reflected light from the gold coated end travelled a longer propagation distance through the fibre which coincided with the above result. It was calculated on average the peak power of the emission spectrum from the dye doped fibre with one end gold coated was ~45% larger than that of it without gold coating.

### 5.3.6 Application as Light Source in Sensor System

The conventional end-pumping experimental setup is shown in Fig. 5-30 [3,16]. Typically a frequency double Q-switched Nd:YAG laser at 532nm is used as the pump source. The light is focused and coupled into the dye-doped fibre using a lens. A microscopic objective is used to couple the output light from the dye-doped

fibre into a collecting fibre, which in turn connected to detectors and oscilloscope.

The emission spectrum is found by a conventional optical spectrum analyzer.

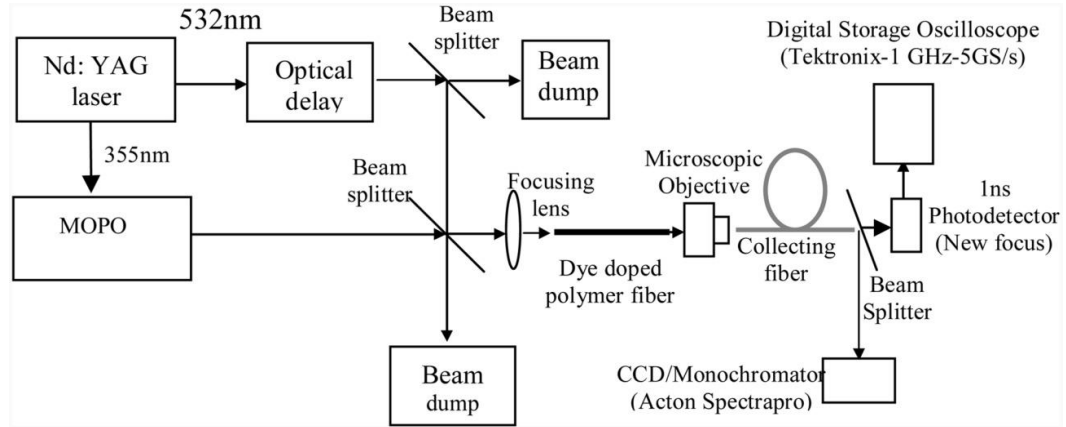


**Fig. 5-30. Experimental setup for pumping the dye doped fibre. (after reference [16]).**

In order to keep our polymer optical sensing system low cost and compact, we have simplified the experimental setup. As mentioned previously, the Nd:YAG laser was replaced by a very low-cost 532nm laser diode. Bulky optical components such as mirrors and lenses have also been eliminated. Then the dye-doped fibre was directly end-pumped by the laser diode as shown in Fig. 5-31. At the output end, the light from the dye-doped fibre was butt-coupled into the sensing fibre. The final output spectrum was found by a low-cost, CCD based spectrometer (Ocean Optics - USB650 Red-Tide™).

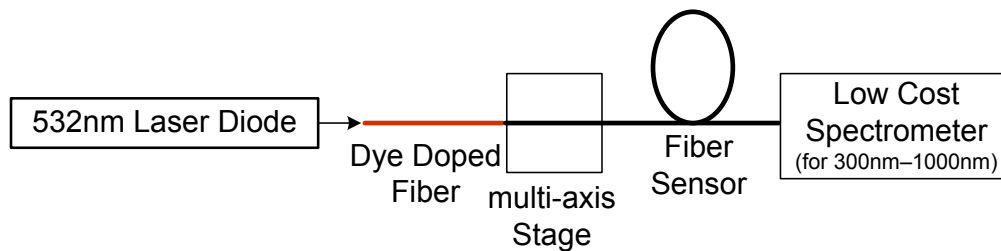


**Fig. 5-31.** Simplified experimental setup of pumping the dye-doped fibre and sensing system.

## 5.4 Conclusion

In this chapter, we have demonstrated how the laser dyes are possible to be doped into POFs and pumped by a low-cost laser diode to become a POF light source. Among different types of laser dyes, R6G, Rh640 and LDS751 are able to be doped into the POFs without losing their fluorescence properties after polymerization and drawing stage. It is also possible to co-dope them into the POFs to achieve a wider fluorescence spectrum over 100nm. We have shown the process to fabricate the dye doped fibre with cladding structure, which is to solve the problem of coupling loss with other available POFs. Both end-pumping and side-pumping technique were carried out and compared. It was concluded that side-pumping technique is superior in suppressing the pumping source spectrum and had many advantages, like the ability to scale up by using numbers of laser diode pumps at the same time (which will be discussed in Chapter 6). Detailed experiments had been done on the Rh640 doped fibre. It was found that the optical conversion efficiency of Rh640 in our case is around 1.509%. The value of the loss of the fibre was also calculated, which gives us useful information about determining the length of the fibre and the power of the pump source in practical applications. Through series of experiments, the effects of the power and position

of the pump source and the dye concentration on the fluorescence intensity and spectrum have been found. Furthermore, we have invented the method to enhance the output power of the dye doped fibre by over 40%, by coating layer of gold at the fibre one end. Finally a simple sensor system is proposed to show that the dye doped fibre light source was applicable in a POF sensing system.



## Reference

1. SCHÄFER, F. P., ed., "Dye Lasers", 3<sup>rd</sup> ed., Springer-Verlag (1990)
2. BARTLETT, R. J., PHILIP-CHANDY, R. and ELDRIDGE, P., "Plastic optical fibre sensors and devices," *Transactions of the Institute of Meas. and Control* 22, 431 (2000)
3. TAGAYA, A., KOIKE, Y., KINOSHITA, T., NIHEI, E., YAMAMOTO, T., and SASAKI, K., "Polymer optical fibre amplifier," *Appl. Phys. Lett.* 63, 883 (1993)
4. PENG, G. D., CHU, P. L., XIONG, Z., WHITBREAD, T. W., and CHAPLIN, R. P., "Dye-doped step-index polymer optical fibre for broadband amplification," *J. Light. Technol.* 14, 2215 (1996)
5. SHEEBA, M., RAJESH, M. and NAMPOORI, V. P. N., "Fabrication and characterization of dye mixture doped polymer optical fibre as a broad wavelength optical amplifier," *Appl. Opt.* 47, 1907 (2008)
6. KURIKI, K., KOBAYASHI, T., IMAI, N., TAMURA, T., NISHIHARA, S., TAGAYA, A., KOIKE, Y. and OKAMOTO, Y., "Fabrication and properties of polymer optical fibres containing Nd-Chelate," *IEEE Photon. Technol. Lett.* 12, 989 (2000).
7. Seymour, Carraher, "Polymer Chemistry," 7<sup>th</sup> Edition, ISBN: 1-4200-5102-4, CRC Press (2008)
8. Askadskii, A. A., "Physical properties of polymers prediction and contro", ISBN: 2- 88449-155-4, Gordon and Breach Publishers, The Netherlands (1996)

9. DAUM, W., KRAUSER, J., ZAMZOW, P. E., and ZIEMANN, O., "POF-Polymer Optical Fibres for Data Communication", ISBN: 3-540-42009-6, Springer-Verlag Berlin Herdelberg, Germany (2002)
10. KRUHLAK, R. J. and KUZYK, M. G., Side-illumination fluorescence spectroscopy. I. Principles," *J. OSA B-Optical Physics* 16, 1749 (1999)
11. DE LA ROSA-CRUZ, E., DIRK, C. W. and RODRIGUEZ, O., "Characterization of Fluorescence Induced by Side Illumination of Rhodamine B Doped Plastic Optical Fibres," *Fibre and Integrated Optics* 20, 457 (2001)
12. SHEEBA, M., RAJESH , M. and MATTEW, S., "Side illumination fluorescence emission characteristics from a dye doped polymer optical fibre under two-photon excitation," *Appl. Optics* 47, 1913 (2008)
13. BLINOVA, L. M., CIPPARRONE, G. and LAZAREV, V. V., "Planar amplifier for a microlaser on a cholesteric liquid crystal," *Appl. Phys. Lett.* 91, 061102 (2007)
14. DRAKE, J. M., LESIECKI, M. L., SANSREGRET, J., and THOMAS, W. R. L., "Organic dyes in PMMA in a planar luminescent solar collector: a performance evaluation," *Appl. Optics* 21, 2945 (1982)
15. AMAT-GUERRI, F., COSTELA, A. and FIGUERA, J. M., "Laser action from a rhodamine 640-doped copolymer of 2-hydroxyethyl methacrylate and methyl methacrylate," *Opt. Comm.* 114, 442 (1995)

16. RAJESH, M., SHEEBA, M. and GEETHA K., "Fabrication and characterization of dye-doped polymer optical fibre as a light amplifier," *Appl. Optics* 46, 106 (2007)
17. CANNING, J., BUCKLEY, E., GROOTHOFF, N., LUTHER-DAVIES, B. and ZAGARI, J., "UV laser cleaving of air-polymer structured fibre," *Opt. Comm.* 202, 139 (2002)
18. KUANG, K. S. C., CANTWELL, W. J. and SCULLY, P. J., "An evaluation of a novel plastic optical fibre sensor for axial strain and bend measurements," *Meas. Sci. and Technol.* 13, 1523 (2002)

## **Chapter 6 Enhancement of Side-illumination Fluorescence by Bending Method**

### **6.1 Introduction**

It was mentioned in the previous chapters that the side-illumination fluorescence (SIF) technique on POFs provides a promising method to make broadband light sources or eliminate coupling between light source and fiber sensor. This proposed novel technology could open up a wide range of inexpensive POF devices to make broadband fiber light sources and low-cost POF sensing systems. To date, most of the work done on laser-dye-doped POFs utilize PMMAs with a dye-doped core, where the fluorescence is generated and guided. Laser dye-doped POFs could also be used as a gain medium to amplify optical signals in the visible spectrum. [1] reported a polymer waveguide with Rh640-doped cladding was utilized for optical signal amplification at 650 nm. However, the attenuation of the guided fluorescence is very high when laser-dye is doped into the core, thus making laser dye-doped core fiber a rather weak light transmission channel.

In this Chapter, we describe a novel approach to eliminate the fiber loss due to laser dye by just doping the fiber cladding with Rh640. The laser dye Rh640 has high quantum efficiency (close to unity) [2] and the fluorescence spectrum is at the low-loss band of the POF. This was then side-pumped by a 532 nm laser diode, with fluorescence light at ~650 nm generated in the cladding, and coupled into the core where relatively low-loss guidance can be maintained in the fiber core with not laser dye dopant. More importantly, any section along the dye-doped POF can

act as an intrinsic light source when it is side-pumped, acting as a combined light source and light delivery system.

The important issue of this proposed novel POF is how to increase the coupling efficiency of generated fluorescence light into the core of the laser dye-doped clad POF. The following sections discussed how it can be achieved with a simple bending method experimentally. The modelling of the bending mechanism will also be shown to support the experimental results.

## **6.2 Principle of Bending Method**

It has been demonstrated that the SIF light can be increased by tapering a POF [3]. In the study, the POF was only coated with fluorescence ink on the surface of the tapered section. The working principle is based on improving the entry angle of the pump and fluorescence light ray-paths from the cladding to the core, thus the coupling of the fluorescence light into the core is enhanced significantly. We demonstrate a simple bending method to optimize the fluorescence light coupling to the fiber core with different incident angles to the POF. In our experiment, the dye-doped POF was side pumped with a compact and low-cost diode-pumped solid-state (DPSS) laser at 532 nm, instead of the more often used, larger laser systems such as He-Ne laser [4], [5], Nd:YAG laser [6] or other femtosecond lasers [7] in the past. The 532 nm DPSS lasers cost less than USD10 each and are commonly used in green laser pointers. These provide an excellent platform for low-cost and compact all-polymer optic sensor system for disposable biomedical application proposed elsewhere [8].

### 6.3 Design of Dye-doped-clad PMMA-core POF

As mentioned previously, a dye-doped-clad PMMA-core POF is preferable because the light will be guided inside a relatively low-loss material. In our experiment, the dye-doped POF was fabricated with cladding diameter of 300  $\mu\text{m}$  and core diameter of 136  $\mu\text{m}$ , with 3% tolerance. The cladding was doped with Rh640 of 50 ppm concentration; poly(benzyl methacrylate) (BzMA) was added to the core to increase the refractive index. An image of an illuminated cross-section of the POF is shown in the inset of Fig. 6-1. The high brightness of the fiber core shows that fluorescence light is coupled and guided in the fiber core.

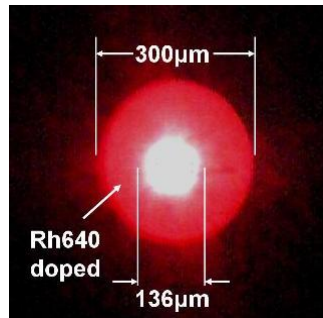


**Fig. 6-1. Cross-section of the dye-doped-clad, PMMA-core POF.**

The loss was measured using the multiple cut-back method. A length of 6.25 m was cut-back 50 mm each time for 45 times to 4 m. An end-coupled input with constant power at 655 nm was used, and the output power was measured for each cut-back length. The average loss was 3.129 dB/m at 655 nm, suitable for meters-long biomedical sensing applications. The mechanism of the light conversion/coupling using the SIF technique on the POF is illustrated in Fig. 6-2.

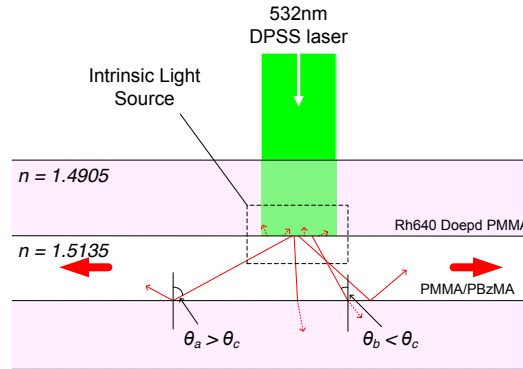


**Fig. 6-2. Mechanism of how a built-in light source is achieved by SIF technique on POF.**

Once the POF is side-illuminated with a pump laser, the chromophores absorb the pump energy and emit the fluorescence light isotropically. Especially at the cladding-core interface, the fluorescence light enters the high-index core and is guided in the core if the total internal reflection condition is satisfied. Although most of the fluorescence light will not be coupled to the fiber core and lost, but sufficient light can be made to couple to the fiber core for sensing purposes.

#### 6.4 Experimental Setup

The experimental setup for studying the coupling efficiency by bending is shown in Fig. 7.3(a). A length of 1.5 m of the dye-doped POF was bent near one end around different sizes of cylindrical stainless steel rods, one rod at a time. The rod radius varied from 0.4 mm to 6.3 mm. The surface of the rods was painted in black to avoid light reflections from the rods to simplify the model used to calculate SIF at the bend of the POF with different bending radius. However, using a good reflective surface rod would increase the coupling of fluorescence light to the fiber core.

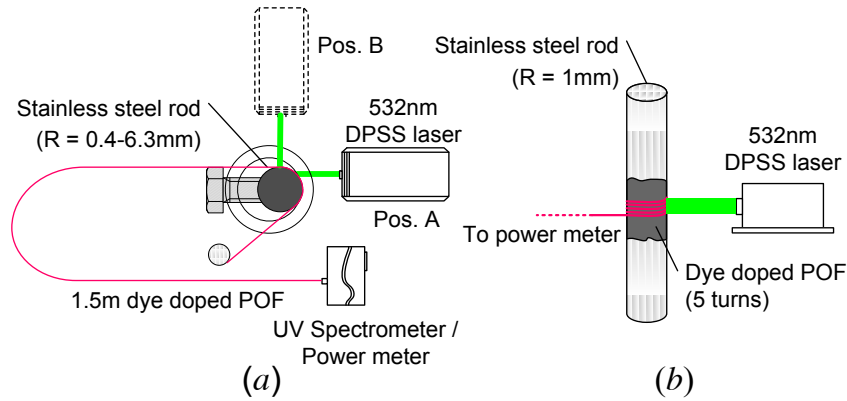


**Fig. 6-3. a) Experimental setup for POE under SIF with different bending radius; b) Experimental setup for POE under SIF with multiple bends on the stainless steel rod.**

A 25 mW CW DPSS laser at 532 nm was used to side-pump the POE. For comparison, the input pump light was arranged to enter the cladding of the dye-doped clad PMMA-core POE from two positions. The first position was at the bend, indicated as Pos. A in Fig. 6-3(a). The angle was adjusted each time until maximum fluorescence output is received (see Fig. 6-6). The second position Pos. B was at a straight section of the POE and as close to Pos. A as possible. The output fluorescence spectrum was recorded by a UV-spectrometer (USB-650, Ocean Optics), which the integration time was 100ms. The output power is measured by a powermeter (2936-C, Newport), which used a silicon photodetector (918D-UV-OD3, Newport) and sampling at 250kHz. The whole experiment was carried out in a dark laboratory to minimize any unwanted ambient light that might be captured by the POE. Moreover, for each measurement, the fluorescence data were taken quickly to minimize photobleaching in the dye, and sufficient recovery time was given in between consecutive data points [9].



It was expected that there were two main factors affecting the output fluorescence power – the entry angle of the fluorescence ray-paths and the bending loss of the POF. There is a trade-off between these two factors. An optimum bending radius can be found in which the maximum fluorescence output power is achieved.

## 6.5 Experimental Results

The results of the output fluorescence power and spectrum are shown in Fig. 6-4 and Fig. 6-5 respectively. Fig. 6-4 shows the normalized fluorescence output power with different input bending radius. It was found that the optimum bending radius was around 1 mm, where the maximum fluorescence output power was  $\sim 0.152 \mu\text{W}$ . In comparison, the fluorescence output power was  $\sim 0.0348 \mu\text{W}$  when pumping at the straight section of the fiber at Pos. B. Therefore, by using a simple bending method, the fluorescence power in the fiber core is at least 4 times greater than that was achieved when side-illuminating without bends.

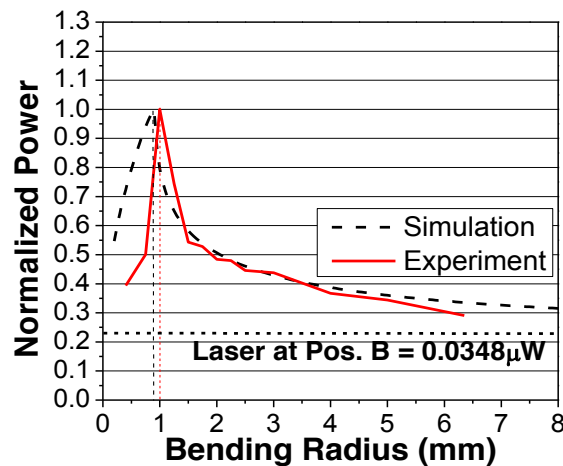
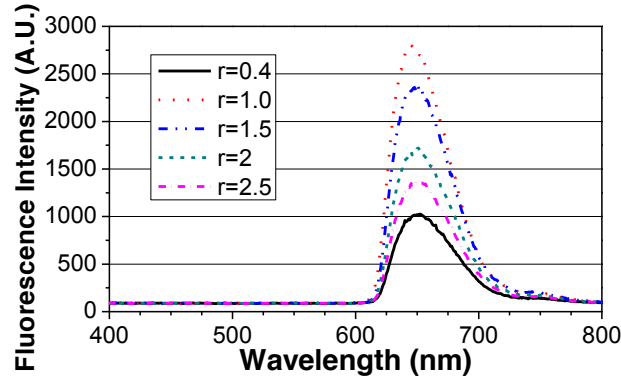


Fig. 6-4. The output fluorescence power of the POF with (a) different bending radius at the input.

The output spectra are shown in Fig. 6-5. It can be observed that the pump light at 532 nm was not detected at the output and the fluorescence peak was found at 649 nm. This suggests that the pump light was not guided by the POF and this is highly desirable, otherwise the received optical signals might be overwhelmed by the pump power.



**Figure**  
**Fig. 6-5. Output fluorescence spectrum of the POF with different bending radius at the input.**

The fluorescence power was further improved to >10 times ( $\sim 0.367 \mu\text{W}$ ) for multiple bends coiled around the rod as illustrated in Fig. 6-3(b). Under this condition, it took at least 45 min for the fluorescence output to drop to half of its initial value, provided that it was continually side-illuminated by the CW DPSS laser at 25mW with spot size of 1.5 mm. It is important to note that the photobleaching effect is not a critical issue here because the pump can be made to scan along the POF at a rate of about 30 min in step of 1.5-mm, to prolong the POF output power.

## 6.6 Modelling of Bending Mechanism

*(I would like to acknowledge that the work and calculations in this section is done*

*by Mr. Liu Zhengyong)*

The mechanism of the improved side-illumination fluorescence can be analyzed with ray optics. In order to describe the model, some assumptions are established:

1) Only the fluorescence emitted at the core-cladding interface covered by the pump source is considered. 2) Once the total internal reflection (TIR) condition is satisfied, the light beams can be guided in the fiber core. 3) The fiber is modeled with one quarter of a circle bend around the cylinder. 4) The intensity is the same for all incident direction (isotropic emission). 5) Each area cell  $ds$  is as the same for any point on the surface of the fiber.

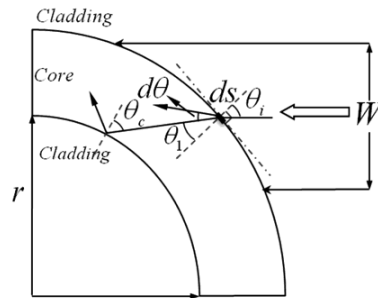


**Fig. 6-6. Fluorescence of one area cell with side-illumination on a bend POF with dye-doped cladding.**

The dye-doped cladding POF is side-illuminated by a uniform beam with width  $W$  and at a wavelength of 532 nm (See Fig. 6-6). For given illuminating area cell,  $ds$ , considering meridional ray (skew rays are ignored due to the high propagation loss), the power for small beams with incident angle  $d\theta$  is:

$$dP = I_0 d\Omega \quad \text{Equation 6-1}$$

where  $I_0$  is the luminous intensity per unit angle,  $\eta$  is the radiation efficiency per unit illumination area. The total power of the whole illuminated area  $S_{irrad}$ , irradiating into the core with angles from 0 to  $\theta$ , can be obtained from the integration of Equation 6-1, expressed as:

$$P = \int_0^\theta I_0 d\Omega = S_{irrad} \times I_0 \times \eta \quad \text{Equation 6-2}$$

From Fig. 6-6, if  $\theta_c$  is the critical angle for TIR and  $\theta_1$  is the angle of incident, then only light beams with incident angle larger than the critical incident angle  $\theta_1$  will be guided:

$$\theta_1 = \arcsin\left(\frac{n_{cladd}}{n_{core}} \cdot \frac{r}{r + 2r_{core}}\right) \quad \text{Equation 6-3}$$

where  $r$  and  $r_{core}$  are the bending radius and fiber core diameter respectively,  $n_{core}$  and  $n_{cladd}$  represent the refractive index of core and cladding respectively.

When the fiber is bent into a circle, the irradiating section (assuming the center of the irradiating section is the center of the arc) can be regarded as a torus. The illuminating area is calculated by Pappus Theorem:

$$S_{irrad} = 4 r_{core} \times (r + r_{core}) \times \arcsin\left[\frac{\sqrt{2}W}{2(r + 2r_{core})}\right] \quad \text{Equation 6-4}$$

substituting Equation 6-3 and Equation 6-4 into Equation 6-2, the total fluorescence power of the illuminating section with the width of  $L$  can be calculated as:

$$P = 4 I_0 \times r_{core} \times (r + r_{core}) \times \arcsin\left[\frac{\sqrt{2}W}{2(r + 2r_{core})}\right] \times \left[ \frac{1}{2} \arcsin\left(\frac{n_{clad}}{n_{core}} \times \frac{r}{r + 2r_{core}}\right) \right] \quad \text{Equation 6-5}$$

Assuming  $r_{core} = 68\mu\text{m}$ ,  $n_{clad} = 1.4905$ ,  $n_{core} = 1.5135$  and  $W = 1.5\text{ mm}$ , the normalized simulation result according to Equation 6-5 is shown in Fig. 6-4. It shows that the simulation result agreed reasonably well with the experimental data, especially the trends and magnitude.

## 6.7 Conclusion

In conclusions, a novel laser-dye-doped clad, PMMA-core POF has been proposed, designed and fabricated to provide a potentially low-cost POF sensing platform where light is generated in the cladding and couples to the fiber core anywhere along the POF with side pumping using low-cost semiconductor laser diodes. The core of the POF was not doped with laser dye so as to permit the coupled fluorescence light to propagate with relatively low attenuation. The cladding of the POF was doped with Rh640 and was successfully pumped by a compact and low-cost 532 nm laser source using the SIF technique. The fluorescence output power of the POF under SIF was enhanced by the proposed bending method by more than ten times. Most importantly, the issue of photobleaching of laser dye doped in the fiber cladding can be overcome by scanning the pump laser along the POF. This scheme offers a practical solution to convert and couple fluorescence light directly into the core of a POF. Furthermore, any point along the POF can act as a light source when that point is under SIF, and the spectrum remains the same along the because of the undoped core. These offer the dye-doped POF a good potential to be used as light source in a biomedical sensing system.

## Reference

1. REILLY, M. A., COLEMAN, B., PUN, E. Y. B., PENTY, R. V. and WHITE, I. H., "Optical gain at 650 nm from a polymer waveguide with dye-doped cladding," *Appl. Phys. Lett.*, vol. 87, 231116 (2005)
2. RAMON, M. C., ARIU, M., XIA, R., BRADLEY, D. D. C., REILLY, M. A., MARINELLI, C., MORGAN, C. N., PENTY, R. V. and WHITE, I. H., "A characterization of Rhodamine 640 for optical amplification: Collinear pump and signal gain properties in solutions, thin-film polymer dispersions, and waveguides," *J. Appl. Phys.*, vol. 97, 73517 (2005)
3. PULIDO, C. and ESTEBAN O., "Improved fluorescence signal with tapered polymer optical s under side-illumination," *Sens. Actuators, B Chem.*, vol. 146, pp. 190–194 (2010)
4. KRUHLAK, R. J. and KUZYK, M. G., Side-illumination fluorescence spectroscopy. II. Applications to squaraine-dye-doped polymer optical s," *J. Opt. Soc. Am. B*, vol. 16, 1756–1767, 1999.
5. DE LA ROSA-CRUZ, E., DIRK, C. W., RODRIGUEZ, P. and CASTANO, V. M., "Characterization of fluorescence induced by side illumination of Rhodamine B doped plastic optical s," *Integr. Opt.*, vol. 20, pp. 457–464, 2001.
6. SAITO, M. and KITAGAWA, K., "Axial and radial fluorescence of dye-doped polymer ," *J. of Lightwave Technol.*, vol. 19, 982–987, 2001
7. SHEEBA, M., REJESH, M., MATHEW, S., NAMPOORI, V. P. N., VALLABHAN, C. P. G. and RADHAKRISHNAN, P., "Side illumination

- fluorescence emission characteristics from a dye doped polymer optical under two-photon excitation,” *Appl. Opt.*, vol. 47, pp. 1913–1921, 2008.
8. TAM, H. Y., PUN, C. F. J., ZHOU, G. Y., CHENG, X. and TSE, M. L. V., “Special structured polymer s for sensing applications,” *Opt. Technol.* 16, pp. 357–366, 2010.
  9. PENG, G. D., XIONG, Z. and CHU, P. L., “Fluorescence decay and recovery in organic dye-doped polymer optical fibers,” *J. of Lightwave Technol.*, vol. 16, pp. 2365–2372, 1998.



## **Chapter 7      Novel Pumping Scheme to Overcome Photobleaching Effect**

### **7.1 Introduction**

In the previous chapter, a novel laser dye-doped clad, PMMA-doped core polymer optical fibre were proposed. We demonstrated light generation in the fiber cladding through side illumination/pumping and enhanced coupling of the generated fluorescence light to fiber core by bending the POF for sensing purposes. In this Chapter, we describe in more details the problem of photobleaching behavior of organic dyes in POFs and how it can be solved by some novel pumping schemes proposed in this study. This invention tackles two main issues: (1) light delivery to a polymer optical fibre sensors, and (2) rapid power degradation due to photobleaching of organic dye. We proposed two novel side-pumping schemes, which are based on a Switch-pumping (SwP) technique and a Scan-pumping (ScP) technique with laser sources. The proposed techniques are scalable by using multiple laser sources to increase the coupled optical power in the core of the POF. We will show how both pumping techniques utilize the property of fluorescence photobleaching recovery (FPR) of laser dyes and the technique of side illumination fluorescence (SIF). The experimental results of the SwP and ScP techniques on POFs will be presented and compared. Finally, we will propose how the novel pumping scheme can be applied in laser dye doped POFs with different designs and how such POFs can be used in sensing applications.

## 7.2 Bleaching Effect and Dye Recovery

Photobleaching is a dynamic process in which the chemical structure of laser dye is destroyed by the excitation light such that the dye loses its fluorescence ability. The rate of photobleaching is a function of the excitation intensity. The photobleaching process occurs over a period of minutes and hours, depending on the excitation intensity and the qualitative form of fluorescence degradation, is commonly observed. This is the main limitation in using laser dyes and laser-dye-doped POFs as a sensing device or broadband light source. We showed the effect of photobleaching in our experiment. A 12cm long Rh640-doped POF was side-pumped in the middle by a 532 nm DPSS laser. Power of the DPSS laser was adjusted such that the output power of the fluorescence from the fibre was around  $1.1\mu\text{W}$ . The POF was kept irradiated by the laser and the output power of the fluorescence was recorded for the first hour. The result is shown in Fig. 7-1.

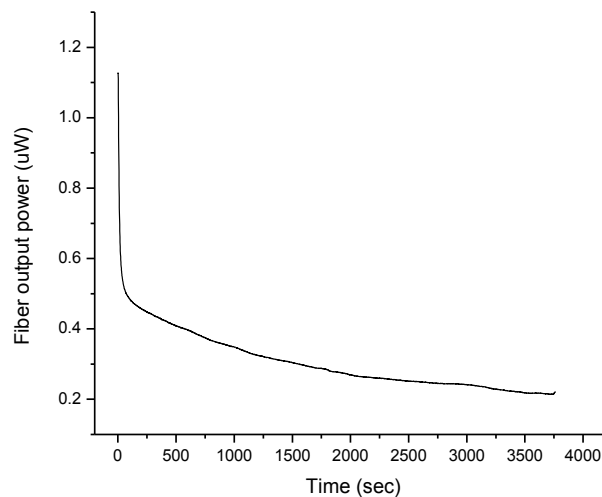


**Fig. 7-1. Photobleaching of laser dye-doped POF over a period of time.**

It can be observed that the fluorescence dropped very rapidly to less than half of its value in just several ten's of seconds and continued to drop even after 1 hour. This power degradation due to photobleaching made the laser dye-doped fibre not practical to act as a light source. This is an issue reported in many publications [1, 2, 3] and not easy to solve for laser dye-doped POFs with end-pumping configuration. To solve this problem, first of all, we proposed side-illumination excitation, and studied the principles of photobleaching and recovery of laser dyes.

The physical mechanisms of photobleaching of laser dye had not been well known until Song explained the photobleaching via photo-oxidation mechanism and dye-to-dye mechanism in 1995 [4] when the dyes were used in quantitative fluorescence microscopy. In mid-1970s, fluorescence photobleaching recovery kinetic was also studied and even applied Rhodamine B to measure cell mobility [5]. The first study of fluorescence bleaching and recovery in organic dye-doped POFs was reported by Peng in 1998 [6]. Rhodamine B was doped into PMMA-based POF and an Argon laser beam at 514nm wavelength was used as the pump source. It was found that the fluorescence in Rhodamine B could partially recover, at medium exposures of laser beam and even fully recover at low intensities. However, the photobleaching process became irreversible once the fluorescence suffered 30% drop in power comparing with its original value. Zhu [7] also reported on the dynamics of photodegradation and subsequent recovery of fluorescence in laser dye-doped polymer, which was also PMMA-based and the

dye was AF455. The polymer was pumped by a Nd:YAG laser with different pulse powers for 3 hours. After that, the laser beam was blocked to allow the dye to recover its fluorescence. The results showed that the dye was bleached and recovered with different rate for different pump powers. But one important issue had not been discussed by the author was that the dye recovery time is obviously longer than the bleaching time. It gives us an important clue to design a novel pumping scheme on the laser dye-doped POFs.

### **7.3 Novel Pumping Scheme**

The objective of the novel pumping scheme on the laser dye-doped clad, PMMA-doped core polymer optical fibre is to minimize the degradation of output fluorescence power due to the photobleaching effect of the laser dye. A continuous and reliable polymer light source could then be achieved, in which the output power is maintained at certain level for sufficient time for practical sensing applications.

The basic concept behind the novel pumping schemes is that the laser dye cannot be intensely pumped by the excitation light and to allow sufficient time for the laser dye to recover its fluorescence ability. It is found that the SIF technique on our dye-doped fibre is a good platform to satisfy these requirements. Subsequently, the two novel pumping schemes, i.e. switched-pumping (SwP) technique and scanning-pumping (ScP) technique are developed based on the SI technique. For all the experiments mentioned in this Chapter, unless specified, the fibre used is a

12-cm long air-clad Rh640 doped POF, which the diameter is 500 $\mu$ m and the dye concentration is 20ppm.

### 7.3.1 Switch-pumping technique (SwP)

The principle of SwP technique is that the dye-doped POF is side-pumped by several laser diodes alternately at different positions along the POF so that the laser dye doped in it, at any location, is only excited for a short time. The DPSS lasers are packed into array (see Fig. 7-2). At any instance, one or more lasers are “ON” and the rest are “OFF” to ensure that no one region of the POF is excited for longer time than necessary. By this means, the laser dye can recover its fluorescence when the laser is switched off. The “ON” and “OFF” operations of the laser diodes are swapped among each other such that the output power from the laser dye-doped fibre remains the same with acceptable margin even during the transition period.

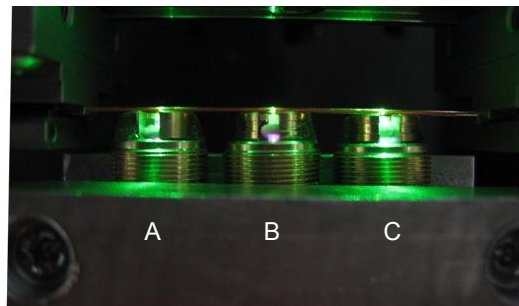


**Fig. 7-2. Photo of dye doped POF sided-pumped by an array of 3 green laser diodes, which are denoted by “A”, “B” and “C”, where “A” is the nearest to the detected fibre output.**

To show the feasibility of SwP technique, we must first prove that the output power of the laser dye-doped POF can be scaled up by pumping at multiple points. In this experiment, Laser A and Laser C were turned on, following a cycle of 10s “ON” and then 5s “OFF”. When Laser A or laser C was “ON”, the fibre output was around 0.5 $\mu$ W. The individual fibre outputs for Laser A and Laser C are shown in Fig. 7-3(i) and Fig. 7-3(ii), respectively. Then both laser diodes were synchronized to operate, the resultant fibre output power is shown in Fig. 7-3(iii).

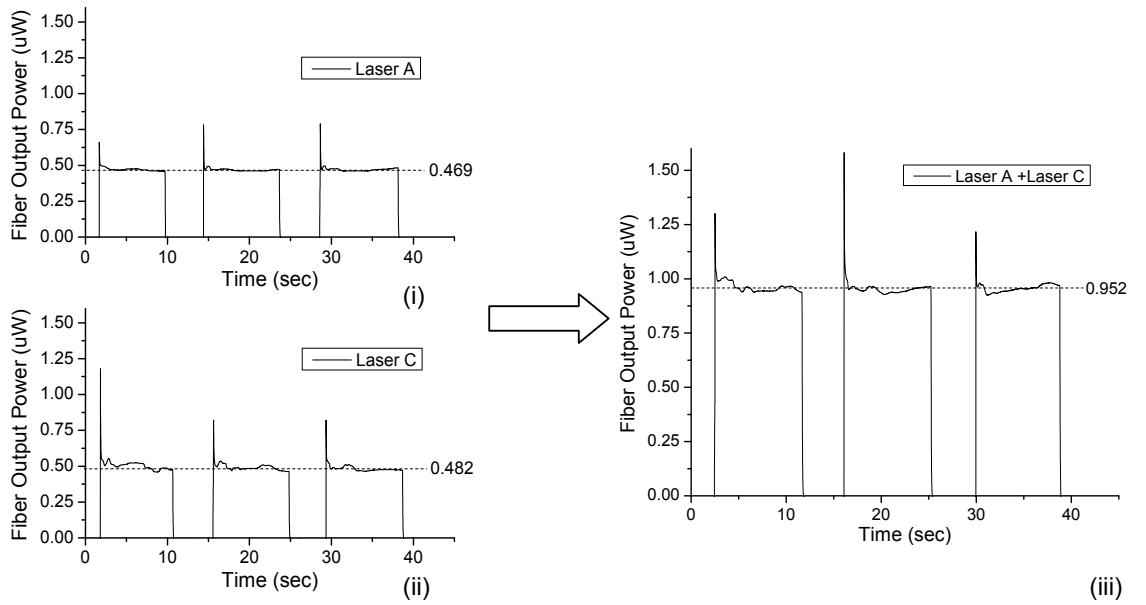


**Fig. 7-3. Graphs of fibre output power when (i) Laser A is in use; (ii) Laser C is in use; and (iii) both laser diodes operate.**

From the graph, the power output of the dyed doped POF pumped by both Laser A and Laser C is approximately equal to the sum of powers of the fibre pumped by

Laser A and Laser C individually. The result shows that the fibre output power can actually be scaled up by adding pump sources at different positions on the fibre. However, it is also observed from the graph that there is always a sudden jump of the output power at the start of the laser “on” command, which may introduce an unwanted signal, i.e. noise, if the fibre is used as a light source. It is suspected the immediate fluorescence power could be very large when the laser dye is rapidly excited by a relatively strong pump. Therefore gradual increase in the pump power is preferred when switching on the pump.

#### 7.3.1.1 Experimental Setup

The following experiment would give an example to show how SwP technique can be done. Three DPSS lasers were used as shown in Fig. 7-4.

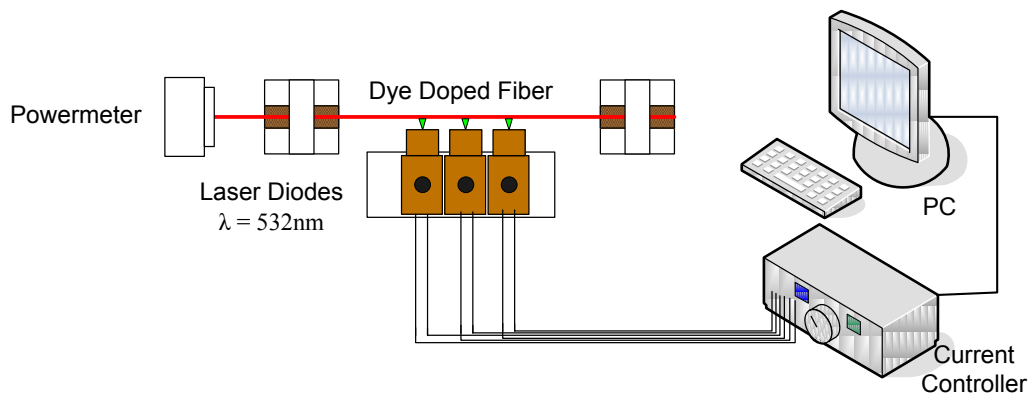


**Fig. 7-4. Experimental setup for multiple pumping technique on dye doped POF.**

Basically the DPSS lasers were controlled with certain power sequence to obtain the desire fibre output profile as illustrated in Fig. 7-5.

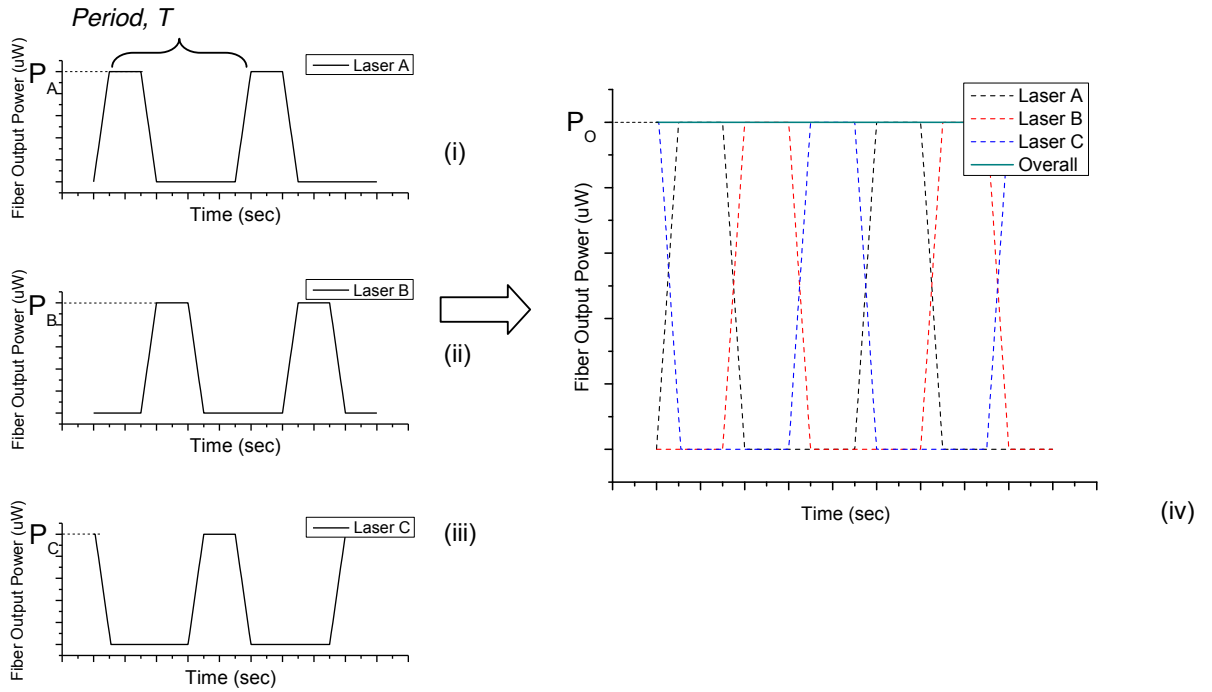


**Fig.7-5. Example of pumping profile e applied in the MPT for dye-doped POF.**

For simplicity, a trapezoidal profile was designed, so that during turning on a laser diode, the power would rise gradually to eliminate a sudden jump in fluorescence power. Moreover, according to the profile, the “off” time of the laser diode in each period was longer than the “on” time, which favour the condition for fluorescence photobleaching recovery (FPR). A time delay was added between each of the operating DPSS lasers. For the transition period between the DPSS lasers, the falling edge of the profile of the laser diode would compensate the rising edge of the profile of the following laser diode. As a result, when all the 3 DPSS lasers were under operation, ideally the output power of the fibre would remain constant, even during swapping between the DPSS lasers.



### 7.3.1.2 Experimental Results

In our experiments, we tried to maintain the fibre output power at  $1\mu\text{W}$ , i.e.  $P_A$ ,  $P_B$  and  $P_C = 1\mu\text{W}$ , (referring to Fig. 7-5), and the whole system operates for 90min. Three different sets of data for the fibre output were recorded for different period of the on-off cycle, i.e.  $T = 18\text{s}$ ,  $36\text{s}$  and  $72\text{s}$ . The results are shown in Fig. 7.6.

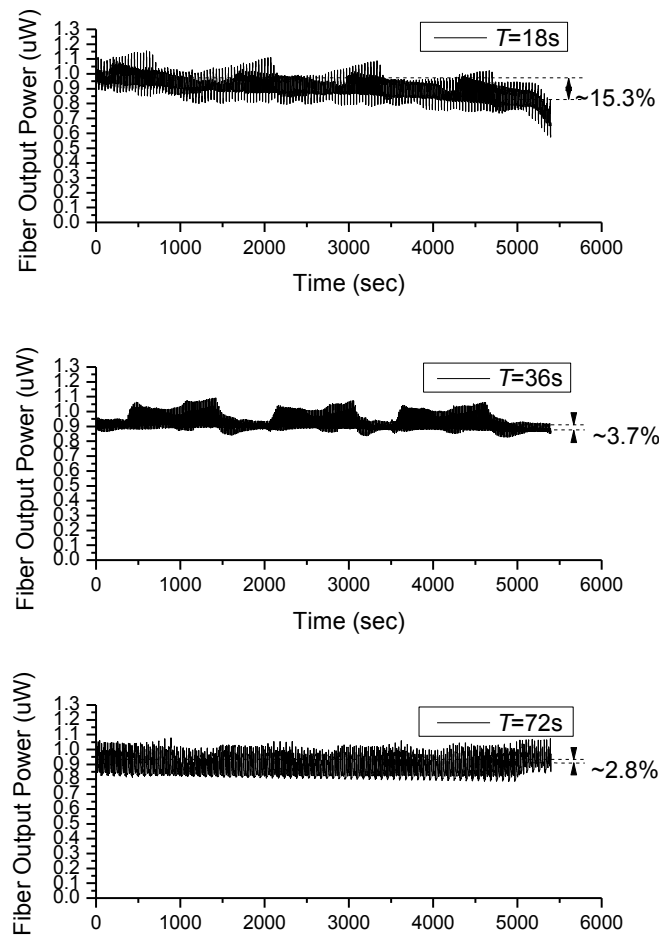


**Fig. 7-6. Fibre output power degradation for different periods of operating cycle by SwP technique with 3 laser diodes.**

It is observed from the graphs that the effect of the photobleaching of the dye-doped POF to output power of the fluorescence light had been reduced significantly compared with the result shown in Fig. 7-1. The improvement in terms of the fibre output power degradation was better when longer operating period of the DPSS lasers was used. It may be explained by the dye getting longer time to recover for longer operating period of the laser diodes. However, there were still small amount of photobleaching of the dye in each case. It was probably caused by the irreversible photobleaching mechanism happened in the laser dye.

### **7.3.2 Scan-Pumping (ScP) Technique**

The principle of scan-pumping technique (ScT) is that the laser dye-doped POF is side-pumped by a single DPSS laser, which is scanned along the fibre to and fro continuously. The output power of the POF can be easily scale up using multiple DPSS lasers scanning over different sections of the POF. The power of the laser diode is adjusted such that wherever the laser diode side-pumped along the POF, the fibre power output remains the same. More pump power is needed when the POF is pumped at a longer distance from its output end because the laser dye-doped fiber exhibits fairly high attenuation.

### 7.3.2.1 SPT Experimental Setup

The following experiment shows how the side-pump technique (SPT) work. As shown in Fig. 7-7, the laser diode was mounted on translation stage so that the fibre could be scanned by the laser beam over a distance of  $d$  cm.

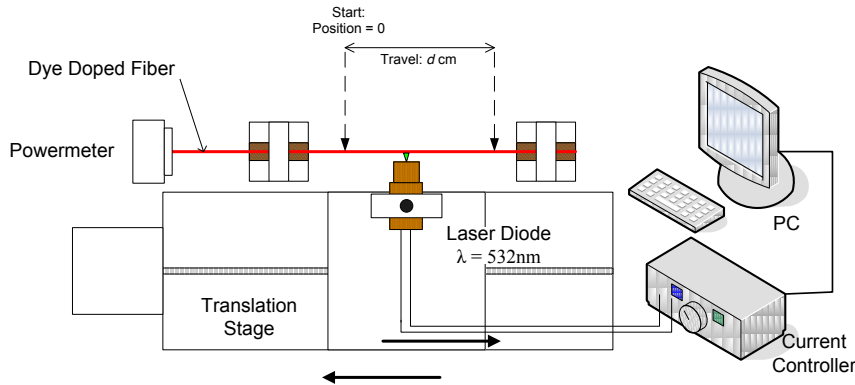


**Fig. 7-7. Experimental setup for SPT on dye doped POF.**

It is also reported by Kruhlak [8], the intensity of the fluorescence spectrum from the dye-doped POF decreases when the propagation distances increases. Therefore for SPT, refer to Fig. 7-7, when the laser diode travelled from the zero position to a distance of  $d$ , the power of the laser diode had to be increased accordingly to maintain the output power from the fibre at nearly the same level, i.e. power of the DPSS laser rose from  $P_{\min}$  to  $P_{\max}$ . It was expected the power of the laser diode would follow the profile as shown in Fig. 7-8, provided that the laser dye-doped POF was homogeneous and the fibre loss was proportional to the length.

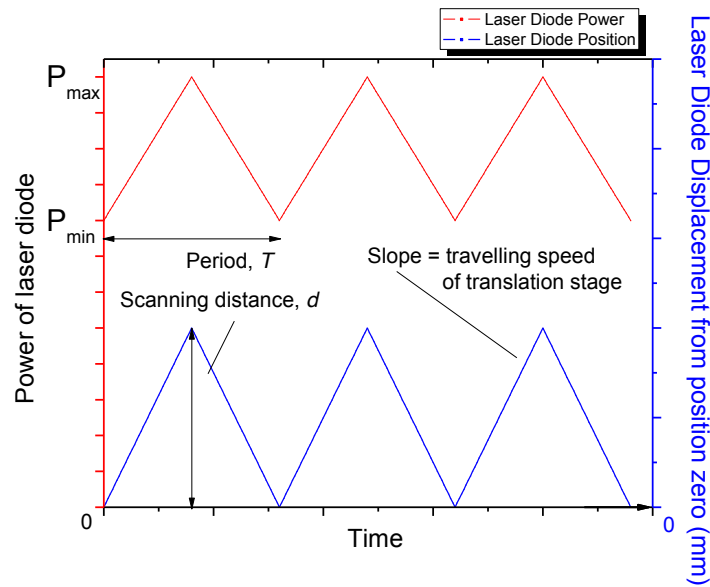
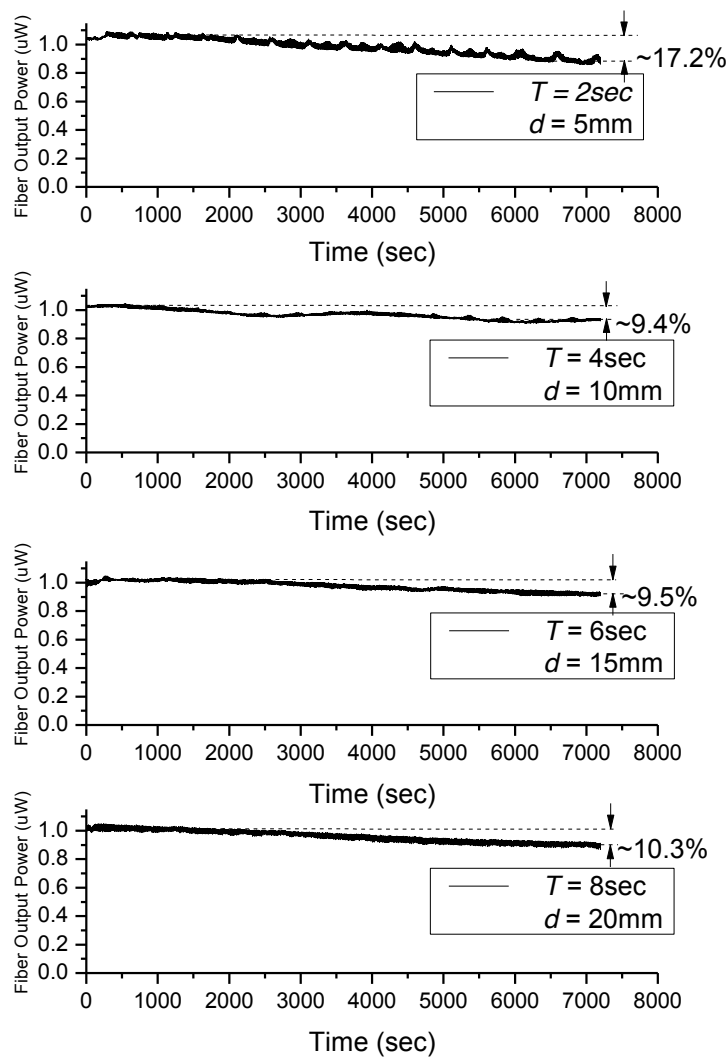


Fig. 7-8. Control of laser diode power according to its displacement from a reference point.

### 7.3.2.2 Experimental Results

In our experiments, a single laser diode “A” was used to get the fibre output power at around  $1\mu\text{W}$  throughout its scanning process. The travelling speed of the translation was  $5\text{mm/sec}$ . Three different sets of data for the fibre output were recorded for  $T = 2\text{s}$ ,  $4\text{s}$ ,  $6\text{s}$  and  $8\text{s}$ , i.e. scanning length,  $d = 5\text{mm}$ ,  $10\text{mm}$ ,  $15\text{mm}$  and  $20\text{mm}$  respectively. The results are shown in Fig. 7-9.



**Fig. 7-9. Fibre output power for different scanning length by ScP technique with a single laser diode.**

From the graph, ScP technique obviously reduced the effect of photobleaching of the dye. More importantly, the power spikes are virtually eliminated. For a relative short scanning length of 5mm, the photobleaching of the dye was still apparent. This is due to the fact that the time provided for the laser dye to recover its

fluorescent ability was not adequate. When the scanning length was increased to 10mm, 15mm, and 20mm, the effect of photobleaching was more or less the same. It is suspected that the loss in power was due to the irreversible photobleaching of the dye. Even if the laser dye was given longer time for recovery, there was already some irreversible photobleaching. However, the output power can still maintained at about 90% even after 2 hours of operation. The power degradation is quite linear and so 10 hours of operation can be expected if 50% power degradation is acceptable.

In the following experiment, it would show how effective of the ScP technique that retained the output power of the laser dye-doped POF. The laser dye-doped fibre was pumped by a single DPSS laser “A” used previously, where period,  $T = 6\text{sec}$  and scanning length,  $d = 15\text{mm}$ . At start, the output power of the fibre was around  $1\mu\text{W}$ . After working for 2 hours, the translation stage stopped at the starting point and the fibre was kept side-pump by the laser diode with constant power for 1 hour. The result is shown in Fig. 7-10.

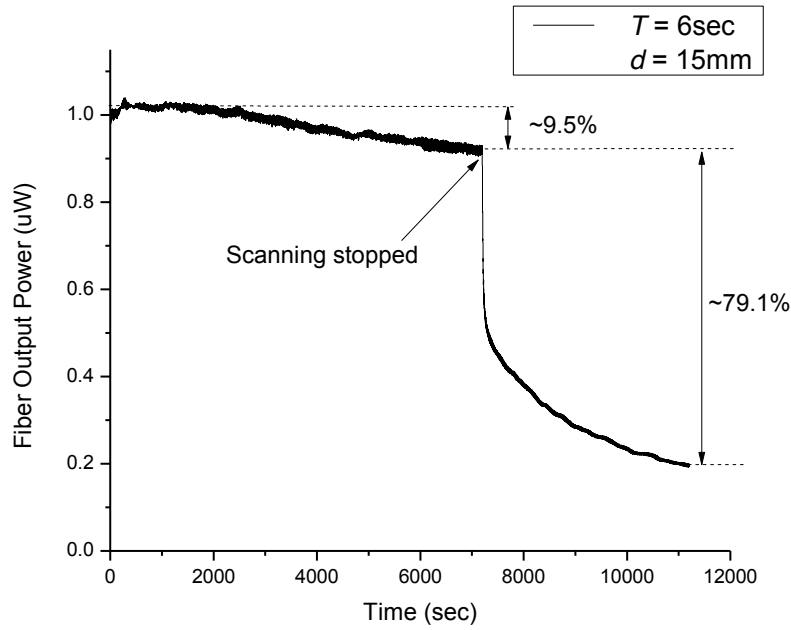


**Fig. 7-10. Illustration of effectiveness of ScP technique for laser dye-doped POF.**

It can be read from the graph that for the first two hours with ScP, the output power of the fibre dropped for around 9.5%. However, once the scanning stops, the pump laser induced a severe photobleaching on the dye. The output power of the fibre fell further to near 79.1% within an hour! In other words, the ScP technique is very effective on the laser dye-doped POF to maintain its output power.

The ScP technique can be carried out by scanning multiple laser diodes at the same time. The following experiment shows how the ScP technique can work by using two laser diodes. Laser “A” and Laser “B” are used. The total power was adjusted so that the fibre output power was around  $1.2\mu\text{W}$ . Then ScP technique was applied

by using these DPSS lasers, where the period,  $T = 2\text{sec}$  and the scanning length,  $d = 5\text{mm}$  for each of the DPSS lasers. The result is shown in Fig. 7-11.

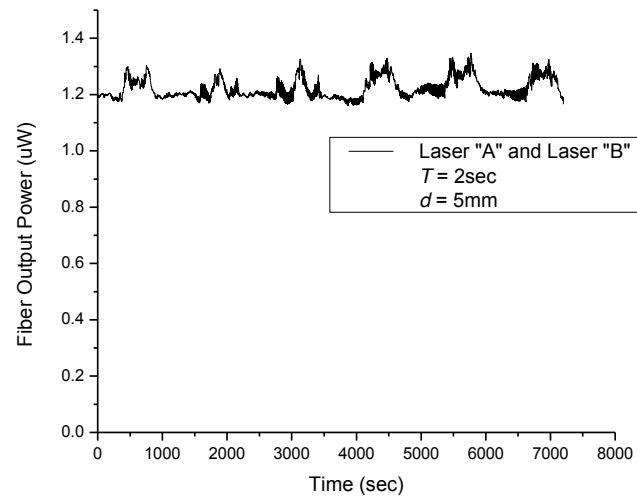


**Fig. 7-11. Fibre output power by ScP technique with using two laser diodes.**

It is found from the graph that the output power of the dye-doped POF nearly remained at the same level after two hours of side-illumination. The photobleaching effect was minimized as the laser dye was pumped locally with a smaller pump power. For higher power requirement, more laser diodes can be used at the same time in the ScP technique.



### 7.3.3 Comparison between SwP and ScP

In summary, advantages and disadvantages of the SwP and ScP techniques are shown in Table 7.1.

**Table 7.1. Summary of advantages and disadvantages of the SwP and ScP techniques**

Switch-pumping Technique (SwP)	Scan-pumping Technique (ScP)
<p><b>Advantage:</b></p> <ol style="list-style-type: none"><li>1. For high power operation, multiple laser diodes can be used</li></ol>	<p><b>Advantage:</b></p> <ol style="list-style-type: none"><li>1. Tuning process is easier for the laser diodes as the profile is simpler.</li><li>2. Photobleaching is nearly eliminated and there is sufficient time for it to recover.</li><li>3. Lower power consumption, as the dye is not intensely photobleached for a long time, early stage of fluorescence which the intensity is higher can be utilized</li></ol>
<p><b>Disadvantage:</b></p> <ol style="list-style-type: none"><li>1. Each laser diode has to be individually tuned and the profile is more complicated.</li><li>2. Space problem on the number of laser diodes can be packed.</li></ol>	<p><b>Disadvantage:</b></p> <ol style="list-style-type: none"><li>1. A translation stage is needed leading to higher cost and maintenance in moving parts. The whole system collapse if the translation is broken out.</li><li>2. For high power operation, when numbers of laser diodes are used, but leads to space problem, as the light beams of them should not be overlapped.</li></ol>

## 7.4 Proposal of Various Pumping Scheme for Laser Dye-Doped POFs

In the following, various pumping schemes of SIF on laser dye-doped POF are proposed (shown in Fig. 7-12). The pumping scheme may make use of SwP or ScP technique, or a combination of both techniques.

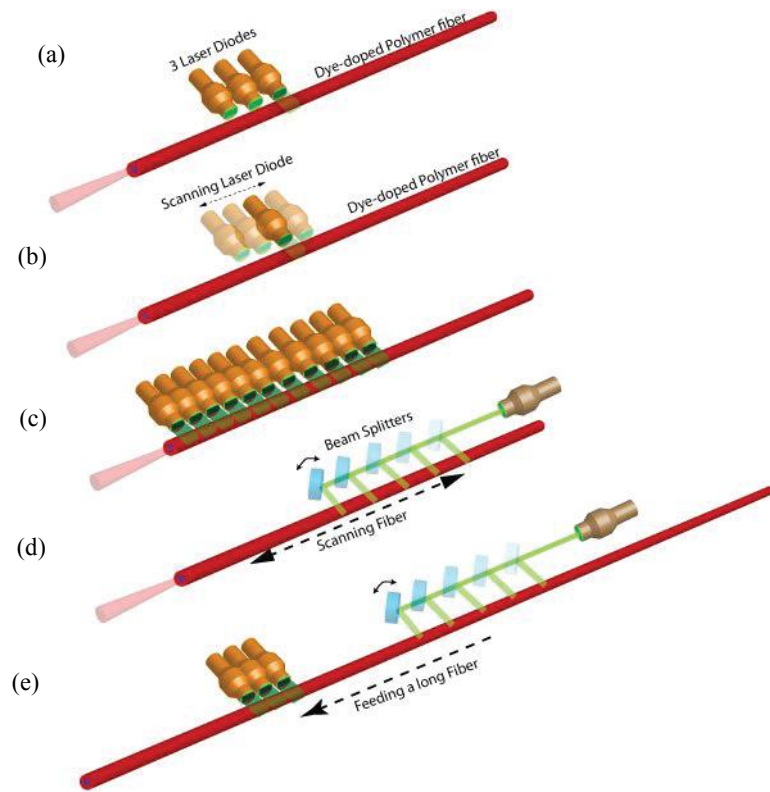


**Fig. 7-12 Various pumping schemes for SIF on laser dye doped POF**

Fig. 7-12 (a) and (b) shows the set-up of using SwP and ScP techniques in our experiments. For high power applications, it is proposed larger numbers of lasers can be added for either SwP or ScP techniques, as it has been shown previously that the laser can be easily scaled-up. From Fig. 7-12 (d), beam splitters can be

used to power-split the pumping source and scan along the laser dye doped fibre, so that the fibre will not be heavily photobleached. From Fig. 7-12 (e), it shows that it is also possible to mix SwP and ScP techniques on the same fibre.

## **7.5 Applications in Fibre Sensing Systems**

The importance of our invention is to combine light source and sensing elements into a single laser dye-doped POF. The applications of the fibre in the fibre sensing systems, especially in biomedical field, depends on the structure of the dye-doped fibre and the available fibre sensing technology. For instance, even a piece of multi-mode SI-POF can be used as a sensor itself for curvature and strain measurements by loss-based applications [9]. Then our proposed laser dye-doped POF can be made as a multi-mode SI-POF for the same applications. The sensing elements for the dye doped POF may include intrinsic types of fibre sensors such as fibre Bragg gratings (FBGs) and long period gratings (LPGs). FBGs can be written into a single-mode POF [10]. Therefore a single-mode POF which is doped with the laser dye emitting the desirable wavelength for Bragg reflection will become a good sensing fibre by writing FBGs into it. The system will be compact and solves the coupling problem between the fibre and the light source. Similarly, it is also possible to create LPGs in dye-doped multi-mode POF and mPOF for sensing applications just like what Li [11] and Hiscocks [12] did respectively but using PMMA-based fibres without laser dye doped. As reported by Homola [13], optical sensors based on the excitation of surface plasmons (SP) have proven to hold great potential for biomolecular interaction analysis and detection of

biological analytes. Wang [14] has demonstrated surface plasmon resonance sensor on an mPOF. Consequently, our laser dye-doped POFs also have potential to be applied in this technology.

## 7.6 Conclusion

In this Chapter, firstly we have demonstrated that the output power of the laser dye-doped POF can be scaled up by SIF technique using multiple pumping points. By exploiting the phenomenon of fluorescence photobleaching recovery, two novel pumping schemes were proposed, based on a SwP technique and a ScP technique with single or multiple laser diodes, to overcome the power degradation problems arising from the photobleaching of the dyes. Generally for both pumping techniques, the total output power deterioration is less than 10% when the dye-doped POF has been continuously pumped by the laser diode(s) to give 1 $\mu$ W optical output for 90min. The pros and cons between SwP and ScP techniques have been described. The side-pump SwP and ScP techniques have great potential to be employed for the interrogation of sensing devices based on Bragg gratings (FBGs), long period gratings (LPGs), or surface plasmons (SP) resonance, such that the light source and the sensing element are combined in a single laser dye-doped fibre.

## Reference

1. WEBER, J., "Photobleaching of rhodamin 6 G dye laser by flashlamp exciting", *Phys. Lett.* 37A, 749 (1971)
2. IPPEN, E., "Rapid photobleaching of organic laser dyes in continuously operated devices", *J. of Quan. Elect.* 7, 178 (1971)
3. KAMINOW, P., STULZ, L. W., CHANDROSS, E. A. and PRYDE, C. A., "Photobleaching of Organic Laser Dyes In Solid Matrices", *Appl. Opt.* 11, 1563 (1972)
4. SONG, L. L., HENNINK, E. J. and YOUNG, I. T., "Photobleaching Kinetics of Fluorescein in Quantitative Fluorescence Microscopy," *Biophysical Journal* 68, 2588 (1995)
5. AXEROD, D., KOPPEL, D. E., SCHLESSINGER, J., ELSON, E. and WEBB, W., "Mobility measurement by analysis of fluorescence photobleaching recovery kinetics," *Biophysical Journal* 16, 1005 (1976)
6. PENG, G. D., XIONG, Z. J. and CHU, P. L., "Fluorescence Decay and Recovery in Organic Dye-Doped Polymer Optical Fibres," *J. Lightw. Techno.* 16, 2365 (1998)
7. ZHU, Y., ZHOU, J. F. and KUZYK, M. G., "Two-photon fluorescence measurements of reversible photodegradation in a dye-doped polymer," *Opt. Lett.* 32, 958 (2007)
8. KRUHLAK, R. J. and KUZYK, M. G., "Side-illumination fluorescence spectroscopy. II. Applications to squaraine-dye-doped polymer optical fibres," *J. OSA B-Optical Physics* 16, 1756 (1999)

9. KUANG, K. S. C., CANTWELL, W. J. and SCULLY, P. J. , “An evaluation of a novel plastic optical fibre sensor for axial strain and bend measurements,” *Meas. Sci. and Technol.* 13, 1523 (2002)
10. XIONG, Z., PENG, G. D., WU, B. and CHU, P. L., “Highly tunable Bragg gratings in single-mode polymer optical fibres,” *IEEE Photon. Technol. Lett.* 11, 352 (1999).
11. LI, Z. C., TAM, H. Y. and XU, L. X., “Fabrication of long-period gratings in poly(methyl methacrylate-co-methyl vinyl ketone-cobenzyl methacrylate)-core polymer optical fibre by use of a mercury lamp,” *Opt. Lett* 30, 1117 (2005)
12. HISCOCKS, M. P., VAN EIJKELNBORG, M. A., ARGYROS, A. and LARGE, M. C. J., “Stable imprinting of long-period gratings in microstructured polymer optical fibre,” *Opt. Express* 14, 4644 (2006)
13. HOMOLA, J., ”Optical fibre sensor based on surface plasmon resonance excitation,” *Sens. Actuators B* 29, 401 (1995).
14. WANG, A., DOCHERTY, A. and KUHLMEY, B. T., ”Surface Plasmon Resonance in lotted Microstructured Polymer Optical fibres,” *Proc. Of 8<sup>th</sup> Inter. Conference on Materials for Advanced Techno.*, Singapore, 41 -43 (2009)

## **Chapter 8 Low-loss Single-mode Perfluorinated Polymer Optical Fibre**

### **8.1 Introduction**

In this Chapter, we are going to discuss how low-loss single-mode perfluorinated polymer optical fibre (PPOF) was fabricated. Firstly, the reasons and importance, especially for fibre grating, of such kind of fibres will be discussed. We will explain how the fibre was particularly useful for biomedical applications by its relative low refractive index of 1.34. The design of the fibre will also be covered that how the fibre could be made from commercial low-loss multi-mode PPOF. We will also investigate the difficulties we had reached to draw the fibre and what the optimum drawing condition for the fibre was. Lastly, the experiments and the results will be demonstrated to understand the optical characteristics of the fibre.

### **8.2 Importance of fabricating low-loss single-mode PPOF**

It is known that FBGs are usually written in single-mode optical fibres so that the Bragg reflection spectrum contains a single peak of the fundamental mode for ease of demodulation of measurand-induced Bragg wavelength shift. For some information about development, fibre Bragg gratings (FBGs) were successfully written in single-mode PMMA based POFs in 1999 [1]. However, so far virtually all reported polymeric FBGs were written at 1550nm telecommunication window [2], [3]. It could be explained by the ready maturity and availability of fibre-optic components and FBG interrogators at that particular wavelength band



However, at this band, the attenuation of PMMA-based POF is extremely large. This results in the limitation of the useful length of the POF to about 10cm as well as its sensing application. The transmission loss of PMMA-based POF can be explained by the absorption of hydrocarbon (C-H) bonds. PMMA contains mainly C-H bonds, in which the overtones of these bonds occur at wavelength from 1300 to 1650nm, resulting in high intrinsic loss at 1550nm [4]. To solve the problem, PPOF could be used which has much lower transmission loss than PMMA. This can be explained in term of vibration frequency. The vibration frequency ( $f_v$ ) is given by Equation 8-1:

$$f_v = \frac{\sqrt{k / \mu}}{2\pi} \quad \text{Equation 8-1}$$

where  $k$  and  $\mu$  are the bond force constant and the effective reduced mass respectively. PPOF contains fluorine atoms which effective masses are much higher than hydrogen atoms in PMMA [5], so the fluorocarbon (C-F) bond overtones are far away from 600-1650nm wavelength. This results in the intrinsic absorption loss of C-F bonds in is several orders of magnitude lower than that of C-H bonds at 1300-1650nm wavelength [6].

On the other hand, high photosensitivity is also essential for writing FBGs. It had been demonstrated that FBGs were possible to be written on PPOF [7]. Furthermore from the same research group, in the form of polymer film, perfluorinated polymer performed better thermal stability of FBGs than both

PMMA and silica fibres [8]. Therefore our low-loss single-mode POF was also based on perfluorinated polymer, which was suitable for the fabrication of FBGs operating at 1310 to 1550nm wavelength range. Moreover, due the relative low refractive index (1.34) of the perfluorinated polymer, the low-loss single-mode PPOF becomes an attractive candidate to realize practical POF grating biosensor. It is because its refractive index is close to that of aqueous solutions of biomaterials, permitting strong optical coupling for biomaterial sensing applications.

### 8.3 Design of single-mode PPOF

The fundamental design problem was how to make use of perfluorinated polymer to fabricate single-mode POF. However, fabrication of single-mode POFs is not easy in control dopant diffusion at both preform polymerization and drawing stage. It is not easy to maintain the refractive index profile and thus the effective diameter of the fibre core for single-mode operation. Besides that our laboratory is not equipped with proper facilities for handling fluorine, which is an extremely toxic material. Therefore we aimed at making use of commercially available multi-mode PPOF to draw it into single-mode fibre, which was our fibre redrawing method.

The graded-index multimode PPOF used in the experiments was taken from Asahi Glass Company, which model number was Lucina™. Fig. 8-1 shows the structure of the Lucina™ and its photo of cross section under microscope.

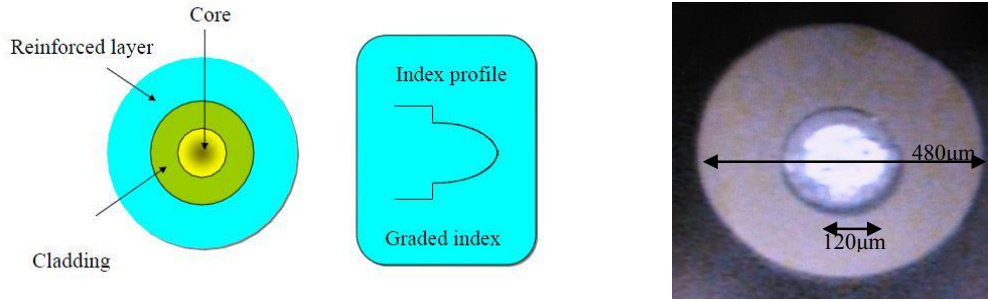


**Fig. 8-1. (left) Structure of Lucina™ reinforced fibre and (right) photo of cross section of that fibre under microscope.**

The core and cladding diameters are 120µm and 480µm respectively. The index profile is approximately parabolic, with core refractive index of 1.355 and cladding refractive index of 1.342. There is enough information to determine the draw-down ratio  $\delta$ , such that the multimode fibre is drawn down to become single-mode at 1550nm.

For a graded-index fibre, the cutoff for the normalized frequency  $V_c$  to support single-mode is governed by Equation 8-2 [9]:

$$V_c = 2.405 \sqrt{1 + \frac{2}{\alpha}} \quad \text{Equation 8-2}$$

where  $\alpha$  is the profile parameter. For parabolic profile,  $\alpha=2$ , then  $V_c \geq 3.4$  for grade-index fibre to operate in single-mode. The normalized frequency is defined in Equation 8-3:

$$V_c = \frac{2\pi a}{\lambda} \sqrt{(n_0^2 - n_c^2)} \quad \text{Equation 8-3}$$

where  $a$  is the core radius and  $\lambda$  is the operating wavelength for the single-mode fibre,  $n_0$  and  $n_c$  are the refractive indexes of the fibre core and cladding

respectively. After solving Equation 8-2 and Equation 8-3 by substituting the Lucina<sup>TM</sup> fibre parameters, the fibre core radius would be  $<4.48$ . In other words, the core of Lucina<sup>TM</sup> fibre has to be drawn from  $130\mu\text{m}$  to less than  $7.57\mu\text{m}$  and  $8.96\mu\text{m}$  for single-mode at  $1310\text{nm}$  and  $1550\text{nm}$  wavelength respectively, which the corresponding values of  $\delta$  are  $15.85$  and  $13.39$  respectively.

#### 8.4 Fabrication of single-mode PPOF

The redrawing method is adopted to draw the multimode PPOF in into single-mode PPOF. Generally, the Lucina<sup>TM</sup> fibre is inserted into a hollow preform and then the whole preform is drawn in the POF drawing tower to a desirable diameter, such that the core of the PPOF becomes small enough to guide the light with single-mode as shown in Fig. 8-2 .

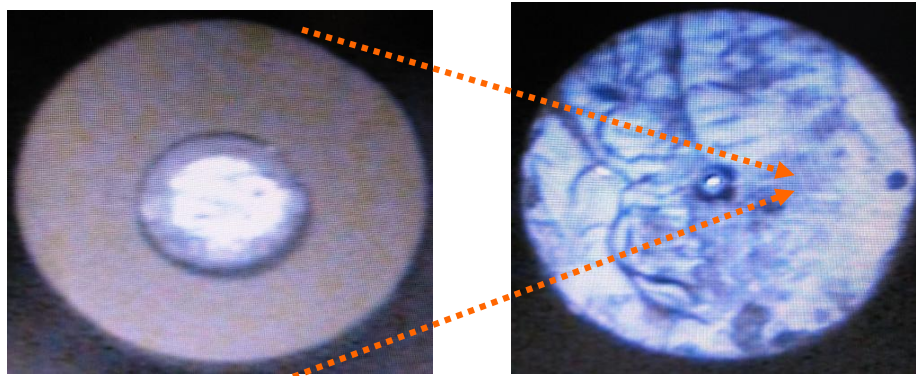


**Fig. 8-2. Illustration of how multimode Asahi fibre is drawn into single-mode.**

The preform was mainly composed of MMA and BMA with molar ratio of 75:25, added with 0.1mol% of LP and 0.25mol% of DT. A glass tubes with inner diameter of 8mm and length of around 20cm was used as the mould for the preform. A

Teflon string with outer diameter of 0.8mm was fixed the centre of the mould. The process of fabrication process is just as that described in Fig., but stopped at Stage B, leaving the preform with 0.8mm hollow centre. Then the Lucina™ fibre was inserted into the preform and fixed by a knot made at the top of the PPOF. Then the whole preform was held by the preform adaptor and drawn at the POF draw tower with suitable vacuum pressure.

#### 8.4.1 Drawing Difficulty

The critical issue in drawing the preform of the single-mode PPOF is to ensure the graded-index profile of the multimode fibre is maintained during the entire process from preform making and fibre drawing. Fig. 8-3 shows the cross section of the successfully drawn single-mode PPOF under microscope and its approximate refractive index profile. The core diameter is around 6.6μm and the cladding diameter is around 400μm. It can be predicted that the refractive index profile is maintained, such that the light can be guided through the centre core.

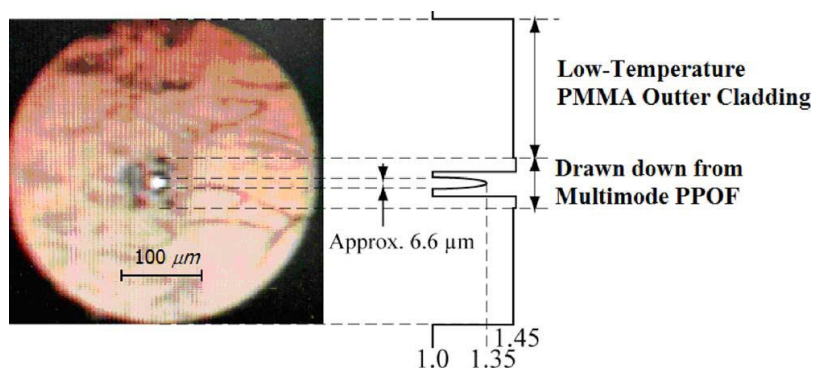
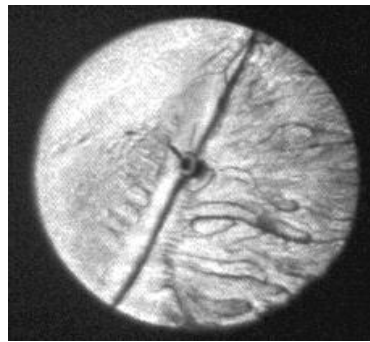


Fig. 8-3. Cross section of the single-mode PPOF and its approximate refractive index profile.

However it is not easy to draw this kind of fibre. If the drawing temperature is too high, then the core material of the PPOF will become molten and diffuse. The graded index profile is destroyed. As the perfluorinated polymer has a low refractive index than PMMA, which means the refractive index of the core is lower than that of the cladding, then the light cannot be guided through the core as shown in Fig 8-4.



**Fig. 8-4. Cross section of PPOF with "dark" core**

On the other hand, the drawing temperature cannot be too low. Otherwise, the preform cannot drop out from the furnace of the POF draw tower; even if it does, the fibre will be very brittle and broken easily when being cleaved. Therefore the temperature control is a crucial factor. Preferably the induction heater, which is what we use in the POF draw tower, is used for drawing this kind of fibre. It is because the preform is being heated unevenly from the outside to the inside by conduction. Then the temperature of the cladding is high enough to melt the PMMA; while the temperature of the PPOF core is low enough to prevent destruction of the graded index profile. Usually for the preform with 8mm diameter, the feeding speed is 120 $\mu$ m/s, the take-up speed varied from 20-30mm/s depending

on the draw ratio, the furnace temperature is kept around 215 to 220°C, and the drawing tension is kept a relatively high value from 100 to 150cN.

#### 8.4.2 Vacuum Pressure Control

It can be observed from Fig. 8-3 that there is an air gap between the Lucina™ fibre and the PMMA cladding. Even for the Lucina™ fibre itself, there is also an air gap between the inside fibre and the reinforced layer. These air gaps may inhibit the FBGs formation during the writing process. To maximize the air gaps, negative pressure is given to the inside of the preform during the drawing process. It has been mentioned in Chapter 3.2.2 about the tower feeding unit that the preform adaptor was designed with the air fitting to be connected with the vacuum controller. Fig. 8-5 shows the comparison between the single-mode PPOF drawn with and without vacuum treatment. For the one with vacuum pump, the pressure was set to 40kPa.

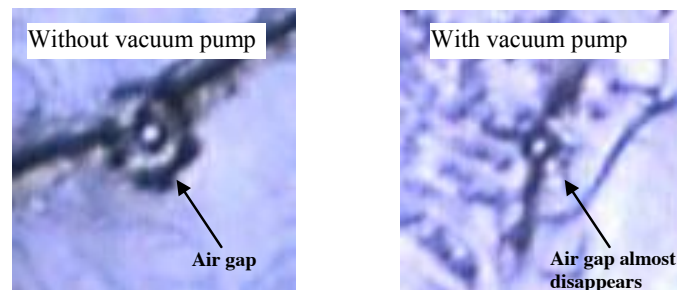


**Fig. 8-5. Comparison between the cross-sections of PPOF drawn (left) without and (right) with the vacuum pump.**

It can be observed that the air gaps are significantly smaller after drawn with vacuum pressure. Moreover, the air gap between the Lucina™ fibre and the PMMA cladding becomes more evenly distributed and the position Lucina™ fibre is more concentric with the outer cladding. From our experience, the vacuum

pressure is adjusted as high as possible to obtain a better result. In our case, the value of the vacuum pressure is 80kPa.

## **8.5 Optical Characteristics**

The approximate refractive index profile of the single-mode PPOF has been shown previously in Fig. 8-3, which is an expectation only until the optical characteristics of the fibre is tested. Therefore after the fibre is drawn, its far field profile is examined to judge whether the fibre is single-mode or not. If the fibre is found to be single-mode, its cut-off wavelength can be found as well. Moreover the transmission loss of the fibre is going to be found to compare with the original Lucina<sup>TM</sup> fibre and see if it remain its low loss property.

### **8.5.1 Far Field Profile**

To view the far field profile of the single-mode PPOF, the fibre was butt-coupled with a light source. The end-face of the fibre was cut by a razor blade perpendicularly to the axis of propagation of the fibre. The output intensity distribution of the fibre was then measured by a far-field profile analyzer (Photon Inc., Model: LD8900 HDR). Two laser sources were used, which wavelength is centered at 1310nm and 1550nm respectively. The results of the far field profile are shown in Fig. 8-6.



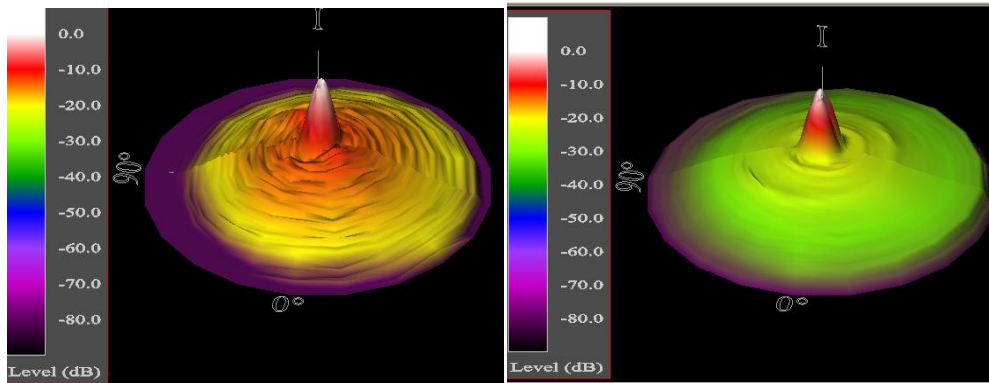


**Fig.8-6. (left) Far field profile of the single-mode PPOF with 1310nm laser source and (right) with 1550nm laser source.**

It can be observed that in the view of far field profile, the fundamental mode in the fibre is dominant for both 1310nm and 1550nm light source. It is concluded that the fibre is single-mode for this wavelength range.

### 8.5.2 Cut-off Wavelength

After proving the fibre is single-mode with the 1310nm to 1550nm telecommunication window, its cut-off wavelength was going to be found by the TIA standard [10]. An 820-nm superluminescent diode was used to illuminate the PPOF. The output power  $P_1(\lambda)$  was measured by an optical spectrum analyzer versus  $\lambda$ , which was around the expected cut-off wavelength. Then the PPOF was replaced by a short length ( $\sim 1.5\text{m}$ ) of multimode fibre which acted as a reference fibre. Similarly its output power  $P_2(\lambda)$  was recorded. The spectral attenuation of the test specimen, relative to the reference power was calculated by Equation 8-5, and plotted into a graph (see Fig. 8-6)

$$a(\lambda) = 10 \log \frac{P_1(\lambda)}{P_2(\lambda)} \quad \text{Equation 8-5}$$

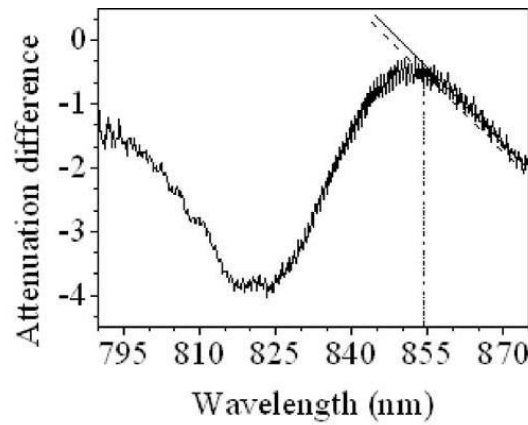


Fig. 8-6. Graph of spectral attenuation of PPOF.

According to the instruction stated in [10], a straight line is fitted with drop of 1dB to the longer-wavelength slope of the graph, then cut-off wavelength can be denoted by the subsequent intersection with the curve. The corresponding value is around 854nm for our PPOF.

### **8.5.3 Transmission Loss**

The transmission loss of the single-mode PPOF was measured by using the cut-back method, in which the fibre was cut by certain length each time, and then the transmission loss was averaged out. A broadband light source with wavelength ranging from 1400nm to 1650nm was used as the input signal, tailed with a conventional single-mode silica fibre. The PPOF was tried to aligned with the silica fibre by a high-precision three-axis stage (Thorlabs, Model: NanoMax-TS). The input signal fibre and the single-mode PPOF fibre were fixed firmly throughout the whole measurement process. The other end of the PPOF was connected to an optical spectrum analyzer via a 400 $\mu$ m diameter fibre adaptor. The initial length of the PPOF was 4.0m. The end-face of the output fibre was cut by a razor blade. Each time 0.5mm of the fibre was cut at the output end and then the output spectrum was measured and recorded. Totally the process repeated 45 times to obtain the average transmission loss of the PPOF. The fibre attenuation measurement errors due to different fibre end-face quality at each time would be reduced by averaging a sufficient number of output spectra. The measurement errors from the cladding-modes were also minimized by a relatively long fibre sample ( $\sim$ 4m in this case). Fig. 8-8 shows the experimental result about the

transmission loss of the single-mode PPOF from about 1410nm to 1650nm wavelength.

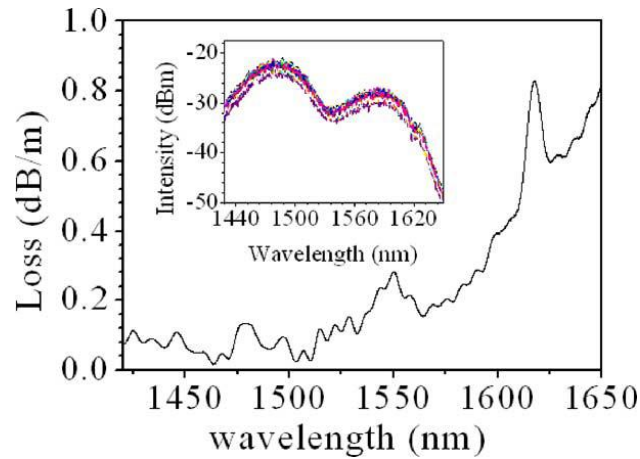


**Fig. 8-7. Graph of measurement of transmission loss of single-mode PPOF and the inset shows the output spectrum with different fibre length.**

Generally the fibre attenuation is less than 0.2dB/m from 1410nm up to near 1540nm. Beyond 1540nm, the attenuation starts to go up, but is still less than 0.5dB/m up to 1610nm. These fibre losses are substantially lower than that of PMMA fibres and should be low enough to allow meters long applications of this kind of fibre.

## 8.6 Conclusion

The single-mode low loss PPOF was successfully fabricated. The fibre was drawn by redrawing method, in which the cladding is made of PMMA-based polymer and the core fibre is a commercially available POF, which is called Asahi Lucina<sup>TM</sup> fibre. The single-mode PPOF has a core diameter of 6.6 $\mu$ m and a cladding diameter of 400 $\mu$ m. The fibre exhibits single-mode characteristics at the wavelength range of 1310nm and 1550nm. It is predicted by TIA standard that the fibre has a cutoff wavelength of 854nm. The transmission loss is less than 0.2 dB/m in the wavelength range of 1410–1540 nm and less than 0.5 dB/m for wavelengths up to 1610 nm, significantly less than the typical transmission loss of 100 dB/m for PMMA fibre. The fibre has a good potential for FBGs inscription and has a low refractive index of 1.34, close to aqueous solution of biomaterials, permitting strong optical coupling for biomedical applications.

## Reference

1. XIONG, Z., PENG, G. D., WU, B., and CHU, P. L., "Highly tunable Bragg gratings in single-mode polymer optical fibres," *IEEE Photon. Technol. Lett.* 11, 352 (1999).
2. KALLI, K., DOBB, H. L., WEBB, D. J., CARROLL, K.I, KOMODROMOS, M., THEMISTOS, C, PENG, G. D., FANG, Q. and BOYD, I. W., "Electrically tunable Bragg gratings in single-mode polymer optical fibre," *Opt. Lett.* 32, 214 (2007)
3. KIM, K. J., BAR-CHEN, A. and HAN, B., "Thermo-optical modeling of an intrinsically heated polymer fibre Bragg grating," *Appl. Opt.* 46, 4357 (2007)
4. YENIAY, A., GAO, R., TAKAYAMA, K., and GARITO, A. F., "Ultra-low loss polymer waveguides," *J. Lightw. Technol.* 22, 154 (2004)
5. PITOIS, C., HULT, A., and WIESMANN, D., "Absorption and scattering in low-loss polymer optical waveguides," *J. Opt. Soc. Amer. B* 18, 908 (2001)
6. YOSHIMURA, R., HIKITA, M., TOMARU, S. and IMAMURA, S., "Low-loss polymeric optical waveguides fabricated with deuterated polyfluoromethacrylate," *J. Lightw. Technol.* 16, 1030 (1998)
7. LIU, H. Y., PENG, G. D., CHU, P. L., KOIKE, Y., and WATANABE, Y., "Photosensitivity in low-loss perfluoropolymer (CYTOP) fibre material," *Electron. Lett.* 37, 347 (2001.)

8. LIU, H. Y., PENG, G. D. and CHU, P. L., "Thermal stability of gratings in PMMA and CYTOP polymer fibres," *Opt. Commun.* 204, 151 (2004)
9. SENIOR, J., "Optical Fibre Communications: Principles and Practice", 2<sup>nd</sup> ed. Englewood Cliffs, NJ: Prentice-Hall ( 1992)
10. "Measuring Cutoff Wavelength of Uncabled Single Mode Fibre by Transmitted Power", *TIA/EIA Standard*, FOTP-80 (Feb. 1996)

## Chapter 9 Conclusion

The POF preforms are fabricated by the “Teflon method” by making use of the Teflon strings, rods or tubes. The principle of the polymerization is studied and it is concluded that the pre-polymerization procedure is necessary to prevent bubble formation during the early stage of the polymerization of monomers. The curing temperature profile in the oven is also strictly controlled so as to guarantee the quality of the preforms. The polymer preform is mainly made from MMA, BMA, and BzMA, in which LP and DT are used as the initiator and the chain transfer respectively. The composition of the POF preform is also investigated such that the glass temperature and the refractive index of the polymer can be adjusted for various fibre designs. Together with the reliable POD draw tower, we can produce POF with quality high enough for research purpose.

The POF draw tower has been built, which mainly comprises of the feeding unit, the furnace, the take-up unit and the control unit. For the performance, the POF draw tower can handle the preform sizes from 6 to 22.2mm and produce the POF with outer diameter from 100 $\mu$ m to as large as 4mm, within 3% accuracy. The drawing parameters such as the feed speed, the take-up speed as well as the furnace temperature and drawing conditions have been tested and optimized for various kinds of POFs.

The light source is one of the major components in a POF sensing system. We have demonstrated how the organic laser dyes are possible to be doped into POFs and



pumped by a low-cost laser diode to become a POF light source. Among different types of laser dyes, R6G, Rh640 and LDS751 are able to be doped into the POFs without losing their fluorescence properties after polymerization and drawing stage but not the case for HITC, IR144, IR125 due to their molecular structures. It is also possible to co-dope R6G, Rh640 and LDS751 into the POFs to achieve a wider fluorescence spectrum over 150nm. The Rh640 doped POF with cladding structure is also fabricated and its fluorescence characteristic have been further studied to know more about relationship fluorescence output of the fibre and the pump source and also the red shift of the fluorescence spectrum due to increase in the fibre length or laser dye concentration. The value of the loss of the fibre was also calculated, which is 0.477db/mm for 532nm wavelength and 0.233db/cm for 658nm wavelength, which gives us useful information about determining the length of the fibre and the power of the pump source in practical applications. It is calculated the optical conversion efficiency of the fibre is 1.509% with the laser dye concentration of 10ppm. Moreover, the output power of dye doped POF can be further enhanced by nearly 45% if one fibre end is coated by thin gold layer.

A laser-dye-doped POF has been specially designed and fabricated in which the cladding of the POF was doped with Rh640. The fibre was successfully pumped by a compact and low-cost 532 nm laser source by the SIF technique. The fluorescence output power of the POF under SIF was enhanced by the proposed bending method by more than ten times. This scheme offers a practical solution to convert and couple fluorescence light directly into the core of a POF. Furthermore,

any point along the POF can act as a light source when that point is under SIF, and the spectrum remains the same along the because of the undoped core. These offer the dye-doped POF a good potential to be used as light source in a biomedical sensing system.

The photobleaching behavior of organic dyes is a great hurdle for the reliability of the dye doped POF to be used as the light source. Based on the scale-up ability of the SIF technique and phenomenon of FPR of the dye doped fibre, there are two novel pumping schemes, based on a Switch-pumping (SwP) technique and a Scan-pumping (ScP) technique with single or multiple laser diodes, are invented. The two pumping schemes minimize the effect of photobleaching of the dyes. The total output power deterioration is less than 10% when the dye doped POF has been continuously pumped by the laser diode(s) to give 1 $\mu$ W optical output for 90min. Different designs of dye doped POFs, with structure of either step-index, graded index or microstructured, are proposed. They have great potential to be inscribed with sensing elements base on Bragg gratings (FBGs), long period gratings (LPGs), or surface plasmons (SP), such that the light source and the sensing element are combined in a single dye doped fibre. Generally for both pumping techniques, the total output power deterioration is less than 10% when the dye doped POF has been continuously pumped by the laser diode(s) to give 1 $\mu$ W optical output for 90min. The pros and cons between SwP and ScP techniques have been stated. The output power of the dye doped POF can be even enhanced by gold coating in several configurations in which gold is coated on one fibre end or

coated along the axial direction of the fibre. Different designs of dye doped POFs, with structure of either step-index, graded index or microstructured, are also proposed. They have great potential to be inscribed with sensing elements base on FBGs, LPGs, or SP, such that the light source and the sensing element are combined in a single dye doped fibre without any coupling devices.

Finally, for some special fibre fabrication, the single-mode low loss PPOF was successfully drawn by the redrawing method, in which the cladding is made of PMMA-based polymer and the core fibre is a commercially available POF, which is called Asahi Lucina<sup>TM</sup> fibre. The single-mode PPOF has a core diameter of 6.6 $\mu$ m and a cladding diameter of 400 $\mu$ m. The fibre exhibits single-mode characteristics at the wavelength range of 1310nm and 1550nm. It is predicted by TIA standard that the fibre has a cutoff wavelength of 854nm. The transmission loss is less than 0.2 dB/m in the wavelength range of 1410–1540 nm and less than 0.5 dB/m for wavelengths up to 1610 nm, significantly less than the typical transmission loss of 100 dB/m for PMMA fibre. The fibre has a good potential for FBGs inscription and has a low refractive index of 1.34, close to aqueous solution of biomaterials, permitting strong optical coupling for biomedical applications.

## **Chapter 10 Future Work**

In order to achieve an all-polymer sensing system, there are so many issues we can further explore and investigate from the thesis. It may involve upgrading the available facilities and setup, applications of the dye doped POFs and even opening several research areas, such as fabricating microstructured polymer fibre and building broadband light source. In this Chapter, some examples of the future work will be suggested.

### **10.1 Inscription of sensing elements in dye doped POF**

The most important future work to do is to inscript sensing elements into the dye doped POF and complete the whole polymer sensing system. As mentioned previously, the sensing elements can be based on the fibre itself, FBGs, LPGs and even SPR. The fibre will be pumped by SwP or ScP technique for the light source components, and the conventional photodetector will be used. Therefore a complete compact and low cost all-polymer sensing system will be achieved.

### **10.2 Building POF Cleaver**

Cleaving POF is a very basic but big problem to handle the POF. As the POF is too soft, it is quite hard to cleave the POF with good end-surface. Now the making use of hot-knife by hand is convenient but involving the human factor. On the other hand, laser cleaving leaves a good end surface but it is restricted to the place and operation cost. It is suggested that a portable POF cleaver may be built.

### **10.3 Modification in Teflon Method**

The Teflon method has been used for making our POFs preforms. However, there are some problems arising from the Teflon itself, such as the surface smoothness of the Teflon strings or tubes surface and the rigidity of them. Therefore we have to investigate a good substituent to the Teflon, and one of the possible ways is to coat a non-stickly layer onto glass rod or stainless steel.

The other problem is related to the glass tube mould for the preforms. After polymerization done, the glass tubes are broken down to take the preform away. It is wasteful and also may damage the surface of the preform. Therefore it is suggested mould is replaced by a well designed Teflon mould such that the mould can be re-used and the dimension of the preform is the identical every time.

#### **10.4 Building boardband fibre laser by dye doped POF**

A short length of the dye doped POF can be used as the resonance cavity, by coating reflection mirror, such as thin gold or chromium layer on both fibre ends. The POF is then side pumped by the laser diode to see if there is any light lasing out from the fibre. By this way, it is possible to make a single-mode POF light source with suitable design of the POF and configuration. It is also possible to dope with several dyes into the fibre to achieve as the broadband light source.

#### **10.5 Fabrication of mPOF**

We have designed a mPOF to eliminate the influence of dopant diffusion and to increase the ultra violet (UV) writing efficiency in fiber Bragg grating inscription. As shown in Fig. 10-1, the proposed design comprises a double-clad layer

structure, in which the inner cladding region is made TS-doped PMMA and the outer cladding is made of undoped PMMA,. Inside the TS-doped region, the fiber core for the single-mode propagation is formed by the three large surrounding air holes.

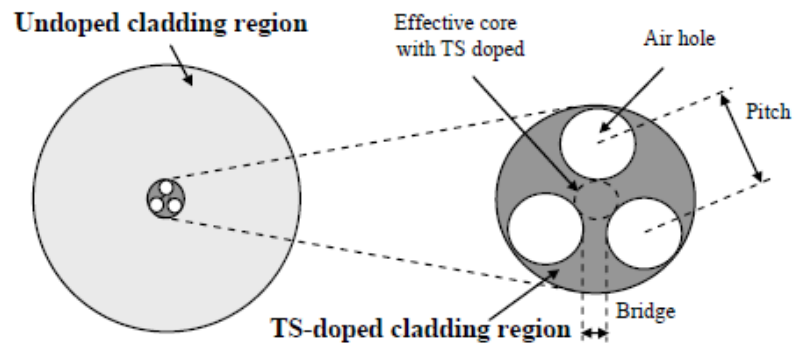


**Fig. 10-1. Schematic Diagram of a PMMA 3-hole-assisted fibre with a structure.**

For some preliminary result, we have fabricated a 3-hole PMMA optical fibre, and observed light guiding at 800 nm. A SEM image of the fibre is shown in Fig. 10-2. We aim to fabricate and examine the proposed TS-doped fibre in the near future.

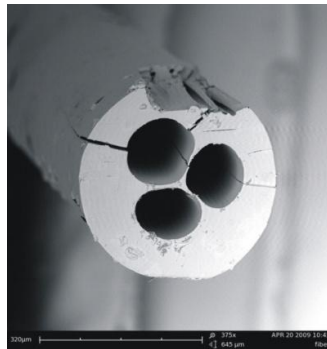


**Fig. 10-2. SEM image of a three-hole-assisted PMMA optical fibre**

We have also designed single-mode mPOF with large core. The cross section of the proposed designed mPOF is shown in Fig. 9-3(left).

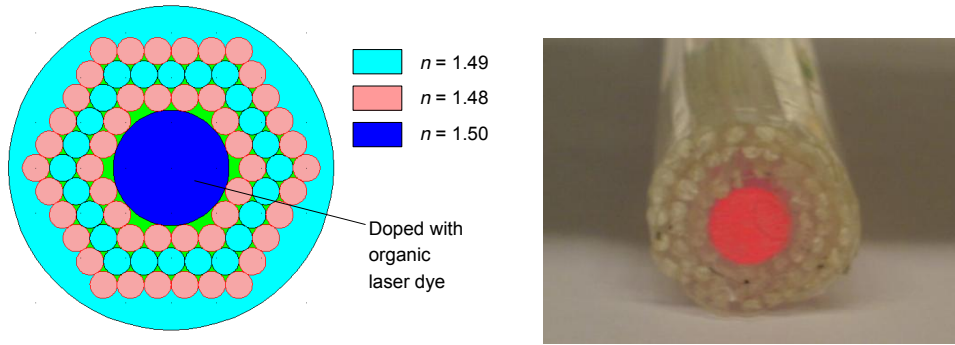


**Fig. 10-3. (left) Cross section of the proposed designed mPOF with large core. (right) Photo of the actual mPOF preform.**

In fact we have actually realized the mPOF preform by stacking method as shown in Fig. 10-3(right). The preform is formed by stacking polymer rods inside a tube, and with a large laser-dye-doped polymer rod in the center. The fibre is composed of three rings in cladding with different refractive index polymer rods. The core was doped with organic laser dye (Rh640 in this case) The effective mode area of the large core mPOF with three homocentric octagonal rings were characterized by using COMSOL software as shown in Fig. 10-4.

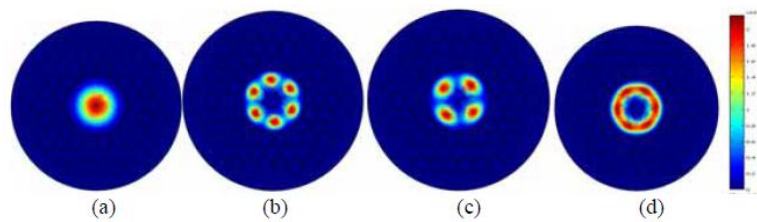


**Fig. 10-4. Field distribution of the first 4 propagation mode groups at the operating wavelength of 640 nm.**

It is simulated that if the diameter of the rod is 7mm and that of the core is 30.1 $\mu\text{m}$ , then the maximum effective mode area can reach up to 335  $\mu\text{m}^2$  for fundamental mode in the structure mPOF. The fabrication of the single mode laser dye-doped mPOF with large core is carried out and further experimental work will be reported afterwards.

### **10.6 Fabrication of Various Structures of Dye Doped POFs**

The novel pumping schemes can be applied in POFs with various structures as far as organic laser dye(s) is doped into it. The dye doped fibre can be single-mode or multi-mode, in which their structures may include (but not limited to) uncladded fibre, step-index POF (SI-POF), guided-index fibre (GI-POF) as well as microstructured fibre (mPOF). The novel pumping schemes can also work with the POFs in which either the core or the cladding, or both of them are doped with organic laser dyes. The dye doped POFs may consist of more complex structure and layers, which may be doped with different types of dyes as well. Fig. 10-5 shows some examples of the dye doped POFs with different structures.



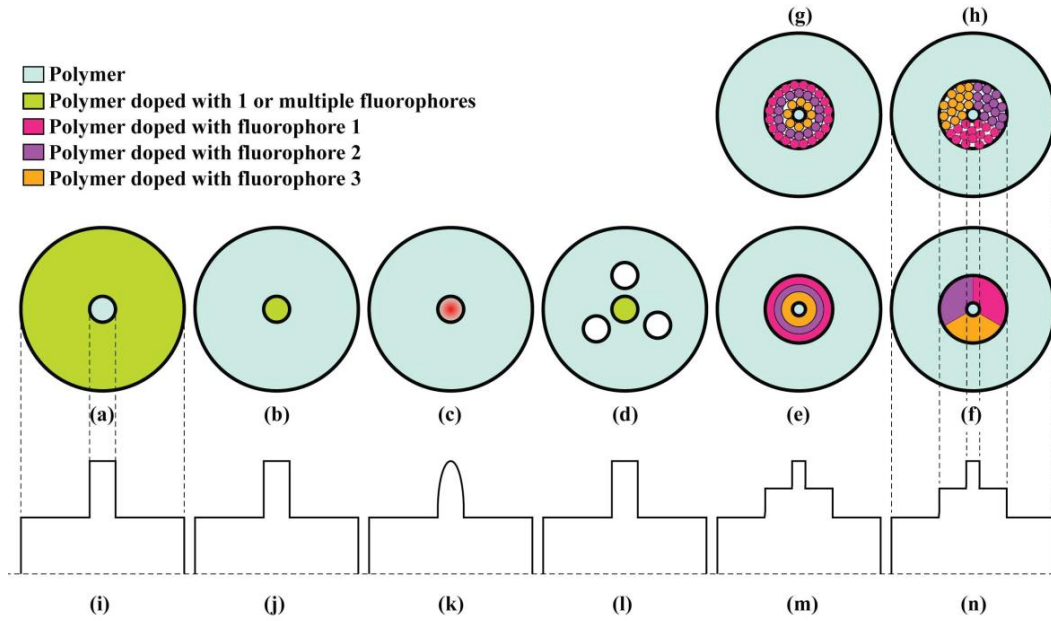


**Fig. 10-5. Cross-section of fluorophore-doped POF of different designs (a) - (h), (g) and (h) are the “stacked” versions of (e) and (f). The refractive index profiles of the different POFs are given in (i) - (n).**

From Fig. 10-5 (a) to (c), it shows that the laser dye(s) can be doped in either core or cladding of the fibre. Also the fibre can be single-index or graded index depends on the applications. From Fig. 10-5 (d), the laser dye(s) can also be applied in the microstructure fibre. From Fig. 10-5 (e) and (f), more complex structures of the laser dye doped POF are proposed. Fig. 10-5 (e) shows that the fibre contains rings of layers, which are doped with different laser dyes respectively. Once the fibre is side-illuminated, it is expected that a broadband fluorescence spectrum will be obtained. Fig. 10-5 (e) shows that the fiber contains three portions, doped with different laser dyes, surrounding the fibre core. It is expected that the switching of

the different fluorescence output can be achieved by side-illuminating the fibre in different orientations.